

Alma Mater Studiorum – Università di Bologna

DOTTORATO DI RICERCA IN

Biologia cellulare e molecolare

Ciclo XXXIV

Settore Concorsuale: 05/E2

Settore Scientifico Disciplinare: BIO/11

Investigating the mechanisms of *Moraxella catarrhalis* resistance to oxidative stress

Presentata da: Sonia Nicchi

Coordinatore Dottorato

Chiar.mo Prof

Vincenzo Scarlato

Supervisore

Chiar.mo Prof.

Vincenzo Scarlato

Co-supervisor

Dott.ssa **Cecilia Brettoni**

Dott. **Domenico Maione**

Esame finale anno 2022

ABSTRACT

Chronic Obstructive Pulmonary Disease (COPD) is a multifactorial inflammatory disease with *Moraxella catarrhalis* (Mcat) being the second bacterial causative agent after non typeable *Haemophilus influenzae* (NTHi). Among the aspects that characterize COPD pathogenesis, oxidative stress (or reactive oxygen species, ROS) is the hallmark. The most biologically relevant sources of ROS include innate immune cells, alteration of the microbiota composition and bacterial load. Most pathogens survive the action of ROS by employing intrinsic mechanisms such as detoxification of radical species. Moreover, few bacterial pathogens exploit extrinsic resistance mechanisms to actively suppress ROS production by eukaryotic cells. Mcat shows a higher innate level of resistance to exogenous oxidative stress compared to the co-infecting pathogens of the respiratory tract but the underlying mechanisms are currently not well defined. We considered this to be of particular interest and thus it became the focus of the work in this thesis.

First of all, we investigated how Mcat and NTHi cope with the oxidative stress produced by differentiated neutrophilic-like dHL-60 cells and primary cells. Here, we showed that Mcat induces ROS and neutrophil extracellular traps (NET) production in dHL-60 and primary cells to a lesser extent compared to NTHi. It is also able to actively interfere with these responses in chemically-activated cells in a phagocytosis/opsonins-independent and contact-dependent manner possibly by engaging host immunosuppressive receptors. Moreover, Mcat subverts the autophagic pathway of the phagocytic cells and survives intracellularly. It also promotes the survival of NTHi which is otherwise susceptible to the host antimicrobial arsenal.

The focus of the second part of this study is the characterization of the Mcat global transcriptional response to oxidative stress. To this aim, we performed an RNA-Seq experiment on exponentially growing bacteria exposed to sublethal amounts of H₂O₂ or CuSO₄. As a consequence of the two treatments, 225 and 140 differentially expressed (DE) genes were identified, respectively. Comparing the two transcriptomes of Mcat treated with H₂O₂ or CuSO₄, 61 commonly regulated genes were found, indicating a significant and previously unknown overlap between the two transcriptional responses. In addition to the known intrinsic resistance mechanisms, other pathways having less obvious associations to oxidative stress resistance were also captured. Ten genes were subsequently selected because of their relevance in DE analysis and functionally characterized through the generation of knock-out (KO) mutants. Among them, deletion mutants for *badM* and *MCR_0349* showed the highest sensitivity to H₂O₂, a reduced virulence in both ROS-induced neutrophil-like cells and in *Galleria mellonella* *in vivo* model. So far, this work provides the most comprehensive picture of the complex Mcat responses to the oxidative environment it normally encounters within the infected tissues.

Disclaimer

Sponsorship:

This work was funded by GlaxoSmithKline Biologicals SA and Alma Mater Studiorum University of Bologna.

Transparency statement:

Sonia Nicchi is a PhD student at the University of Bologna Alma Mater Studiorum and participates in a post graduate studentship program at GSK, Siena, Italy. CB and DM are employees of the GSK group of companies. VS is an employee of University of Bologna, Department of Pharmacy and Biotechnology.

Human samples:

The three human sera (ID:2543, 6002, 2151 from Phleb001_20180404-AXB-1805_Phleb001 generic) used in the study were obtained according to Good Clinical Practice in accordance with the declaration of Helsinki and patients have given their written consent for the use of the samples of study MENB REC 2ND GEN-074 (V72_92). The study was approved by the Western Institutional Review Board (WIRB). The sera have been pooled and used as human complement source for the research purpose. The studies involving venous blood from healthy human individuals (for neutrophils isolation) were reviewed and approved by a GSK commercial provider, CHU Tivoli (BELGIUM). The patients/participants provided their written informed consent to participate to further research.

CONTENTS

1. INTRODUCTION	1
1.1 <i>Moraxella catarrhalis</i> : from a commensal to established pathogen.....	1
1.2 Chronic obstructive pulmonary disease.....	4
1.3 Neutrophil-mediated Oxidative stress: the hallmark of COPD	6
1.4 Neutrophil Fc, CEACAM and Siglec receptors: phagocytosis and ROS pathways.....	8
1.5 Killing effects of ROS	11
1.6 ROS-related antimicrobial weapons: NET and autophagy.....	13
1.7 Role of Copper in the oxidative stress response.....	17
1.8 <i>Galleria mellonella</i> as a valuable <i>in vivo</i> model for bacterial infections	19
2. AIM.....	21
3. BACKGROUND 1 ST PART AND GRAPHICAL ABSTRACT.....	22
4. RESULTS 1 ST part	23
4.1 <i>M. catarrhalis</i> and NTHi: two different ways to interact with neutrophil-like cells.....	23
4.2 Mcat actively interferes with cellular ROS production while NTHi does not.....	25
4.3 Mcat limits ROS production in a contact-dependent and phagocytosis-independent manner by possibly binding immunosuppressive receptors.....	28
4.4 NET generation is differently modulated by NTHi and Mcat.....	32
4.5 Mcat interferes with the autophagic pathway surviving intracellularly and reducing the killing of NTHi	34
4.6 Human opsonins increase Mcat and NTHi neutrophil uptake without affecting their ROS response	38
4.7 Mcat and NTHi behaviours in primary cells strongly reflect those observed in dHL-60 cells ...	41
5. DISCUSSION 1 ST part	44
6. BACKGROUND 2 ND PART AND GRAPHICAL ABSTRACT	49
7. RESULTS 2 ND part	50
7.1 Identification of a previously unknown overlap between Mcat transcriptional responses to H ₂ O ₂ and CuSO ₄	50
7.2 Co-expression network analysis, relevance in DE analysis and functional categories guide the selection of ten genes for functional characterization	57
7.3 <i>badM</i> transcriptional regulator and <i>MCR_0349</i> unknown genes emerged as fundamental factors for Mcat resistance to oxidative stress.....	61
7.4 $\Delta badM$ and ΔMCR_0349 mutants are less virulent in <i>Galleria mellonella</i> larvae, a valuable <i>in vivo</i> model for Mcat.....	66
8. DISCUSSION	68
9. MATERIALS AND METHODS.....	71
9.1 Cell culture and differentiation.....	71
9.2 Bacterial Strains and Cultures	72
9.3 Phagocytosis Studies by FACS	72

9.4 Reactive Oxygen Species Detection.....	73
9.5 Flow cytometric analysis of <i>M. catarrhalis</i> engagement of human recombinant receptors CEACAM-1, Siglec-5 and Siglec-9	73
9.6 Recombinant OmpCD preparation	74
9.8 NET: quantification and visualization by confocal microscopy.....	75
9.9 Autophagic response and intracellular survival assay	76
9.10 Electron microscopy (EM)	77
9.11 Mcat and NTHi opsonization with human sera	77
9.12 Isolation of human neutrophils	78
9.13 Statistical Analysis	78
9.14 Determination of the H ₂ O ₂ and CuSO ₄ MBC for <i>M. catarrhalis</i>	78
9.15 RNA isolation for and real-time reverse transcription-PCR (RT-PCR) analyses.....	78
9.16 RNA-Seq data analysis.....	79
9.17 Mcat O35E and CCRI-195ME experiment data retrieval and mapping.....	80
9.18 Co-expression network analysis	80
9.19 Generation of directed mutants.....	81
9.20 Genetic complementation of <i>badM</i> and <i>MCR_0349</i> directed mutants.....	82
9.21 Use of growth curves to assess the response to exogenous H ₂ O ₂	82
9.22 Intracellular survival of deletion mutants and complementant strains in dHL-60 cells	82
9.23 <i>In vivo</i> virulence assay of <i>Galleria mellonella</i> infected with Mcat.....	83
10. REFERENCES.....	83
11. SUPPLEMENTARY MATERIALS.....	94
Table S1. List of cell lines, bacterial strains and oligonucleotides used in this study.	94
Table S2. Health Index Score system in <i>Galleria mellonella</i>	99

LIST OF ABBREVIATIONS

$1O_2$	Singlet oxygen superoxide anion
AMP	AntiMicrobial Peptides
AMPK	AMP-activated kinase
ATG5	Autophagyrelated protein 5
BER	Base excision repair
C3	Complement component 3
Ca^{2+}	Calcium
CEACAM	CarcinoEmbryonic Antigen-related Cellular adhesion Molecules
CGD	Chronic Granulomatous Disease
Col IV	Collagen IV
COPD	Chronic Obstructive Pulmonary disease
ECM	Extracellular matrix
ECT	Electron Transport Chain
eDNA	Extracellular DNA
ER	Endosplamisc Reticulum
Fn	Fibronectin
FPRs	Formyl peptide receptors
H_2O_2	Hydrogen peroxide
HIF-1 α	Hypoxia Inducible Factor-1
HO•	Hydroxyl free radical
HOBr	Hypobromous
HOCl	Hypochlorous
HOSCN	Hypothiocyanous
Ig	Immunoglobulin

ITAM	Immunoreceptor tyrosine-based activation motif
ITIM	Immunoreceptor tyrosine-based inhibitory motif
LC3	Microtubule-associated protein light chain 3
LOS	Lipooligosaccharide
MAMs	Mitochondria- Associated endoplasmic reticulum Membranes
Mcat	<i>Moraxella catarrhalis</i>
MFI	Mean fluorescence intensities
MHC	Major histocompatibility complex
MPO	MyeloPerOxidase
mTOR	Mammalian target of rapamycin complex
mtROS	Mitochondrial ROS
NADPH	Nicotinamide Adenine Dinucleotide PHosphate
NDP52	Nuclear dot protein 52 kDa
NE	Neutrophil Elastase
NETs	Neutrophil Extracellular Traps
NLRP3	Nod-Like Receptor family, Pyrin domain containing 3 inflammasome
NTHi	Nontypeable <i>Haemophilus influenzae</i>
O ₂	Oxygen
O ₂ ⁻	Superoxide anion
O ₂ ^{·-}	Superoxide anion
OMVs	Outer Membrane Vesicles
OPTN	Optineurin
PA	<i>Pseudomonas aeruginosa</i>
PAD4	Protein-Arginine Deiminase type 4
PKC	Protein Kinase C

PMA	Phorbol 12-Myristate 13-Acetate
PRRs	Pattern Recognition Receptors
PTP	Permeability Transition Pore
PO	Phenoloxidase
RN	Rhinovirus
ROS	Reactive Oxygen Species
RSV	Respiratory Syncytial Virus
SCN	Thiocyanate
Sias	Sialic acids
Siglecs	Sialic acid-binding immunoglobulin-type lectins
SNPs	Single Nucleotide Polymorphisms
SOD	SuperOxide Dismutase
SP	<i>Streptococcus pneumoniae</i>
SQSTM1/p62	Sequestosome
TCA	TriCarboxylic Acid cycle
TLRs	Toll Like Receptors
TREM-1	Triggering receptor expressed on myeloid cells-1
VDAC	Voltage-dependent anion channels
Vn	Vitronectin
$\Delta\Psi_m$	Mitochondrial transmembrane potential

1. INTRODUCTION

1.1 *Moraxella catarrhalis*: from a commensal to established pathogen

Moraxella catarrhalis (Mcat) is a nonmotile, unencapsulated, aerobic, oxidase-positive diplococcus Gram-negative human pathogen (Verhaegh et al., 2015). For most of the past century, Mcat was thought to be a harmless commensal bacterium because of its resemblance to commensal *Neisseria spp*, which are part of the normal flora (Murphy and Parameswaran, 2009). Thus, despite being often detected on sputum cultures in previous studies, *M. catarrhalis* was ignored as it was considered a non-pathogenic bacterium. Indeed, in an article published in 1953, this bacterium, previously named *Neisseria catarrhalis*, was described as an “organism whose pathogenic propensities are known to be slight or nonexistent” (May, 1953). Although it is able to colonize asymptotically, it is now clear that Mcat is actually a harmful opportunistic human pathogen that represents the second most prevalent bacterium found in sputum of Chronic Obstructive Pulmonary Disease (COPD) patients with exacerbation (Perez and Murphy, 2017, Murphy and Parameswaran, 2009) and the third aetiological agent of otitis media in children behind *Streptococcus pneumoniae* (SP) and nontypeable *Haemophilus influenzae* (NTHi) (Mather et al., 2019). It is also occasionally the causative agent of sinusitis, meningitis and conjunctivitis (Verduin et al., 2002). The species is composed of two main lineages called RB1 and RB2/3 based on the sequence of the 16s rRNA gene (Pingault et al., 2007). Even if several groups indicated that serum-resistant isolates belonged to the RB1 lineage, a clear relationship between genetic lineage and disease was absent (Earl et al., 2016). Only later, a supragenome modelling carried out on 31 *M. catarrhalis* strains revealed that its main virulence factors are present in strains belonging to both RB1 and RB2/3 lineages, indicating that all isolates have equal potential to cause disease (Davie et al., 2011), depending on environmental and host factors (Choudhury and MacNee, 2017).

A growing body of evidence pointed out that *M. catarrhalis* often acts as a co-pathogen (Figure 1A), providing a less hostile environment to the establishment of both viral and bacterial infections (Figure 1B), (Barker et al., 2015, D’Anna et al., 2020). A myriad of studies has demonstrated the reciprocal beneficial mutualism between *M. catarrhalis* and several viruses such as the respiratory syncytial virus (RSV), influenza, and rhinovirus (RN) (Suarez-Arrabal et al., 2015, George et al., 2014). Primary viral infections modulate innate defenses facilitating Mcat colonization and survival within the host (Brockson et al., 2012). On the other hand, it has been shown that Mcat downregulates crucial mediators in innate antiviral responses, favoring viral infections (Heinrich et al., 2016a). In the case of bacterial infections, it has been found that 20–30% of Mcat infections are

associated with the presence of NTHi (Perez and Murphy, 2019). Furthermore, Mcat releases outer membrane vesicles (OMVs) and other secreted products, important in polymicrobial infections. Its OMVs, enriched with beta-lactamase enzyme and complement resistance factors, act distally providing a safer niche for co-infecting pathogens such as NTHi and *S. pneumoniae* that would otherwise be susceptible to beta-lactam antibiotics and host innate immune factors (Schaar et al., 2011, Tan et al., 2007). Interestingly, pneumococcus produces millimolar amounts of hydrogen peroxide (H₂O₂) causing the reduction in the viability of competing bacteria such as NTHi (Johnson et al., 2015b, Wypych et al., 2019) but not that of *M. catarrhalis* (Hoopman et al., 2011). Therefore, by targeting Mcat, the burden of the diseases associated with the other co-infecting pathogens can be possibly reduced.

The colonization of the respiratory tract by *M. catarrhalis* is multifactorial. It requires the cooperation between multiple adhesins, including fimbriae, pili type IV, and non-fimbriae type adhesins, mainly autotransporters and porins (Figure 1C) (Blakeway et al., 2017). Some of these adhesins also function as pulmonary extracellular matrix ECM-binding proteins capable of binding to fibronectin (Fn), laminin and vitronectin (Vn). Importantly, initial adhesion to the airway mucoid epithelial cell lining is mediated by the interactions of OmpCD porin with mucins (Reddy et al., 1997). Subsequently, many other interactions can take place. Among them, the trimeric autotransporter called UspA1 exploits its distal head domain to bind to cell integrin $\alpha 5 \beta 1$ -associated Fn and its stalk region to have a close contact with carcinoembryonic antigen-related cellular adhesion molecules, CEACAM1 receptor (Brooks et al., 2008). Mcat makes multiple contacts with human receptors and ECM to colonize and persist in the pulmonary airways (Riesbeck et al., 2006) (Su et al., 2012) (Perez and Murphy, 2019) and a schematic representation of them is reported in Figure 1C. Nevertheless, due to the lack of an *in vivo* model capable of mimicking Mcat-caused diseases, some aspects of its pathogenesis remain to be elucidated. The most widely employed *in vivo* model for evaluating vaccine candidates for COPD is the mouse pulmonary clearance model (Smidt et al., 2013). However, regardless of a very high inoculum of bacteria, Mcat does not survive for a long time, being efficiently cleared out within 24 hours from the airways of challenged mice. The inability to colonize limits the window in which the immune responses against this bacterium can be tested (Perez and Murphy, 2019). The chinchilla model is also used for the otitis media but shows the same drawbacks (Shaffer et al., 2013). As a consequence, an effective vaccine capable of preventing Mcat infections is still missing (Ren and Pichichero, 2016).

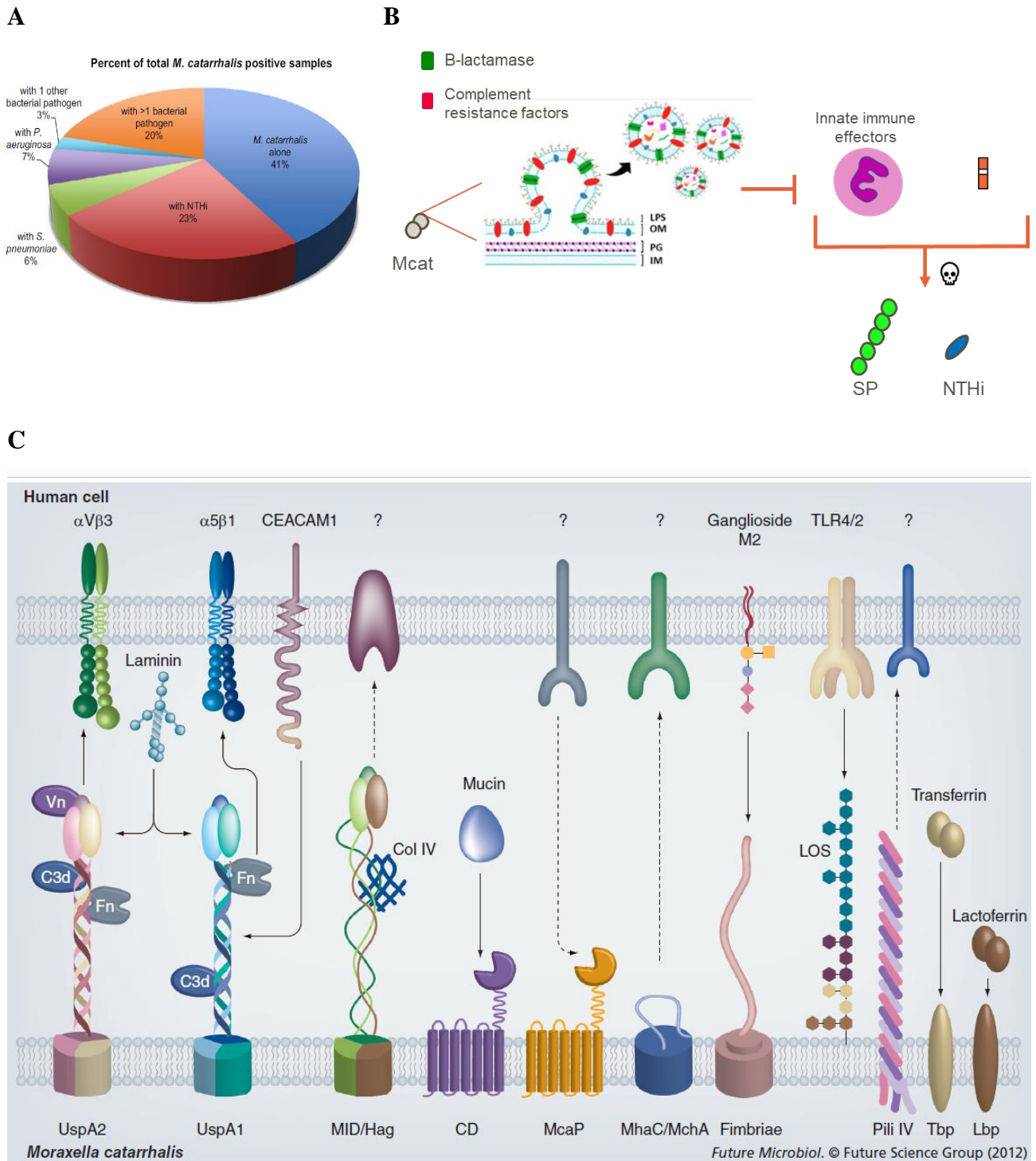


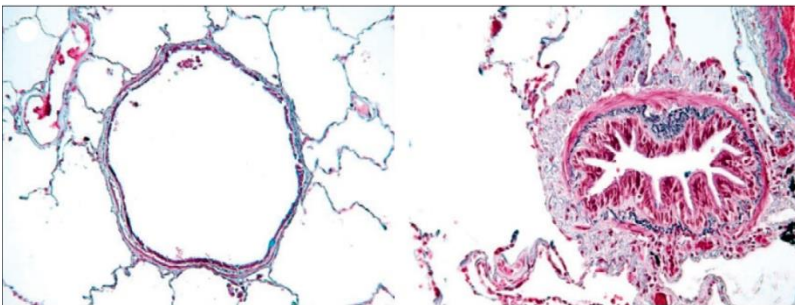
Figure 1. *Moraxella catarrhalis*: from a commensal to an established pathogen. **A)** Percentages of *M. catarrhalis* positive samples based on the number of culture and/or qPCR positive sputum samples across different prospective COPD studies. Image reproduced by courtesy of *Vaccine* (2019) (Perez and Murphy, 2019). **B)** *M. catarrhalis* acts as an important co-pathogen in bacterial infections providing protection against antibiotics and the host complement factors. **C)** Mcat establishes multiple interactions with human cell receptors and proteins by using different adhesins. Image reproduced by courtesy of *Future Microbiol* (2012) (Su et al., 2012).

1.2 Chronic obstructive pulmonary disease

Chronic obstructive pulmonary disease (COPD) is a debilitating disease of adults affecting 65 million people globally. It is the third most common cause of death in the world after ischaemic heart disease and stroke ([The top 10 causes of death \(who.int\)](#)). The course of COPD is marked by intermittent periods of worsening symptoms, called exacerbations, responsible for the progressive decline in lung functions (Pavord et al., 2016). This disease is characterised by a persistent airway inflammation, protease-antiprotease imbalance and over-production of cytokines and oxidative radicals (Stockley et al., 2013, Jaroenpool et al., 2016). All these responses determine a continuous remodeling of the small airways and degradation of ECM of the pulmonary tissues resulting in airflow limitation, pulmonary emphysema, chronic bronchitis and fibrosis (Figures 2A and 2B) (Choudhury and MacNee, 2017). Several epidemiological studies have revealed that the excessive inflammation and ECM destruction observed in COPD are strongly linked to the increased incidence of lung cancer. Additionally, the component of humans' genetic susceptibility required for the establishment of both lung cancer and COPD is similar (Houghton, 2013). Among the several identified common single nucleotide polymorphisms (SNPs), the most widespread one is a hereditary deficiency of α 1 antitrypsin (A1AT, encoded by *SERPINA1*). This protein is the inhibitor of neutrophil elastase (NE), a proteinase responsible for the degradation of elastin, the 'rubber band' protein that enables the lung to recoil after inhalation (Greene et al., 2016). Other candidate gene families are proteinases, detoxifying enzymes and inflammatory cytokines (Chitkara and Hurst, 2012). Of note, two candidate genes *CHRNA3* and *CHRNA5*, which encode nicotinic acetylcholine receptors, are also associated with cigarette smoke and nicotine dependence (Kupiainen et al., 2016). Therefore, also the surrounding environment plays a crucial role for the establishment of COPD. Indeed, several mechanisms such as oxidative stress, telomere length regulation, immunosenescence and changes in the number of anti-ageing molecules are thought to be important as pathogenic mechanisms in COPD (Choudhury and MacNee, 2017). This disease is also characterized by viral and bacterial aetiology (D'Anna et al., 2020). The occurrence of viruses during exacerbation has been estimated to be the 43%, identifying mainly RSV, influenza, and rhinovirus, and to a lesser extent, parainfluenza viruses, adenovirus, and coronavirus (Jafarinejad et al., 2017). Virus–bacteria coinfections may exist, and bacterial exacerbation accounts for up the half of the total COPD (Moghoofei et al., 2020) with nontypeable *Haemophilus influenzae* (NTHi), *Moraxella catarrhalis* (Mcat), *Streptococcus pneumoniae* (SP), and *Pseudomonas aeruginosa* (PA) being the predominant pathogens (Figure 2C) (Garcha et al., 2012, Perez and Murphy, 2019). Another emerging aspect we need to consider is the different lungs microbiota composition of healthy people compared to COPD. Far from the idea of

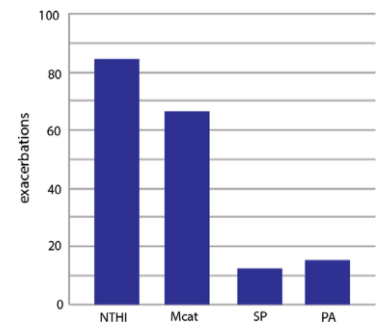
the lungs as sterile organs and similar to the gastrointestinal tract, an ecosystem of viruses and bacteria populate the lungs and the microbiota composition keeps changing during stable and exacerbation states (Wypych et al., 2019). As quantity and functions of immune cells change during disease, microorganisms can show a different degree of pathogenicity (Bagdonas et al., 2015). In healthy individuals, 88% of the microbial population is represented by *Firmicutes*, *Bacteroidetes* and *Actinobacteria* phyla, with *Veillonella*, *Streptococcus*, *Actinomyces*, *Prevotella* and *Rothia* being the dominant genera. In COPD subjects, the most predominant phylum is *Proteobacteria* accounting for 50% of the lung microbiome with *Haemophilus* and *Moraxella* genera contributing for the 25% and 3%, respectively (Haldar et al., 2020, Mayhew et al., 2018), (Figure 2D). Therefore, due to the identified increase in bacterial load and microbial diversity, it is now evident that the lung microbiome can play a crucial role in COPD (Yagi et al., 2021).

A



B

C



D

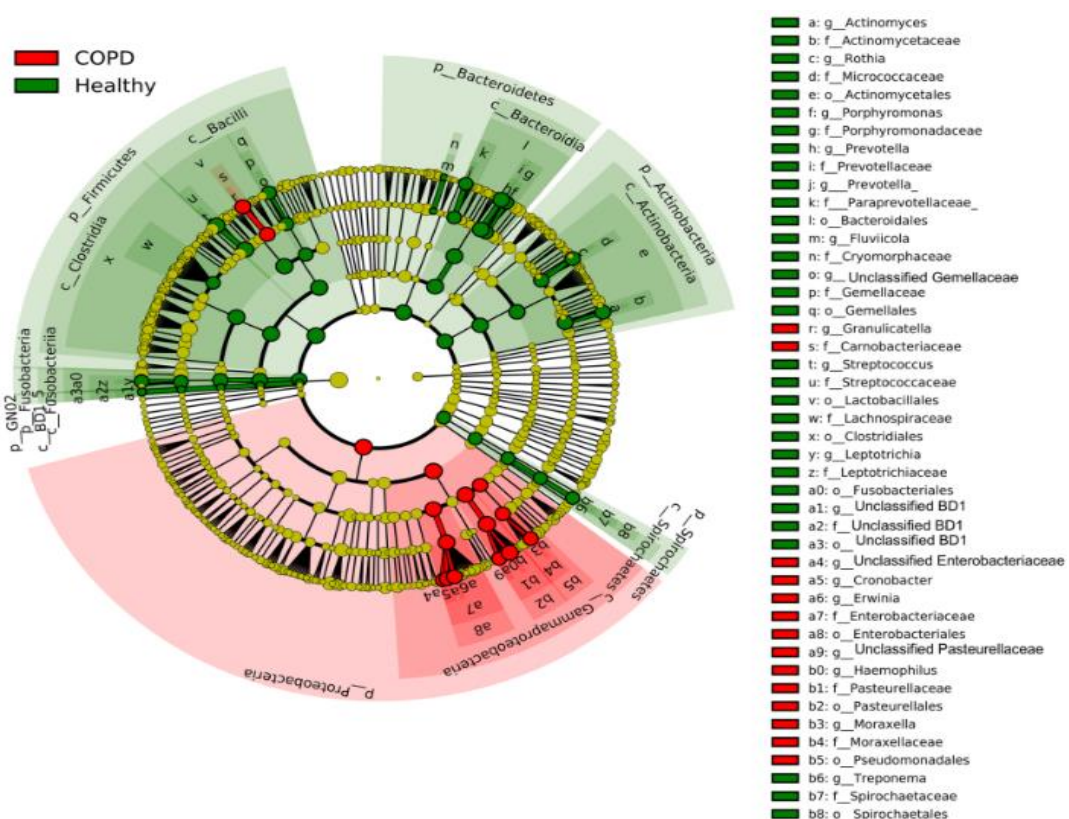


Figure 2. Chronic Obstructive Pulmonary disease: histopathological features and bacterial exacerbations.

A) Healthy individual showing normal airway features and **B)** a patient with COPD showing narrowed airways due to the infiltration of inflammatory cells and mucosal hyperplasia. Images reproduced by courtesy of *The Lancet* (2012) (Decramer et al., 2012) **C)** Bacteria associated with clinical symptoms of exacerbations. Image reproduced by courtesy of *Vaccines* (2019) (Perez and Murphy, 2019). **D)** Health (green zones) and COPD (red zones) microbiome. In the cladogram, each circles represent a bacterial taxa. List of abbreviations: phylum (p), class (c), genus (g), family (f) and order (o). Image reproduced by courtesy of *Respiratory Research* (2020) (Haldar et al., 2020).

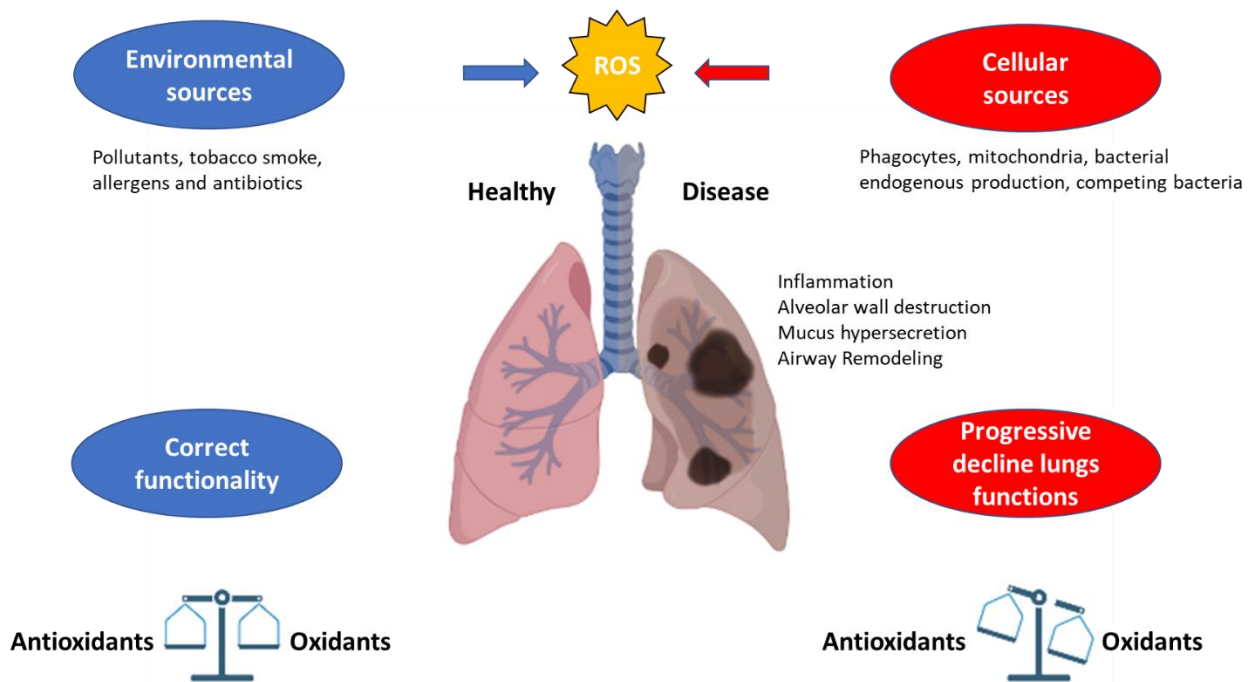
1.3 Neutrophil-mediated Oxidative stress: the hallmark of COPD

Among the aspects that characterize COPD pathogenesis, the oxidative stress is one of the most important hallmarks (Choudhury and MacNee, 2017, Jaroenpool et al., 2016). The sources of reactive oxygen species (ROS) can be classified as both environmental and cellular (Figure 3A). The lung, *per se*, is far more exposed to ROS compared to other anatomical sites (Cheresh et al., 2013). Under physiological conditions, thousands of liters of air are inhaled every day and every breath contains a myriad of exogenous oxidative compounds, such as pollutants, tobacco smoke, and allergens (Marino et al., 2015). In addition to this, there is a massive exposure to antibiotics in patients with recurrent infections, which themselves have a role in ROS production (Van Acker and Coenye, 2017). Joined to these exogenous sources, the lung is constantly exposed to endogenous oxidants which are mainly produced by phagocytic cells, mitochondria (Murphy, 2009, Dupre-Crochet et al., 2013), bacteria themselves through respiration and competing bacteria, as in the case of *Pneumococcus* and also *lactobacilli* which are able to produce millimolar amounts of H_2O_2 (Johnson et al., 2015b, Wypych et al., 2019). Under normal conditions, there is a balance of oxidants and antioxidants for the correct functionality of this anatomical site (Aydemir et al., 2019). Under pathological conditions, such as COPD or cystic fibrosis, there is an oxidant/antioxidant imbalance in favor of oxidants, resulting in oxidative stress (Figure 3A) (Shuto et al., 2016, Cheresh et al., 2013).

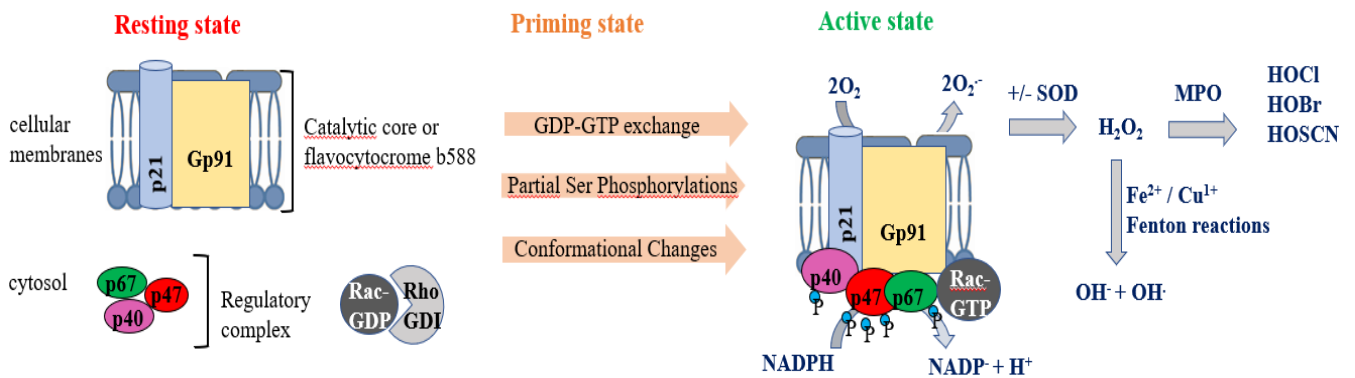
The oxidative burst represents one of the most powerful phagocytic antimicrobial weapon (Nathan and Cunningham-Bussel, 2013). Among phagocytic cells, neutrophils are the most abundant leukocytes (50%–70%) and represent the first line of innate defense and effectors of adaptive immunity (Mayadas et al., 2014). Neutrophils migrate from the circulation to the sites of infection in response to certain stimuli (Ley et al., 2007), carrying out a variety of microbicidal activities (Winterbourn et al., 2016) including phagocytosis, ROS generation, autophagy, degranulation with the release of antimicrobial peptides (AMP), proteases, and as a last line of defense, neutrophil extracellular traps (NETs) (Delgado-Rizo et al., 2017). Neutrophils generate ROS by using a multicomponent oxidase complex named nicotinamide adenine dinucleotide phosphate NADPH oxidase complex (NOX2), and complex I, II, and III within the mitochondrial respiratory chain

(Glasauer and Chandel, 2013, Dan Dunn et al., 2015, El-Benna et al., 2009) (Figures 3B and 3C). In severe COPD, ROS generation is markedly enhanced due to the presence of activated neutrophils, which promote the excessive formation of ROS and ROS-related responses (Di Stefano et al., 2004).

A



B



C

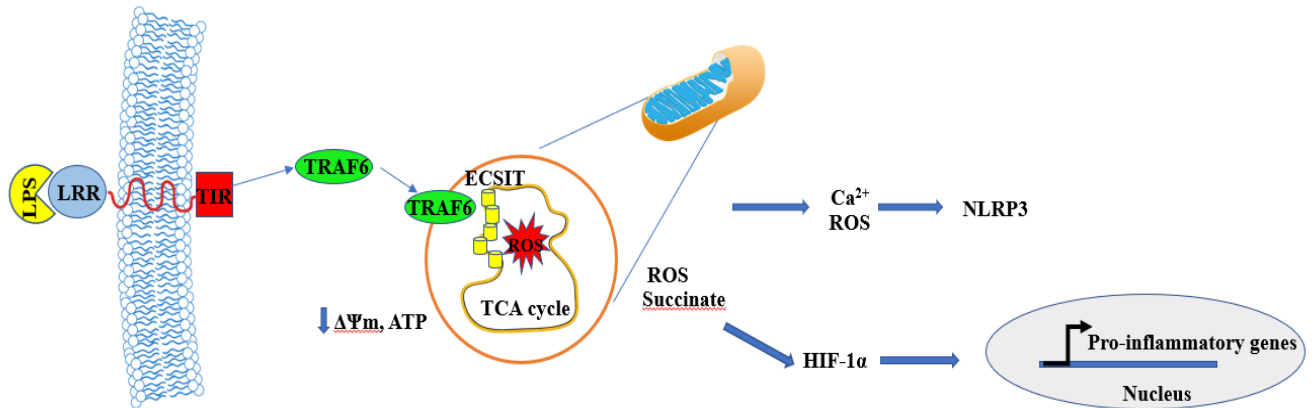


Figure 3. Main sources of ROS. A) Increased oxidative stress is the hallmark of COPD lungs result from both environmental source (pollutants, tobacco smoke, allergens and antibiotics) and cellular sources (phagocytic cells, mitochondria, endogenous production and competing bacteria). Created with Biorender.com (B and C) Cellular sources: NADPH oxidase and mitochondria. B) NADPH oxidase: in the resting state, the two membrane-bound subunits gp91phox and p22phox that represent the catalytic core, are localized on cellular membranes. Four additional soluble proteins including the Rac2 GTPase bound to its inhibitory partner Rho-GDI and the regulatory complex (p40phox, p47phox, and p67phox) dwell in the cytosol of resting cells. An intermediate (prime) state represents a ‘boosting’ step, preparing the NADPH oxidase for a stronger activation. Priming induces NADPH oxidase components phosphorylation, conformational changes and Rac2 undergoing GDP-GTP exchange. As a result, Rac and cytosolic oxidase subunits translocate to the membranes leading to ROS production. Upon NADPH oxidase assembly, the generated superoxide anions can lead to the hydrogen peroxide (H_2O_2) production. H_2O_2 can be transformed into hypochlorous acid (HOCl), hypobromous acid (HOBr) or hypothiocyanite (HOSCN) by the myeloperoxidase enzyme (MPO) or can react with superoxide to produce hydroxyl radicals (OH^\bullet). This reaction occurs in the presence of metals such as Fe^{2+} or Cu^{2+} (Fenton Haber Weiss reaction). gp91phox, p22phox p40phox, p47phox, p67phox, Rac-GDP or-GTP, Rho-GDI and phosphoryl group are in light yellow, light blue, purple, red, green, dark gray, light gray and cyan, respectively. C) Mitochondrial ROS (mtROS) are produced within the electron transport chain (ECT, complex I-III, yellow rectangles). The process is mediated by pattern recognition receptors (PRRs) such as toll like receptors (TLRs). Activation of TLR4 leads to the translocation of TNF receptor associated factor 6 (TRAF6, green) to mitochondria, interacting with evolutionarily conserved signaling intermediate in Toll pathways (ECSIT), and increasing ROS production. In addition, the availability of intermediates of TCA cycle like succinate is shown to increase mtROS production by reversing the electron transport through complex-I of ETC, rise the stability of hypoxia inducible factor-1 HIF-1 α which induces the expression of pro-inflammatory genes. mtROS activates a multiprotein complex called Nod-like receptor family, pyrin domain containing 3 (NLRP3) inflammasome that leads to caspase-1 activation resulting in increased cytokines activities (e.g., IL-1 β) and an inflammatory cell death named as ‘pyroptosis’. Downstream effects of mtROS include the opening of the permeability transition pore (PTP), a high-conductance inner membrane channel involved in the apoptotic response, due to the loss of mitochondrial transmembrane potential ($\Delta\Psi_m$), decline in ATP levels, loss of mitochondrial structural integrity and impair of Ca^{2+} homeostasis.

1.4 Neutrophil Fc, CEACAM and Siglec receptors: phagocytosis and ROS pathways

Both immunoactivating and immunosuppressive receptors are involved in ROS generation in neutrophils. The immunoactivating receptors include the formyl peptide receptors (FPRs), Toll-like receptors (TLRs) (Botos et al., 2011), Triggering receptor expressed on myeloid cells-1 (TREM-1) (Bouchon et al., 2000), Fc receptors, and members of the carcinoembryonic antigen (CEA) family, a subset of the immunoglobulin (Ig) superfamily of proteins. The last two aforementioned receptors are of particular importance in oxidative burst and phagocytosis (Buntru et al., 2011).

Fc γ receptors (Fc γ Rs) are transmembrane proteins that bind to the Fc portion of IgG and are mainly involved in the recognition and phagocytosis of opsonized pathogens (i.e., when serum complement or immunoglobulins coat the bacteria) (García-García and Rosales, 2002, Bruhns, 2012). Three distinct pathways are generally activated during pathogen infections: the classical, the lectin and the alternative pathways, all of which converge with the formation of the complement component 3 (C3) convertase enzymes, which cleave the C3 producing the active complement component C3b. The binding of C3b molecules to the pathogen surface induces the phagocytic cells' recognition or stimulate cell lysis through the formation membrane-attack complex (Lubbers et al., 2017, Noris and Remuzzi, 2013). Thus, the complement system is an important component of the innate immune response having the potential to modulate the intracellular bacteria's fate, thus determining the outcome of infections (Merle et al., 2015).

CEACAM3 (CD66d) is only expressed in humans and exclusively in neutrophils and consists of a cytoplasmic domain encoding an immunoreceptor tyrosine-based activation motif (ITAM) (Bonsignore et al., 2019), resulting in kinases recruitment and downstream signaling, in a process very similar to the pathway activated by the ITAM-containing Fc receptors (Buntru et al., 2012). In both cases, Src family kinase (SFK)-dependent phosphorylation of tyrosine residues within the ITAM domain activate the protein tyrosine kinase, Syk (Sarantis and Gray-Owen, 2007). This leads to activation of class I PI3K, capable to initiate ROS production due to its phosphorylation of Akt and ERK, downstream of CEACAM-3 and Fc γ R activation (Kulkarni et al., 2011). Syk is also important for the RAC-GTPase-dependent assembly of polymerized actin into phagocytic cup-like structures that ultimately engulf bacteria (Schmitter et al., 2004). This occurs both in an opsonin-independent and opsonin-dependent manners for CEACAM-3 and Fc γ R, respectively.

Inhibitory receptors play key roles in regulating aspects of the immune response mainly by blocking activating pathways. These are usually composed of a cytoplasmic tail that contains at least one immunoreceptor tyrosine-based inhibitory motif (ITIM), as it is observed in some receptors of the CEACAM family and Siglecs (Pysz et al., 2006). CEACAM1 (also known as CD66a) is expressed by different cell type such as epithelial, endothelial, lymphoid, and myeloid cells (Prall et al., 1996). The receptor can recruit signaling molecules upon activation, including Src homology 2 (SH2)-domain-containing protein tyrosine phosphatases (SHP-1/2). It has been demonstrated that bacteria can exploit ITIM inhibitory function to suppress the immune response in T cells, B cells, dendritic cells and epithelial cells (Rowe et al., 2007, Boulton and Gray-Owen, 2002). Interestingly, interactions with CEACAM1 confers survival signals that prevent neutrophil apoptosis, which might allow the persistence of these cells at a site of infection (Singer et al., 2005).

Sialic acid-binding immunoglobulin-type lectins (Siglecs) are cell surface receptors belonging to the immunoglobulin (Ig) superfamily. In mammalian cells sialic acids (Sia) comprise a family of nine-carbon keto-sugars ubiquitous on mucous membranes as terminal modifications of mucin glycoproteins (Haines-Menges et al., 2015). Being the most prevalent monosaccharides at the host–pathogen interface (Prado Acosta and Lepenies, 2019), several pathogens display Sia on their surface to pretend to act as “self” and thereby eluding the host immune response (Chang and Nizet, 2014). The neutrophil inhibitory Siglecs (Siglec-5 and Siglec-9) contain an ITIM motif in their intracellular domain, conferring the ability to have an immunosuppressive role through the recruitment of the SHP phosphatases (Macauley et al., 2014). By engaging these inhibitory human neutrophils’ receptors, bacteria can impair oxidative burst and NET formation (Chang and Nizet, 2020), as it occurs for *P. aeruginosa* (Khatua et al., 2012). Interestingly, Siglec-14 with an activating ITAM-motif is nearly identical to Siglec-5 in its ligand-binding domain (Ali et al., 2014). Since neutrophils express both Siglec-14 and Siglec-5, there is the possibility that these function as paired Siglec receptors to balance immune responses in response to certain pathogens.

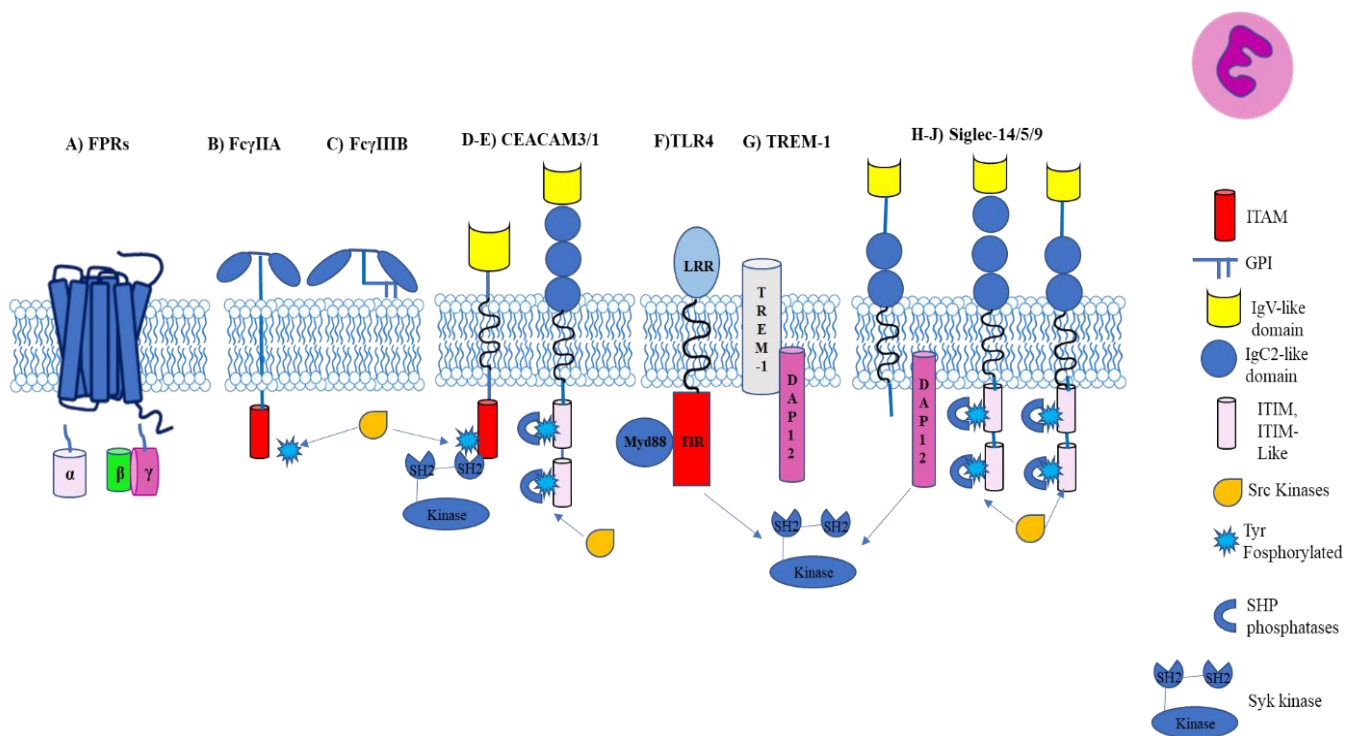


Figure 4. Main immunoactivating and immunosuppressive receptors present on neutrophils surface. The immunoactivating receptors include the formyl peptide receptors (FPRs), Toll like receptors (TLRs), Triggering receptor expressed on myeloid cells-1 (TREM-1), Fc receptors and member of the carcinoembryonic antigen (CEA) family. Sialic acid-binding immunoglobulin-type lectins (Siglecs) include the inhibitory Siglec-9 and Siglec-5 receptors and its counterpart activating Siglec-14.

1.5 Killing effects of ROS

The notion of oxidative stress has been proposed in biology only in 1985 when the chemical concepts of oxidation-reduction such as electron transfer, free radicals, oxygen metabolites were merged with a biological concept of stress, first developed in 1936 by Selye in his studies of adaptive responses (Sies, 2015, Sies, 2018). Four ROS can be spontaneously produced by consecutive reduction from O₂: Singlet oxygen (1O₂), superoxide anion (O₂⁻), hydrogen peroxide (H₂O₂), and hydroxyl radical (OH•) (Imlay, 2013). 1O₂ is the result of spin-orbit coupling by energy transfer, not by electron transfer, but its roles in bacteria have not been revealed. Once one electron moves to 1O₂, O₂⁻ is generated. In the presence of protons, superoxide dismutases (SODs) are the enzymes that catalyze the dismutation of O₂⁻ into O₂ and H₂O₂. H₂O₂ shows the highest stability of any other ROS, can cross the cell membranes and diffuses more readily (Kim et al., 2019). Importantly, a wide variety of detoxification systems have evolved for this molecule. For example, catalases are the enzymes that catalyze the dismutation of H₂O₂ into O₂ and H₂O, resulting in complete detoxification (Imlay, 2008). Moreover, H₂O₂ is highly reactive toward reduced forms of the transition metals Fe²⁺ or Cu⁺ generating OH•, a type of ROS with an extremely short half-life (10⁻⁹ sec) in solution at 37°C (Becker and Skaar, 2014). Its notoriety is due to the fact that no detoxification systems exist to neutralize its toxicity (Kim et al., 2019, Imlay, 2008).

ROS are involved in clearing infection and resolution of inflammation, limiting bacterial growth by damaging their protein, DNA, and lipid molecules (Sies et al., 2017).

Arginine, lysine, proline, and threonine can be carbonylated (Nystrom, 2005), histidine can be modified to oxo-histidine (Traore et al., 2009), and cysteine and methionine residues are particularly sensitive to oxidation due to their electron-rich sulfur atom in their side chain (Ezraty et al., 2017). All these reactions can have deleterious effects on proteins functions, especially in iron-sulphur dehydratases and mononuclear iron proteins (Imlay, 2008). Oxidation of DNA bases can produce several damaging byproducts. Due to lower reduction potential, electrons of guanine bases can easily jump to electron holes in adjacent oxidized base radicals (Imlay, 2013). The resulting 8-hydroxyguanine is highly mutagenic due to its ability to frequently mismatch with adenine (Hogg et al., 2005). Additionally, ribose oxidation by ROS can induce strand breaks in bacterial DNA (Imlay, 2008). Lipid peroxidation is a universal outcome of oxidative stress in eukaryotic systems, but this seems less likely in most bacteria as their lipids are not polyunsaturated (Imlay, 2013). An exception to this rule is provided by that *Borrelia burgdorferi*, an intracellular pathogen that can incorporate

polyunsaturated fatty acids from the eukaryotic host, thereby being quite susceptible to ROS (Boylan et al., 2008).

Bacteria have developed several strategies to counteract killing by ROS, including i) detoxification of these radical species into less damaging byproducts, ii) metal homeostasis and iii) DNA damage repair systems. These three ROS tolerance systems have been shown to be quite conserved in most bacterial species (Imlay, 2013) and they can be classified as “intrinsic” resistance mechanisms. Regarding radical species detoxification, in many Gram-negative bacteria, OxyR is a master regulator that senses the intracellular level H_2O_2 through oxidation of its conserved “sensing” Cys residue to a sulfenic acid (-SOH) that can then react with a second Cys, resulting in conformational changes. As a result, OxyR can function both as a transcriptional activator and repressor (Chiang and Schellhorn, 2012) (Jo et al., 2015). OxyR regulon includes primarily antioxidant defense mechanisms such as those involved in H_2O_2 detoxification (glutaredoxin, thioredoxin, catalases, and peroxiredoxin protein families), heme biosynthesis, Fe-S cluster assembly (Isc and Suf operons), DNA protection and metal uptake (Imlay, 2008) (Imlay, 2015). In the context of metal homeostasis, vertebrate hosts withhold metals to curtail bacterial proliferation but at the same time, the toxicity of metals is exploited to directly poison intracellular bacteria. These are referred to as nutritional immunity (Becker and Skaar, 2014) and this aspect is discussed in more detail in section 1.7. Base excision repair (BER) and SOS response pathways, which induces the UvrABC excision nuclease and the Rec recombinational machinery, are fundamental to coping with DNA damages (Asad et al., 2000). Not specific for a particular lesion, DNA glycosylases endonuclease IV and VIII scan for helical distortions removing any disparate adducted bases that can be generated by oxidation (Mullins et al., 2019). Post-replication recombination is the back-up strategy when the excision systems do not recognize these lesions (Sun et al., 2020).

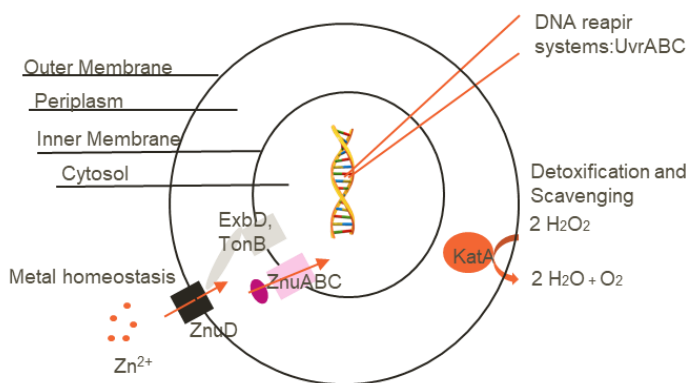
Additionally, few bacterial pathogens employ “extrinsic” resistance mechanisms to directly suppress ROS production in eukaryotic cells (Nguyen et al., 2017) as in the case of *P. aeruginosa* and *Chlamydia trachomatis* through a contact-dependent mechanism and the expression of extracellular effector, respectively (Vareechon et al., 2017, Rajeeve et al., 2018). *P. aeruginosa* has a type III secretion system (T3SS), a molecular syringe that can directly introduce effector proteins into the host cells cytoplasm (Williams McMackin et al., 2019). Among them, ExoS and ExoT ADP-ribosylate Ras preventing neutrophils-mediated clearance. ADP-ribosylated Ras can no longer bind to PI3K, thus interfering with ROS production (Sun et al., 2004). *C. trachomatis*, an obligate intracellular human pathogen associated with sexually transmitted diseases (Ljubin-Sternak and Mestrovic, 2014), impairs ROS generation by the secreted protease-like activating factor (CPAF) that is responsible for the cleavage of the immunoactivating FPR2 receptor (Rajeeve et al., 2018). Other

bacteria, such as *Franciscella tularensis* and *N. gonorrhoeae* (not expressing Opa proteins), essentially disrupt NADH oxidase activity by not fully elucidated mechanisms (McCaffrey et al., 2010, Smirnov et al., 2014).

A

Intrinsic mechanisms

1. Detoxification and Scavenging
2. Metal Homeostasis
3. DNA Damage Repair



B

Extrinsic Mechanisms

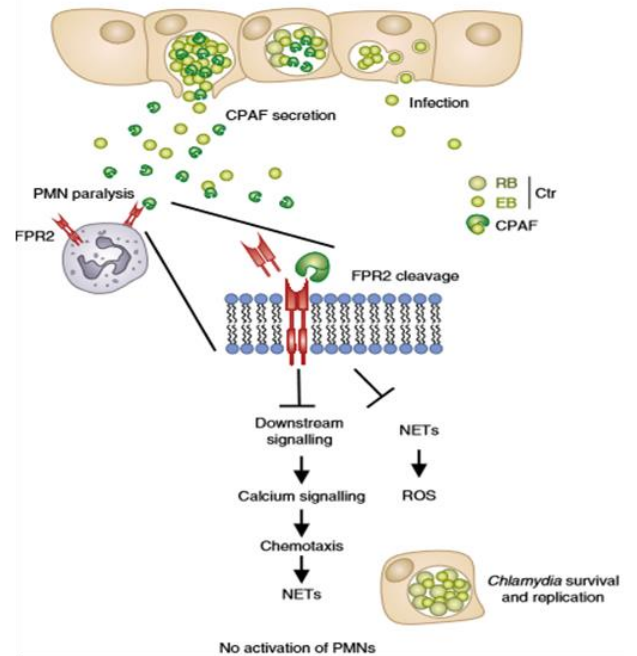


Figure 5. Strategies mounted by bacteria to tackle the oxidative stress. A) Intrinsic mechanisms include: scavenging enzymes, metal homeostasis and DNA repair systems. **B)** Extrinsic mechanisms refer to the ability to actively interfere with eukaryotic ROS production, as in the case of *Chlamydia trachomatis*. This bacterium dampens ROS generation by secreted protease-like activating factor (CPAF), which is responsible for the cleavage of FPR2. Image reproduced by courtesy of *Nature Microbiology* (2018) (Rajeeve et al., 2018).

1.6 ROS-related antimicrobial weapons: NET and autophagy

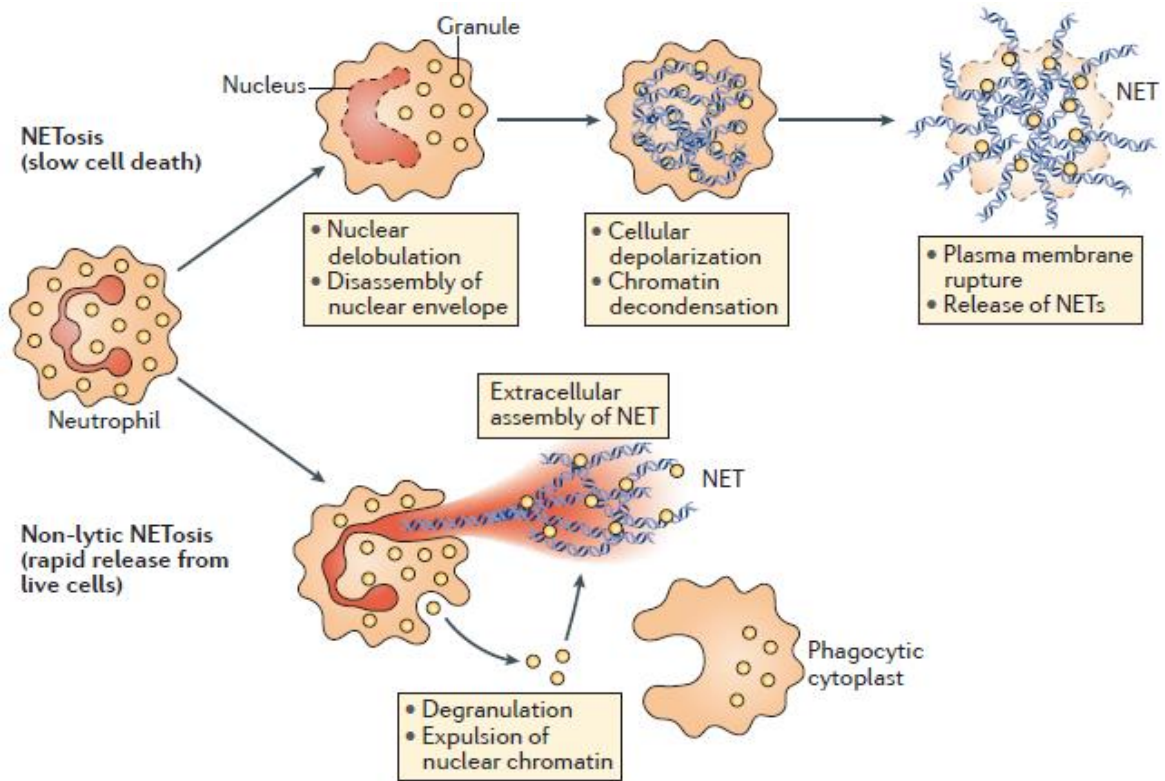
Neutrophil extracellular traps (NETs) are major contributors to chronic inflammation and lung tissue damage in COPD (Grabcanovic-Musija et al., 2015, Twaddell et al., 2019). NETs are related to ROS release and represent a pathway of cellular death that is different from apoptosis and necrosis (Fuchs et al., 2007). NETs are extracellular web-like structures composed of a backbone of histones and extracellular DNA (eDNA) fibers decorated with antimicrobial proteins such as myeloperoxidase (MPO) and neutrophil elastase (NE) (Pires et al., 2016). NETs generation, or NETosis, follows these sequential steps: 1) a proper stimulus activates Raf/MEK/ERK kinases pathway and increases calcium concentration leading to the phosphorylation of gp91phox subunit, responsible for NADPH complex activation (Hakkim et al., 2011). 2) The consequent ROS generation stimulates MPO that,

in turn, triggers the activation of NE. 3) NE degrades F-actin filaments (cytoskeleton) and translocates from azurophilic granules to the nucleus (Metzler et al., 2014), where it proteolytically processes histones interfering with chromatin packaging (Papayannopoulos et al., 2010). 4) Chromatin decondensation is also promoted by MPO and protein-arginine deiminase type 4 (PAD4), a nuclear enzyme that promotes the citrullination of histones (Rohrbach et al., 2012). Citrullination converts positively charged arginine residues into non-charged citrulline residues, making the overall charge of histones less positive. This conversion results in a lower affinity for the negatively charged DNA, stimulating chromatin decondensation (Leshner et al., 2012). 5) Subsequently, the integrity of the nuclear membrane is lost, and the decondensed chromatin becomes associated with antimicrobial peptides (AMP). 6) After the damage of the plasmatic membrane, DNA is released out of the cell as extracellular traps. NETs trap, neutralize and kill bacteria, and by preventing bacterial dissemination, these structures concentrate the antimicrobial efforts at sites of infection (Delgado-Rizo et al., 2017). Bacteria with mutations in NET-degrading nucleases (Juneau et al., 2015) or in capsule genes (Wartha et al., 2007) are impaired in their ability to disseminate, increasing their NET trapping *in vitro* (Papayannopoulos, 2018). Surprisingly, bacteria may even use NETs to their advantage. The pore-forming toxin leukotoxin GH of *S. aureus* is sufficient to drive NETosis (Malachowa et al., 2013), exploited to provoke macrophage killing around abscesses (Thammavongsa et al., 2013). Similar to this bacterium, *S. pneumoniae* can produce a nuclease named EndA that enables this bacterium to survive within NETs and disseminate from the upper respiratory tract to the lungs (Beiter et al., 2006). *N. gonorrhoeae* interferes with the phagosome-azurophilic granules fusion and promotes NETosis (Johnson and Criss, 2013). Finally, mutants of *Porphyromonas gingivalis* for phagocytosis-promoting protease induce NETosis (Jayaprakash et al., 2015), suggesting the ability of phagocytosis to modulate NETosis. In addition, microorganisms attenuate NETosis by engaging host receptors that suppress neutrophil activation such as Sialic acid-binding immunoglobulin-type lectins (Siglecs) (Schwarz et al., 2015). By engaging the inhibitory Siglec-9 and Siglec-5 human neutrophils' receptors, bacteria such as group B *Streptococcus* and *P. aeruginosa* can impair oxidative burst and NET formation (Carlin et al., 2009) (Khatua et al., 2012).

In all cell types, autophagy is a process that maintains cellular homeostatic functions leading to the degradation of the sequestered cargos, such as damaged organelles and misfolded proteins, recycling them for anabolic processes (Yoshimori, 2004). Although the Greek words (*auto* and *phagein* stand for 'self' and 'to eat', respectively) suggest the role in cell homeostasis, in professional phagocytes, autophagy is also involved in the capture of invading bacteria, a process referred to as xenophagy (Levine and Kroemer, 2008, Jo et al., 2013). By controlling bacterial replication,

autophagy plays an important role in activating the innate and adaptive immunity (Lamark et al., 2009). With respect to the latter, autophagy is involved in delivering certain microbial antigens to the major histocompatibility complex MHC class II antigen-presenting molecules, leading to the activation of CD4⁺ T lymphocytes (Levine and Deretic, 2007). Five phases can be identified in the autophagic process: induction, elongation, maturation, transport to lysosomes, and degradation (Tooze and Dikic, 2016, Choi et al., 2013). 1) The signal induction (e.g., after ROS release (Dan Dunn et al., 2015)) is regulated by the serine threonine kinases AMPK (AMP-activated kinase) and mTOR (mammalian target of rapamycin complex 1). Autophagic adaptors including sequestosome 1 (SQSTM1/p62), nuclear dot protein 52 kDa (NDP52), optineurin (OPTN), and neighbor of *BRCA1* gene 1 (NBR1) are receptors functioning for the selective targeting of substrates to the autophagy-related family of proteins (Lamark et al., 2009). 2 and 3) The nucleation of a cup-shaped structure called phagophore which then progressively elongates to form a double-membrane vesicles called autophagosomes, is the hallmark of this pathway (Levine and Kroemer, 2008). Autophagosomes are formed at mitochondria-associated endoplasmic reticulum (ER) membranes (MAMs), membranous structures at the interface of ER-mitochondria, pivotal for processes such as mitochondrial morphology, autophagosome formation, inflammasome activation and apoptosis (Escoll et al., 2017). Two ubiquitin-like conjugation systems are essential for these phases: the autophagy related protein 5 (ATG5) and the microtubule-associated protein light chain 3 (LC3) (Riebisch et al., 2021). 4 and 5) In the last two steps, autophagosomes fused with lysosomes allowing the content to be degraded and recycled (Escoll et al., 2016). Throughout the autophagic pathway, including the recognition of cargoes, autophagosomes formation and the fusion of these structures with lysosomes, LC3 plays a fundamental role and the increased lipidated form (called LC3-II) is a molecular autophagic marker (Deretic et al., 2013). Numerous medically important pathogens, including *Salmonella enterica*, are degraded by xenophagy (Wild et al., 2011). Nevertheless, successful intracellular pathogens may antagonize both the signaling pathways that activate autophagy as well as the membrane trafficking events required for lysosomal delivery and degradation, as in the case of *Mycobacterium tuberculosis* (Gutierrez et al., 2004) (Padhi et al., 2019). In the case of *Legionella pneumophila*, a secreted effector called LpSPL mimics the functions of its eukaryotic counterpart sphingosine-1-phosphate lyase (SPL), modulating sphingolipid levels thereby limiting autophagosome formation at MAMs and thus the host autophagic response (Rolando et al., 2016).

A



B

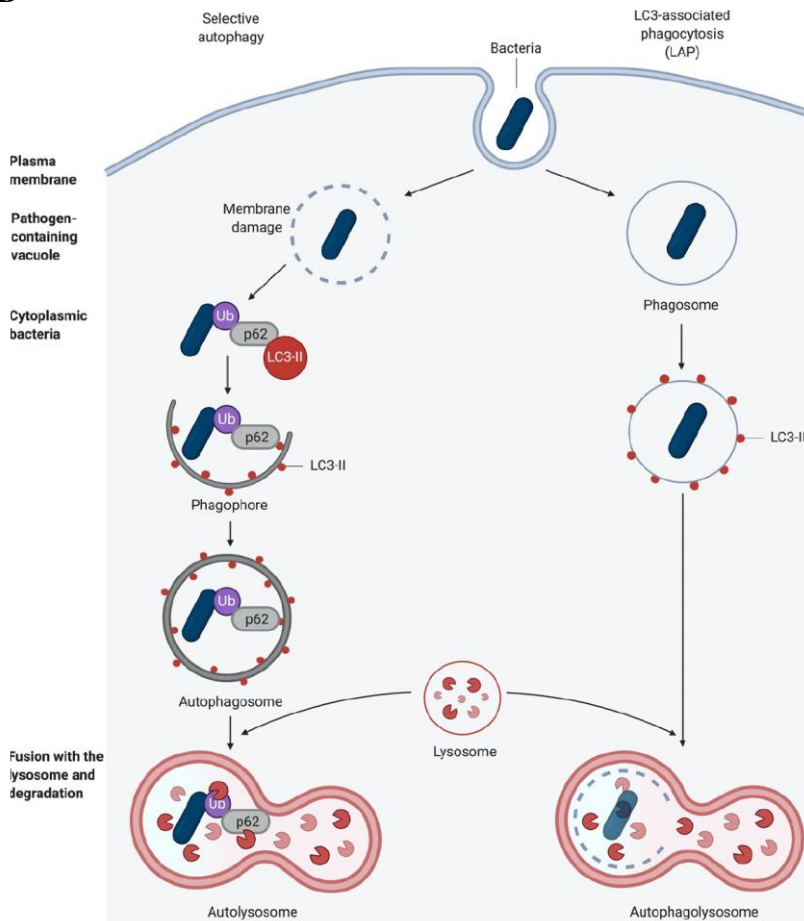


Figure 6. NET formation pathways and autophagic elimination of invading bacteria.

A) Neutrophil extracellular traps (NETs) formation occurs via two pathways: a cell death pathway termed NETosis which is accompanied by the morphological changes here reported and a non-lytic form of NETosis that involves the secreted expulsion of nuclear chromatin and degranulation. The resulting anucleated cytoplasts keep ingesting microorganisms. Image reproduced by the courtesy of *Nature Review* (2018) (Papayannopoulos, 2018). **B)** Internalized bacteria, either cytoplasmic or within phagosomes, can be eliminated through autophagy. After sequestration, the double membrane vesicle autophagosome fuses with a lysosome to

form an autophagolysosome. Bacteria capable of escaping the phagosome are polyubiquitinated and thus susceptible of recognition by autophagy receptor proteins. These bacteria are then directly delivered to the phagophores (left panel).

Bacteria entrapped within the phagosomes are degraded via LC3-associated phagocytosis (right panel). Image reproduced by the courtesy of *Pathogens* (2021) (Riebisch et al., 2021).

1.7 Role of Copper in the oxidative stress response

Regarding metal homeostasis, the six 3d-block transition metals manganese (Mn), iron (Fe), cobalt (Co), nickel (Ni), copper (Cu), and zinc (Zn) are essential micronutrients to both hosts and bacterial pathogens. Still, at the same time, they also represent an important antimicrobial weapon for phagocytic cells (Diaz-Ochoa et al., 2014, Sheldon and Skaar, 2019). Among them, copper appears to play a unique role in the context of nutritional immunity. The concept that Cu is fundamental in controlling infections is not so unexpected since humans with a deficiency related to this metal, called Menkes disease, present higher incidences of infections, especially in the lung (Tumer and Moller, 2010, Jomova and Valko, 2011). In phagocytic cells, CTR1 is a high-affinity copper importer located on the plasma membrane mediating Cu influx into the cell while ATP7a is P-type ATPase, localized in the trans-Golgi network, transporting Cu into the phagolysosome to kill engulfed bacteria (White et al., 2009). The antimicrobial activities of Cu are multifaceted. Due to the high redox potential, Cu catalyzes hydroxyl radicals production via the Fenton and Haber-Weiss reactions (Ladomersky and Petris, 2015), in which copper (I) is oxidized in the presence of hydrogen peroxide, producing copper (II) + $\cdot\text{OH}$ + OH^- . Bacterial cellular macromolecules, including proteins, lipids, and DNA can irreversibly be damaged by the resulting free radicals (Letelier et al., 2010). Another mechanism of Cu toxicity includes the targeting of solvent-exposed [Fe-S] cluster enzymes (Besold et al., 2016) and the outcompetition of all other transition metals from key biosynthetic enzymes (mismetallation) with the consequent loss of protein functions (as described by the Irving-Williams series, Cu is a highly competitive metal for protein binding) (German et al., 2016). Indeed, when Cu displaces Fe, the released Fe atoms may further induce ROS generation (Sheldon and Skaar, 2019). To cope with this harmful effects, the transcriptional regulator Fur helps in suppressing loose-iron levels (Varghese et al., 2007) and importers of manganese ions are important as this transition metal can supplant iron in mononuclear enzymes (Anjem et al., 2009).. Mechanisms of copper tolerance in bacteria are quite functionally conserved underlying the importance of copper homeostasis for bacterial virulence (Besold et al., 2016, Samanovic et al., 2012, Ladomersky and Petris, 2015). These strategies include Cu export systems from the cytoplasm into the periplasm or extracellular environment, sequestration by metallothioneins and multicopper oxidases that convert Cu(I) into Cu(II) ion that is less toxic (Fu et al., 2014). Inactivation of copper exporter genes has been shown *in vivo* to reduce the virulence of bacterial pathogens such as *Mycobacterium tuberculosis* (Shi et al., 2014), *S. pneumoniae* (Johnson

et al., 2015a) and *P. aeruginosa* (Schwan et al., 2005). Therefore, these notions highlight that copper plays a key role in the antimicrobial weaponry of the innate immunity to curtail bacterial infections.

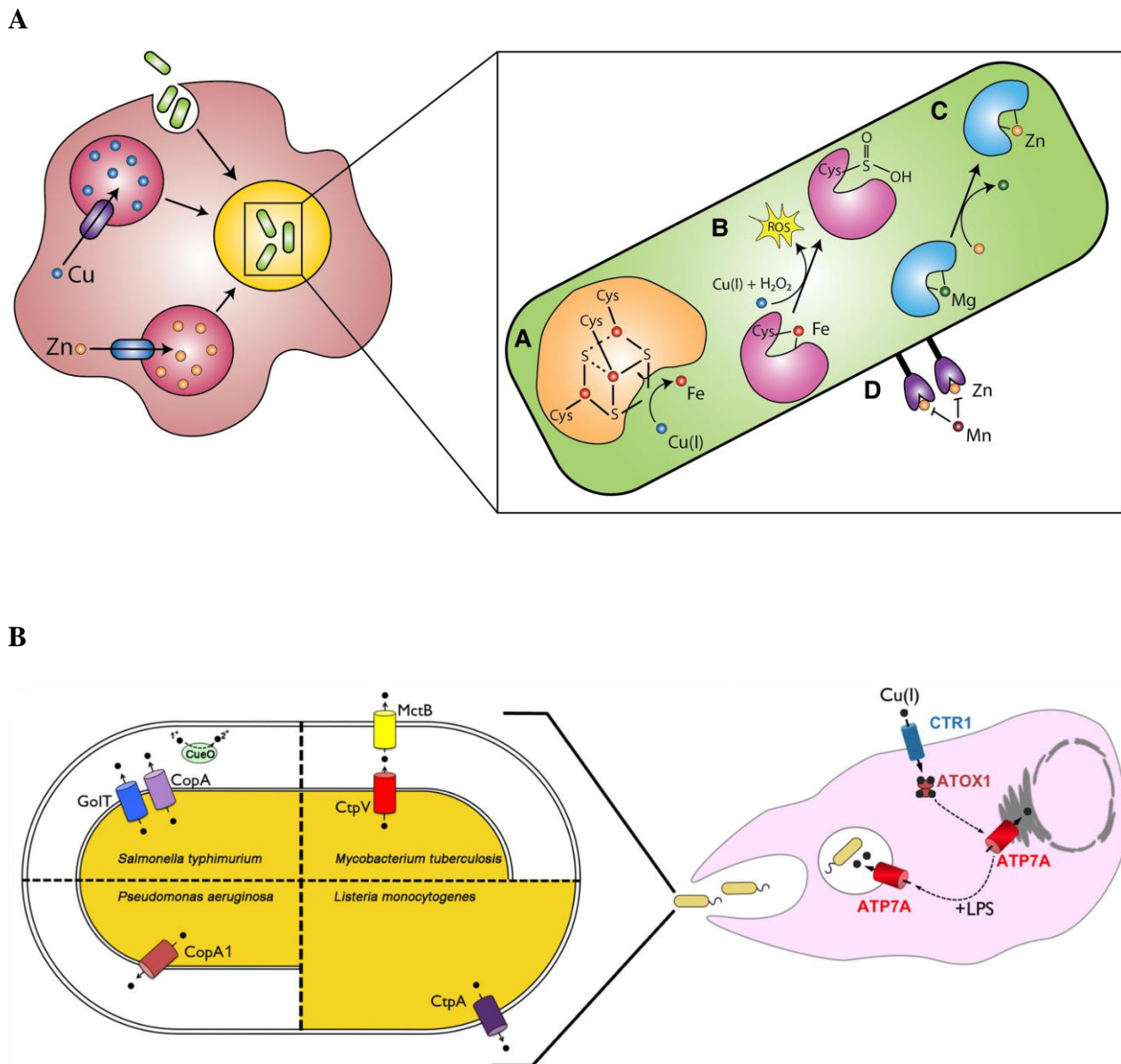


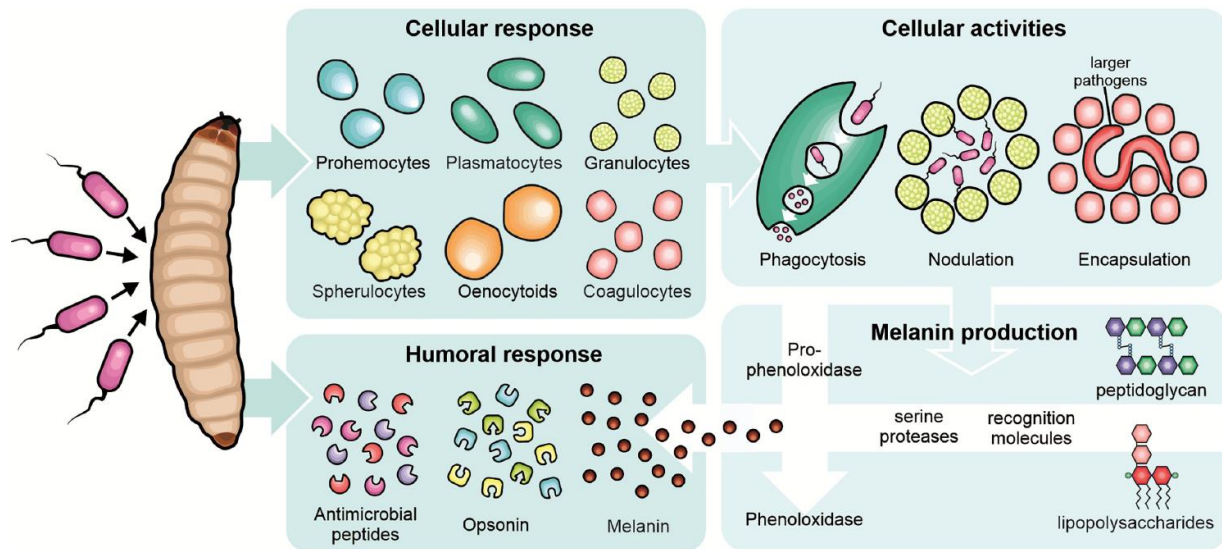
Figure 7. Role of Copper in the oxidative stress response. Via the Fenton and Haber-Weiss reactions, copper catalyzes the production of hydroxyl radicals. **A)** The metal intoxication mechanisms include (a) replacement of Fe with Cu(I) in Fe–S clusters of cellular proteins; (b) ROS generation leading to oxidation of Fe-coordinating cysteine residues with the consequent loss of function; (c) mismetallation, inactivation of cellular proteins via adventitious binding by competitive, non-cognate metals such as Zn.; (d) Cellular Mn starvation. Image reproduced by the courtesy of *Biochemical Society Transactions* (2019) (Begg, 2019). **B)** On the left, mechanisms of copper tolerance in bacteria. On the right, inflammatory agents such as bacterial lipopolysaccharide promote the expression of the CTR1 copper importer, which mediates copper influx across the plasma membrane. This metal is then delivered to the ATP7A copper pump in the trans-Golgi network by the chaperone ATOX. ATP7A is then partially relocated from the Golgi to phagolysosomes, filling this compartment with bactericidal copper. Image reproduced by the courtesy of *Metallomics* (2016) (Ladomersky and Petris, 2015).

1.8 *Galleria mellonella* as a valuable in vivo model for bacterial infections

Although insects have diverged from vertebrates approximately 500 million years ago and lack an adaptive immune response, their innate immune response still retains remarkable similarities with the human one (Browne et al., 2013). The most frequently used alternative animal models are *Drosophila melanogaster*, *Danio rerio* (zebrafish), *Caenorhabditis elegans* (roundworm) and *Galleria mellonella* (greater wax moth or honeycomb moth). As demonstrated by the increased number of published articles, this latter alternative model is gaining popularity in the scientific community. *G. mellonella* is a member of the Pyralidae family of the Lepidopteran order that naturally infests beehives. Four distinct life stages exist: egg, larva, pupa, and adult (Killiny, 2018). The insect *larvae* have increasingly been used as a surrogate to study microbial infection in a range of microorganisms including Gram-positive and Gram-negative bacteria and fungi (Cook and McArthur, 2013, Firacative et al., 2020), and as a rapid model to screen novel antimicrobial drug candidates (Cutuli et al., 2019). From a practical consideration, *G. mellonella larvae* are low-cost to establish and easy to manipulate due to their large size (2–3 cm long and 0.3 to 0.5 g) and no special lab equipment is required. Additionally, their use is ethically more acceptable than that of vertebrates and their short life cycle (7-8 weeks) makes them ideal for screening studies. Unlike other invertebrate models such as *C. elegans* and *D. melanogaster*, *G. mellonella larvae* can survive at 37 °C, equivalent to the mammalian body temperature, allowing the study of temperature-dependent virulence factors (Pereira et al., 2020). The immune response of *G. mellonella* consists of two components: cellular and humoral responses. The cellular response is mediated by phagocytic cells, termed hemocytes, present in the hemolymph, which is analogous to mammalian blood. Hemocytes are involved in the nodulation, phagocytosis and encapsulation (for larger microbes, such as nematode and protozoa) of invading agents. Phagocytosis in insects and mammals is believed to be very similar. Once phagocytosed, pathogens are killed mainly by the oxidative burst, which is promoted by the NADPH oxidase complex. Indeed, homologous proteins p47 and p67 were identified in *G. mellonella* hemocytes, and it was shown that Phorbol 12-Myristate 13-Acetate (PMA) can trigger superoxide production, as in the case of human neutrophils. The humoral response involves soluble effector molecules such as ROS, AMPs, complement-like proteins (opsonins), melanin and products of proteolytic cascades. The melanization is an essential process for the defense against microbial pathogens. Typically, melanization begins with black spots on the larval surface and, as the infection progresses, the *larva* becomes completely black and thus dies (Killiny, 2018, Firacative et al., 2020, Cutuli et al., 2019, Tsai et al., 2016). To conclude, wax worms are used extensively as an alternative infection model for the study bacterial pathogens such as *S. pneumoniae* (Cools et al., 2018), *P.*

aeruginosa (Jeon and Yong, 2019), *Mycobacterium strains* (Li et al., 2018) and *S. aureus* (Li et al., 2020), shedding light on the virulence mechanisms and new therapies for important pathogenic bacteria.

A



B

Table 2. The *G. mellonella* Health Index Scoring System.⁴⁹

Category	Description	Score
activity	no movement	0
	minimal movement on stimulation	1
	move when stimulated	2
	move without stimulation	3
cocoon formation	no cocoon	0
	partial cocoon	0.5
	full cocoon	1
melanization	black larvae	0
	black spots on brown larvae	1
	≥3 spots on beige larvae	2
	<3 spots on beige larvae	3
	no melanization	4
survival	dead	0
	alive	2

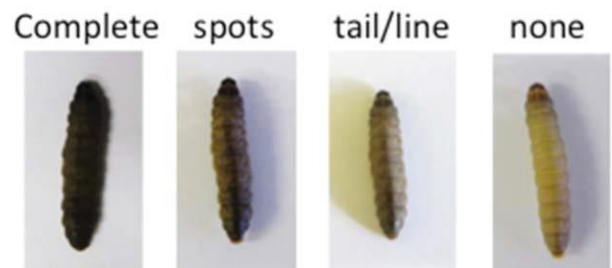


Figure 8. *Galleria mellonella* as an infection model. **A)** *G. mellonella* immune system is composed by components of a cellular response and a humoral response. The cellular response comprehends six types of cells. Among them, plasmatocytes, granulocytes and coagulocytes are involved in the clearance of invading agents by phagocytosis, nodulation and encapsulation, respectively. Molecular patterns associated to pathogens can trigger the phenoloxidase pathway, to produce melanin. Melanin, along with antimicrobial peptides and opsonins, is one of the components of the humoral response. Image reproduced by the courtesy of *Pathogens and Disease*, 78, (2020) (Pereira et al., 2020). **B)** According to the Health Index Score, larvae are considered for their 1) survival (dead or alive), 2) cocoon formation, 3) movement (no movement at all, or inability to right themselves, movement that is minimal or upon stimulation e.g., shaking of the petri dish or touching with a pipette tip) and 4) melanization (how is different from the healthy creamy color: > 0 < 3 spot on beige larvae, or spots in brown larvae and black larvae). Image reproduced by the courtesy of *Virulence*, (2016) (Tsai et al., 2016).

2. AIM

The first objective of this thesis was to investigate how Mcat and NTHi cope with the antimicrobial arsenal mounted by neutrophilic cells by using both primary cells and the HL-60 cell line (extrinsic resistance mechanisms). To this purpose, a number of responses were considered: adhesion and invasion, ROS evaluation, NETs and the autophagic response, survival of internalized bacteria and bacterial interplays in co-infections.

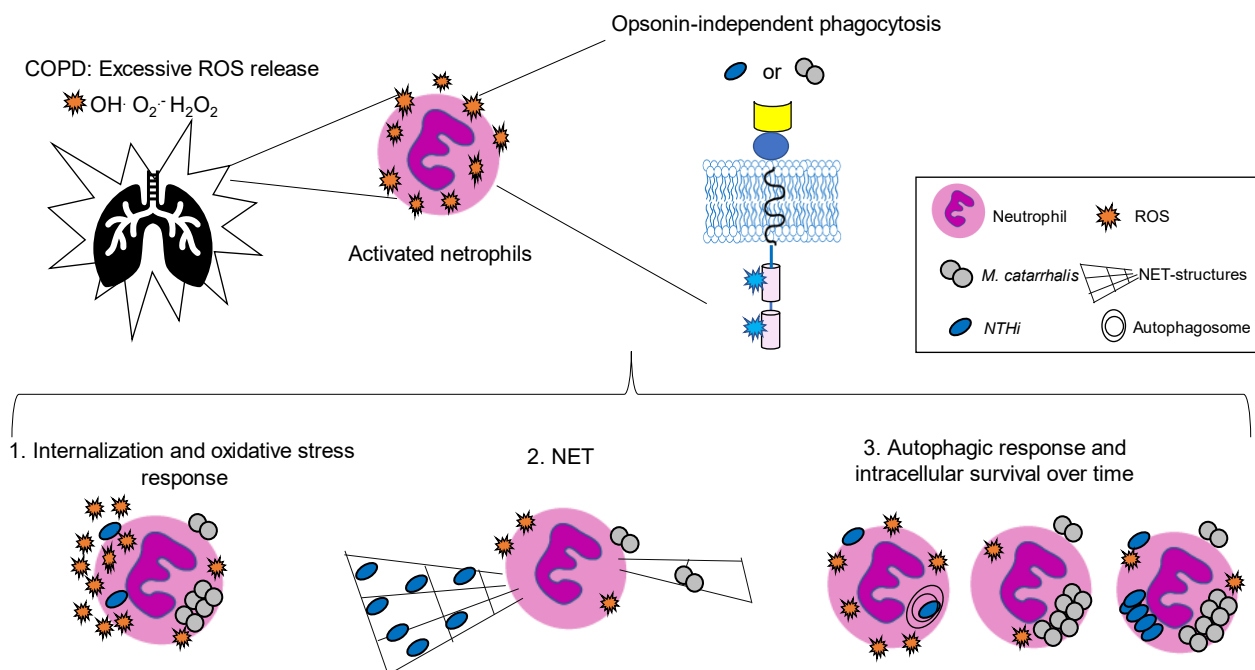
The second aim of the research in this thesis was to expand the knowledge of Mcat intrinsic resistance to exogenous oxidative stress. Therefore, RNA-Seq of exponentially growing Mcat exposed to sublethal amounts of H₂O₂ or CuSO₄ was performed thus, providing a comprehensive picture of Mcat global transcriptional response to stimuli that mimic *in vitro* the oxidative stress. A subset of genes was functionally characterized in terms of sensitivity to H₂O₂, survival in both ROS-induced neutrophil-like cells and, for the first time in Mcat, in *G. mellonella in vivo* model.

Therefore, the thesis aimed to explore the strategies that Mcat exploits to tackle the antimicrobial arsenal mounted by neutrophilic cells shedding light on its interplay with NTHi and to provide a comprehensive picture of the Mcat global transcriptional response to stimuli that mimic *in vitro* the oxidative stress.

3. BACKGROUND 1ST PART AND GRAPHICAL ABSTRACT

The first objective of this thesis was to investigate a number of responses such as adhesion and invasion, ROS evaluation, NETs and the autophagic response and survival of internalized Mcat and NTHi bacteria in neutrophils. In our study, we used exponentially-growing *M. catarrhalis* BBH18 (de Vries et al., 2010) and NTHi 658 (Mayhew et al., 2018) clinical isolates derived from COPD patients, to challenge human HL-60 cell line, differentiated into neutrophil-like cells (dHL-60) or primary cells. We demonstrated that, differently from NTHi, *M. catarrhalis* is able to dampen the host's innate immune response by directly interfering with ROS production and ROS-related responses. The underlying mechanisms are shown to be phagocytosis and opsonins-independent but contact-dependent, probably due to the engagement of the immunosuppressive receptors, CEACAM-1 and Sialic acid-binding immunoglobulin-type lectins (Siglec-5 and Siglec-9). In addition to the well-known interaction between the eukaryotic CEACAM-1 receptor and Mcat UspA1, we showed that Mcat is able to engage Siglec-5 and Siglec-9 receptors through its porin OmpCD. Furthermore, under co-infection experiments, NTHi intracellular survival is greatly enhanced by the presence of Mcat, which provides a less hostile environment for NTHi in the host cells.

GRAPHICAL ABSTRACT



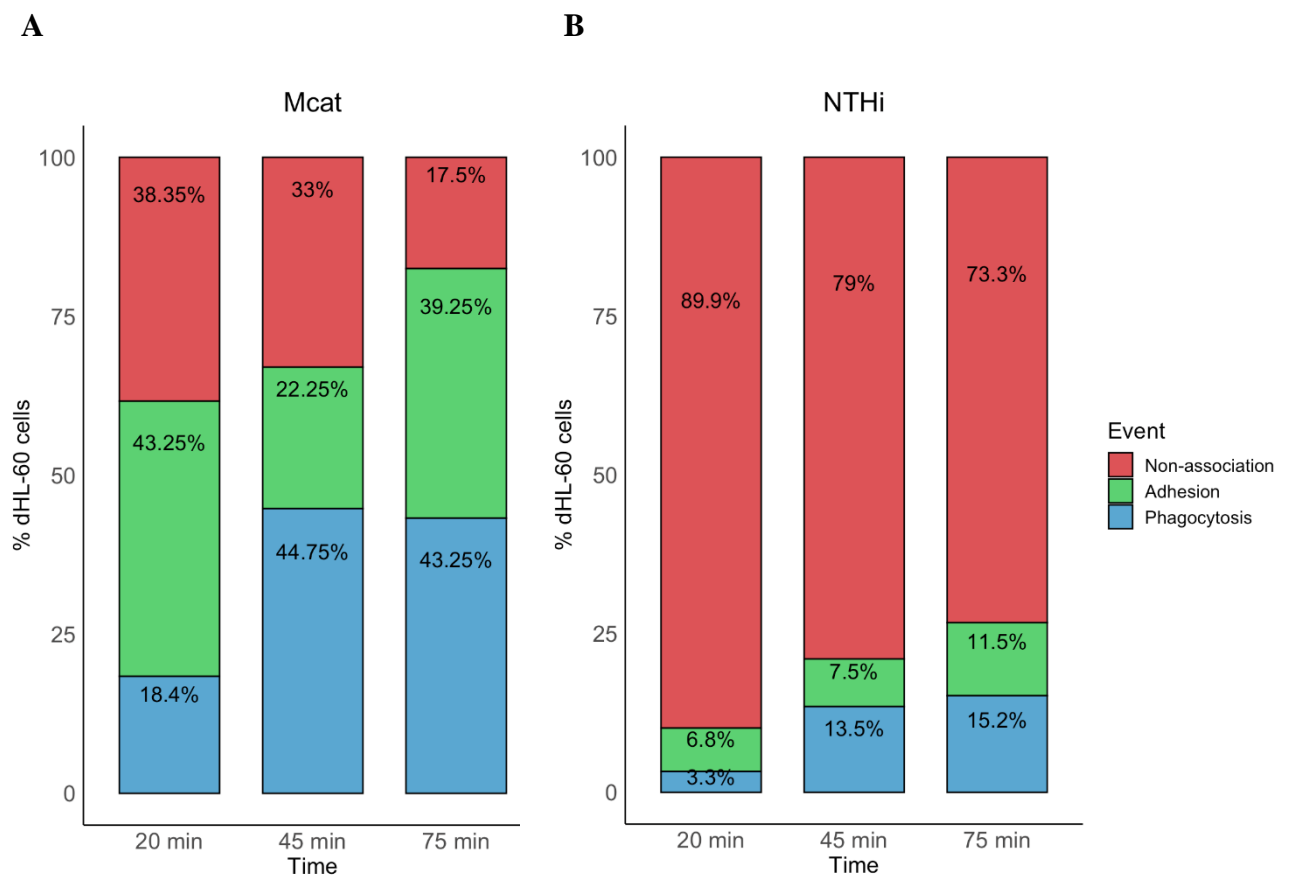
4. RESULTS 1st part

4.1 *M. catarrhalis* and NTHi: two different ways to interact with neutrophil-like cells

We first evaluated the interactions and the opsonin-independent uptake of *M. catarrhalis* and NTHi with differentiated neutrophil-like cells (dHL-60), chemically activated *in vitro* by treatment with Phorbol 12-Myristate 13-Acetate (PMA), known to elicit a strong oxidative burst. Activated dHL-60 cells were left untreated or treated with cytochalasin D, a known inhibitor of phagocytosis, and infected with exponentially-growing, unopsonized Mcat or NTHi (multiplicity of infection, MOI=50). After an incubation of 20-, 45- and 75 minutes at 37°C, samples were fixed, permeabilized, and then stained with bacteria-specific polyclonal anti-sera. By flow cytometry, we measured the percentage of infected cells (cytochalasin D-untreated samples: cells with adherent and internalized bacteria) or the percentage of cells with adherent bacteria (cytochalasin D-treated samples: adhesion only). From the total interaction (cytochalasin D-untreated samples), we subtracted the percentage of adhesion (cytochalasin D-treated samples), (Figures 9A and B, green bars) to calculate the percentage of cells with phagocytosed bacteria (Figures 9A and B, light blue bars). The resulting percentage of uninfected cells is reported as red bars (Figures 9A and B). As shown in Figure 9A, *M. catarrhalis* was readily internalized into dHL-60 cells as the percentage of cells with internalized bacteria was 18,4% at the earliest time point. The percentage of infected activated neutrophil-like cells increased over time with the percentage of host cells with internalized bacteria ranging from 18.3% to 43.25%, and those of uninfected cells from 38.3% to 17.5%, at 20 and 75 minutes, respectively. Unlike Mcat, during NTHi infection, the percentage of non-infected cells passed from 90% to 73.3% at 20 and 75 minutes, respectively. Indeed, only 3.3% of cells with internalized NTHi was recorded at 20 min post-infection (Figure 9B). This percentage slightly increased to 15.2% at 75 min post-infection indicating a lower kinetic of internalization compared to that of *M. catarrhalis*. For both bacteria, while a strong increase in the percentages of cells with phagocytosed bacteria at 45 min compared to 20 min was recorded, no differences were observed between 45- and 75 minutes post-infection.

These bacterial adhesion and invasion phenomena on PMA-activated dHL60 cells were visualized by transmission electron microscopy. Representative images of electron microscopy cross sections of uninfected cells (control) and cells infected by unopsonized Mcat or NTHi at MOI of 50 for 20- and 75 minutes are reported in Figure 9C. At 20 minutes post-infection, grape-like aggregates of *M. catarrhalis* were present on the cell surface which exhibited membrane protrusions (or lamellipodia) at the site of bacterial contact (black arrow). Interestingly, at this earliest time point, bacteria were found not only in the early stages of phagocytosis but also in later ones, as indicated by

the presence of bacteria surrounded by electrodense materials (phagolysosomes, white arrow). At 75 minutes, PMA-activated dHL-60 cells were packed with an increased number of *M. catarrhalis* bacterial cells while showing intact mitochondria and heterochromatin condensation of nuclei. Unlike Mcat, a small portion of the dHL-60 cells were found to be infected by NTHi and few bacterial cells were found to be phagocytosed both at 20- and 75 minutes post-infection. Moreover, regardless of the presence of a small number of phagocytosed bacteria, more prominent events of apoptosis such as extensive cytoplasmic vacuolization were observed. These observations suggest that unopsonized *M. catarrhalis* is rapidly phagocytosed into neutrophil-like cells and accumulates intracellularly over time interfering with the cell attempts to clear the pathogen. Conversely, a low amount of NTHi bacterial cells remains intracellularly, strongly affecting the host cell viability.



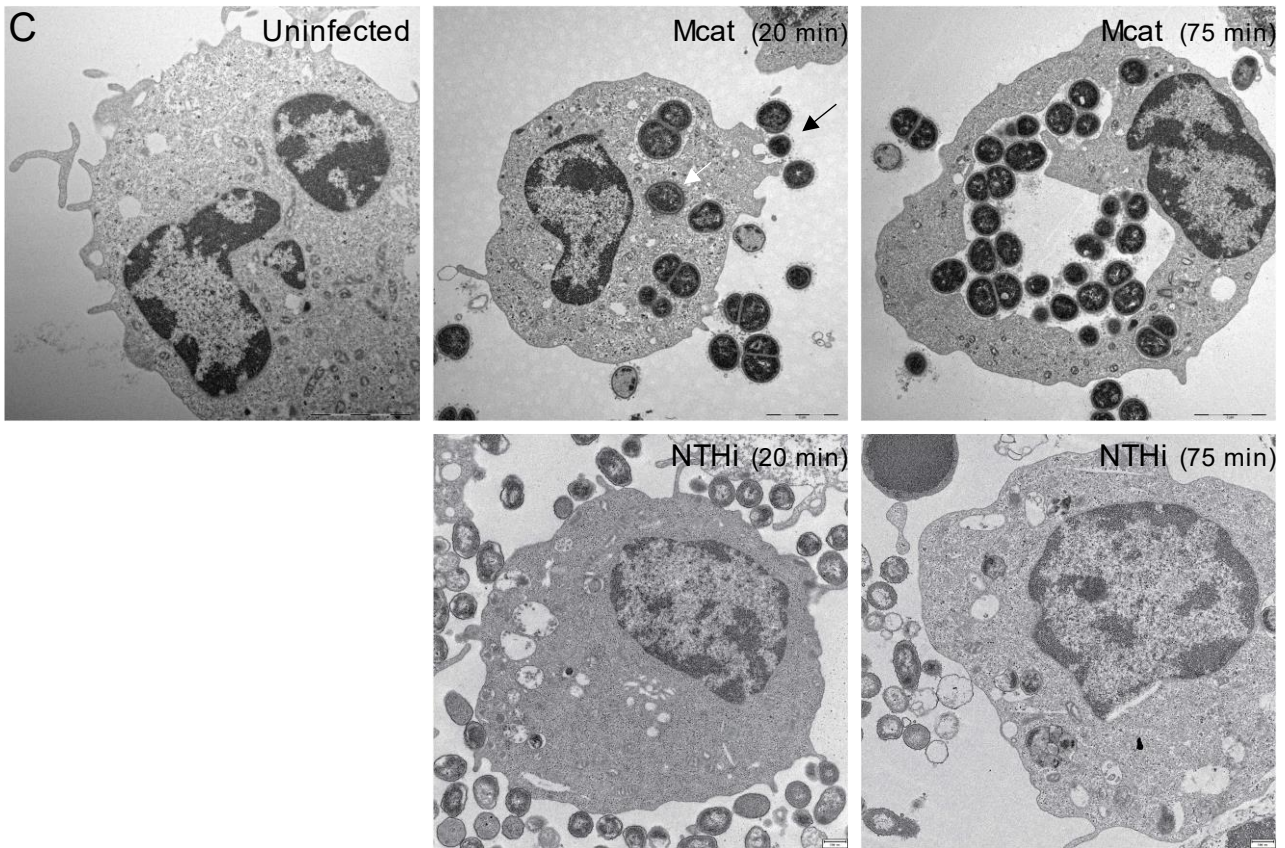
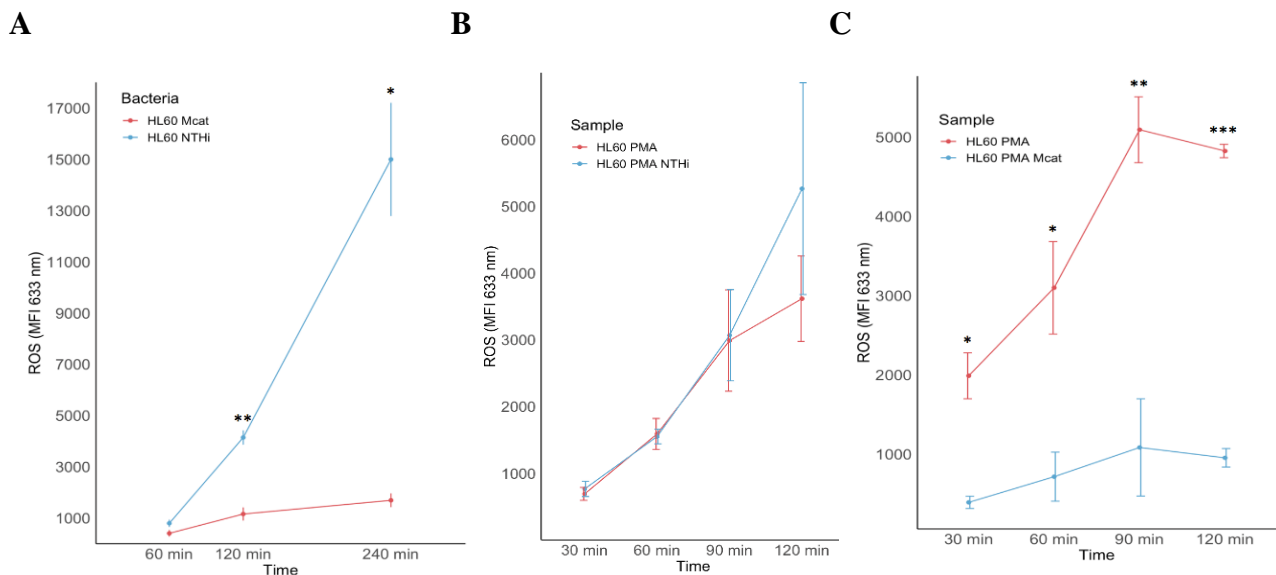


Figure 9. Mcat and NTHi: two different ways to interact with neutrophil-like cells. (A and B) ROS-induced dHL-60 cells were left untreated (total association) or challenged with cytochalasin D (for bacterial adhesion). They were infected with Mcat (A) or NTHi (B) at MOI of 50 for 20-, 45- and 75 min. Cells were permeabilized and bacteria were stained for UspA2 (rabbit polyclonal antibodies) or for whole bacteria for Mcat or NTHi, respectively. By flow cytometry, cells were evaluated and reported as the percentage of bacteria positive-cells. Light blue bars: phagocytosis; Green bars: adhesion; Red bars: non infected cells. (C) Transmission electron microscopy imaged of uninfected ROS-induced cells (left panel) and infected by unopsonized Mcat (top panels) or NTHi (bottom panels) at MOI 50 for 20- and 75 min. Scale bars, 2 μ m.

4.2 Mcat actively interferes with cellular ROS production while NTHi does not

We subsequently examined the possible impact of Mcat and NTHi on the oxidative burst, a pivotal weapon of innate immune cells against invading bacteria. To this purpose, we challenged neutrophil-like cells with unopsonized Mcat or NTHi at MOI=50 and the intracellular ROS production was measured by flow cytometry at 60-, 120- and 240- minutes post-infection using CellRox fluorogenic dye. Measurements of the mean fluorescence intensities (MFI) from infected cells, normalized by fluorescence signals of uninfected cells, are reported in Figure 10A. The reason behind the choice of subtracting the MFI obtained in uninfected cells from infected cells is linked with the fact that the process of phagocytosis itself leads to ROS release, and it is already known that both NTHi and Mcat elicit ROS production after internalization. Thus, the purpose of panel A of this image is to compare the different levels of ROS generation upon Mcat and NTHi infections. In

unstimulated cells, NTHi induced a marked increase of the oxidative burst over time (MFI from 796 to 14,994, at 60- and 240- min, respectively). Indeed, the MFIs recorded at the last two time points were significantly higher compared to that of Mcat (MFI from 404 to 1692, at 60- and 240- min, respectively). Next, we verified if NTHi and Mcat were able to dampen ROS production in chemically activated dHL-60 cells (Figures 10B and 10C). To this aim, MFI of PMA-activated uninfected cells and Mcat or NTHi infected cells (MOI=50) were evaluated at 30-, 60-, 90-, and 120 minutes post-infection by flow cytometry using the aforementioned dye, CellRox. As shown in Figure 10B, no reduction in ROS production was detected when cells were infected by NTHi at any of the indicated time points. By contrast, intracellular ROS production in PMA-stimulated dHL-60 cells was dampened by Mcat infection over time (Figure 10C), and this was not the result of cell death (Figure 10D). We subsequently investigated if this suppression was also effective on the extracellular ROS response. Therefore, we treated uninfected cells or cells infected with bacteria at different MOI (MOI of 100, 50, 25 and 12) with PMA. The kinetics of extracellular ROS production were recorded every 180 seconds within 120 minutes using a luminol-dependent chemiluminescence assay. As shown in Figure 10E, a peak of luminescence at 42 minutes of treatment was observed in uninfected dHL-60 cells after PMA exposure. When PMA-activated cells were challenged with Mcat, the respiratory burst was suppressed in a MOI-dependent manner. From the above data, we conclude that, unlike NTHi, Mcat does not elicit a strong oxidative response in unstimulated cells and it can actively interfere with ROS generation in chemically activated dHL-60 cells.



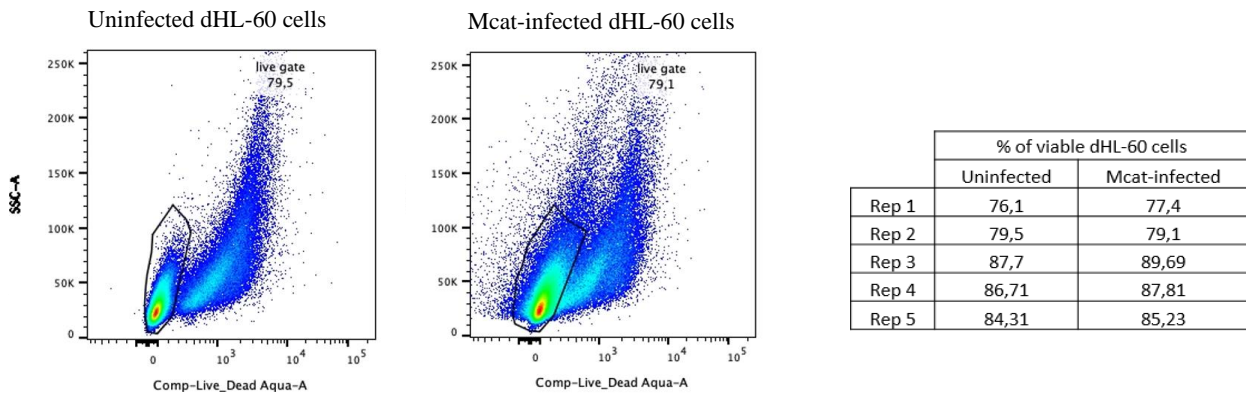
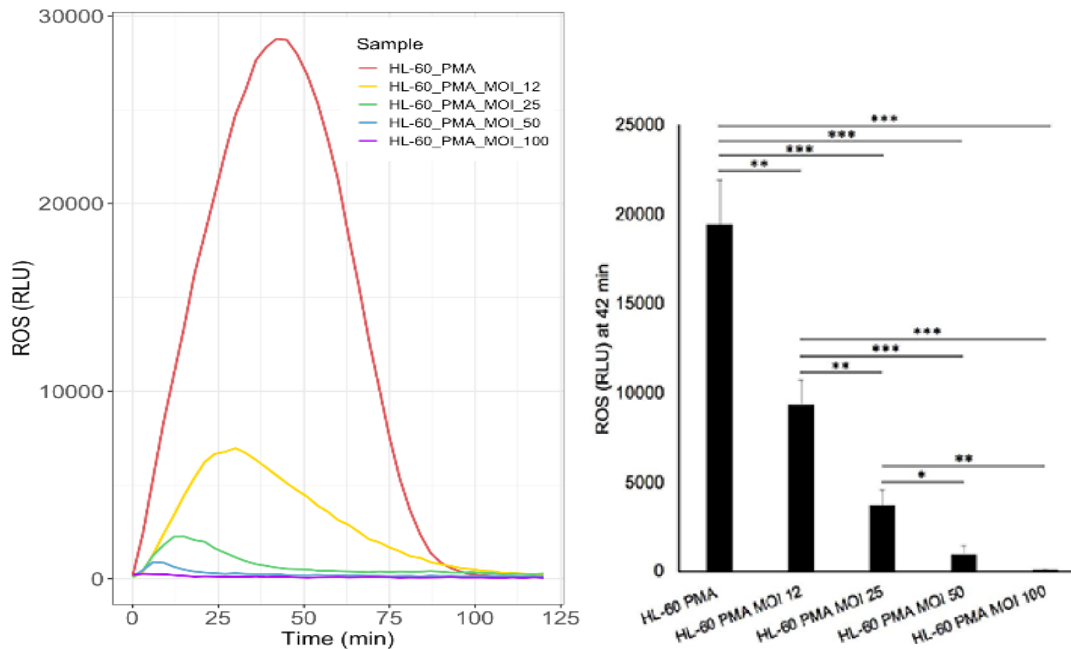
D**E**

Figure 10. *M. catarrhalis* actively interferes with cellular ROS production while NTHi does not. (A) Unstimulated differentiated HL-60 cells were infected with the *M. catarrhalis* BBH18 or NTHi 658 at MOI 50 for at 1, 2 and 4 h. (B and C) dHL60 cells were stimulated for ROS production and infected with *M. catarrhalis* BBH18 (B) or NTHi 658 (C) at MOI 50. (A-C) Intracellular ROS production was monitored by flow cytometry, using a fluorogenic dye, CellRox. MFI at 633 nm from at least three independent experiments at the indicated time point after infection was determined by flow cytometry and was the result of subtraction from fluorescence signals of uninfected cells for the corresponding time point. Bars represent means \pm SE. MFI, Mean fluorescence intensity. * $p < 0.05$; ** $p < 0.01$; *** $p < 0.001$. (D) Representative example of viability (LIVE/DEAD Fixable Aqua Dead Cell Stain) for ROS-induced, non-infected and Mcat infected dHL-60 cells (MOI 50) at 75 minutes after infection. Summary data of the percentage of viable cells across multiple replicate experiments. (E) dHL60 cells were stimulated for ROS production and infected with *M. catarrhalis* BBH18 at MOI 100, 50, 25 and 12. Representative experiment showing generation of chemiluminescence measured every 3 minutes within 2 hours along with the quantification of ROS at 42 minutes from at least three independent experiments. Bars represent means \pm SE. RLU, relative luminescence units. * $p < 0.05$; ** $p < 0.01$; *** $p < 0.001$ by chemiluminescence.

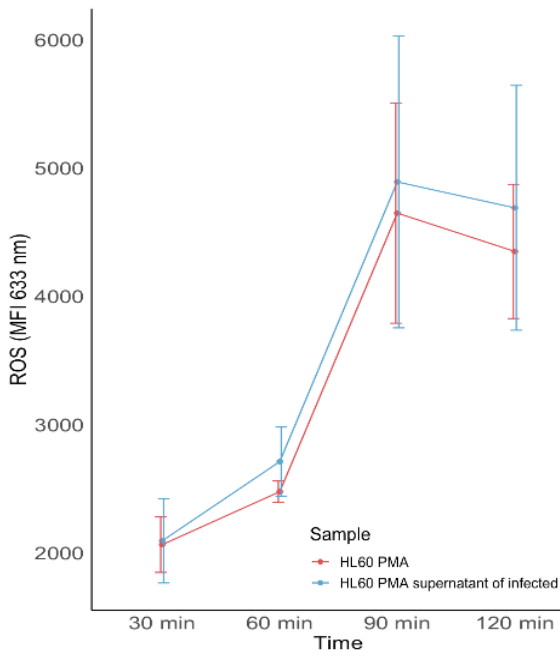
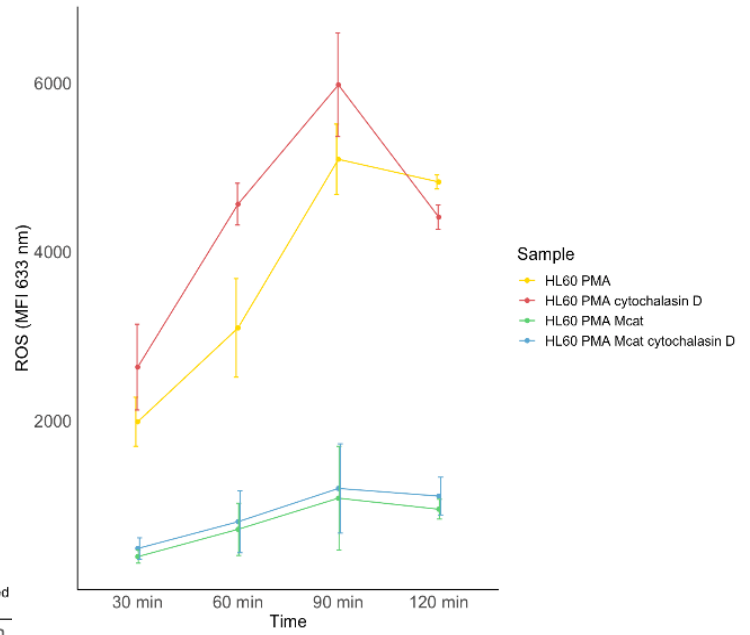
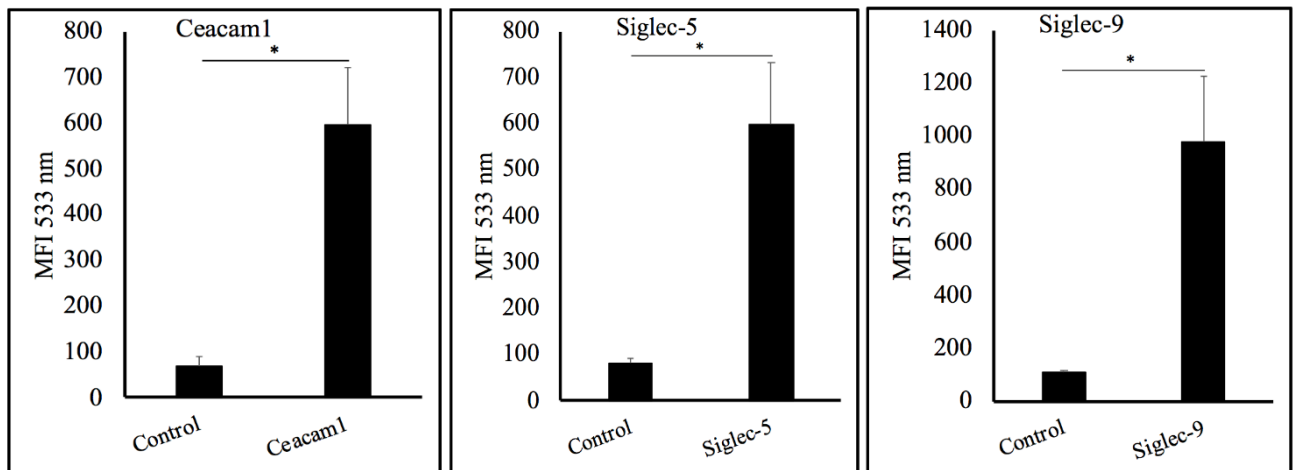
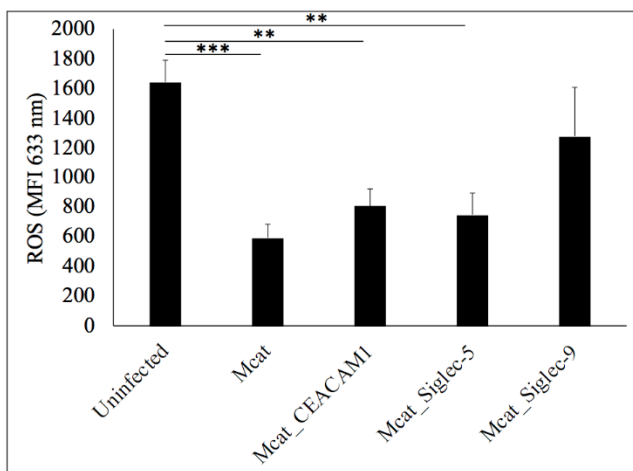
4.3 Mcat limits ROS production in a contact-dependent and phagocytosis-independent manner by possibly binding immunosuppressive receptors

To better explore the mechanisms by which Mcat actively limits ROS production in neutrophil-like cells, we investigated whether the interference was mediated by secreted effectors or required direct bacterial contact with the host cells. To this purpose, we measured intracellular ROS production on dHL60 cells treated with conditioned supernatants of infected cells or cytochalasin D. Cells were first infected by *M. catarrhalis* (MOI=50), and at 42 min post-infection (time point at which we measured the peak of ROS generation in PMA-stimulated dHL-60 cells), the resulting supernatant was exposed to naïve uninfected PMA-activated cells. Under these conditions, no interference with the oxidative response was observed (Figures 11A), indicating that the underlying mechanism was not likely due to factors released in the supernatant derived from *M. catarrhalis* infecting cells. Subsequently, we verified whether bacterial internalization by the host cells was required to enable Mcat to exert its inhibitory effect. dHL-60 cells were exposed to cytochalasin D (10 µg/ml), to inhibit phagocytosis. The presence of this molecule did not alter the extent of ROS inhibition in PMA-activated infected dHL-60 cells (Figures 11B), indicating that the bacterial uptake was not necessary to limit ROS production in dHL-60 cells. These results point out that *M. catarrhalis* impairs the oxidative stress response in cells chemically activated with PMA with a contact-dependent (not due to the secretion of effector proteins or toxins) and phagocytosis-independent mechanism.

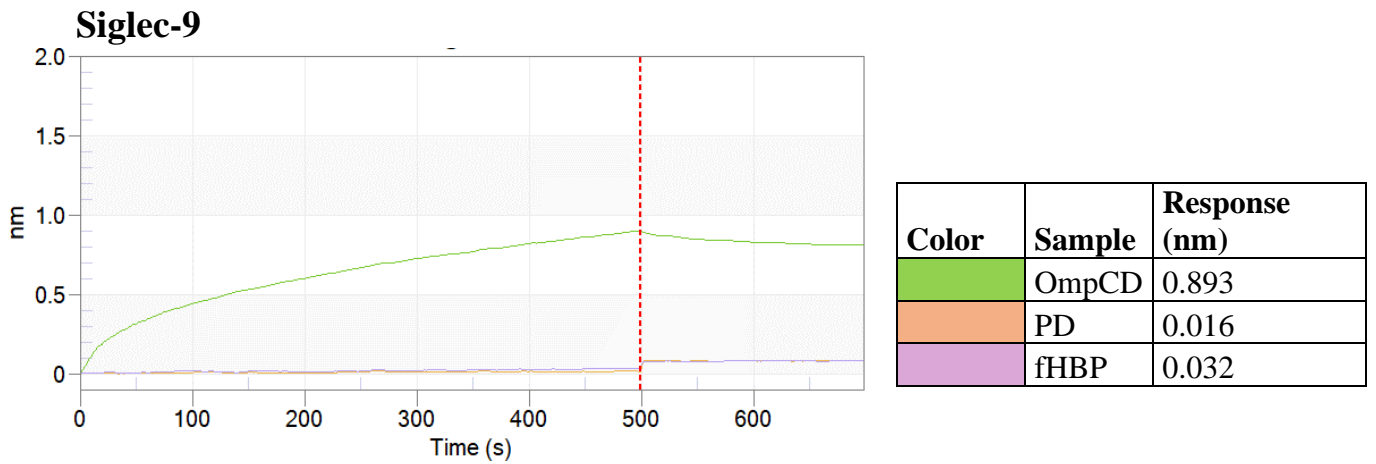
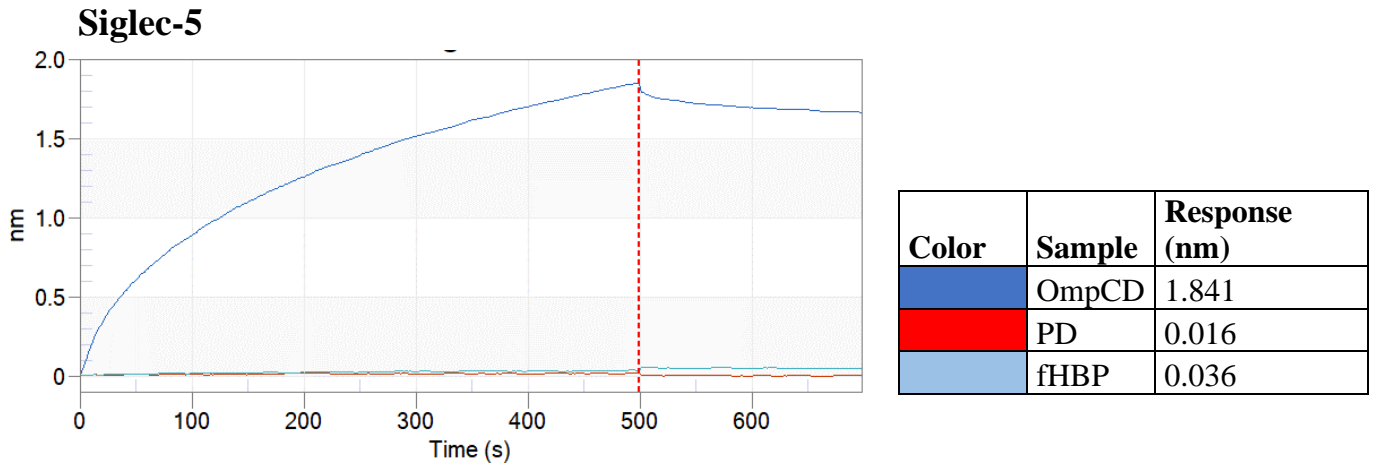
Once assessed bacteria-cell contact is necessary for dampening the oxidative stress response, the Mcat binding to immunosuppressive receptors has been evaluated. Several neutrophil inhibitory receptors, such as some Siglec receptors (Siglec-5 and Siglec-9) and receptors of the CEACAM family (such as CEACAM-1), modulate the immune responses mainly by blocking ROS activating pathways (Pyz et al., 2006). To this purpose, Mcat was incubated or not, with 2 µg of each recombinant protein: CEACAM-1 (known interactor of the bacterium), Siglec-5 and Siglec-9 inhibitory receptors. The engagement of these soluble receptors by Mcat was determined by flow cytometry using antibodies specific to each recombinant protein. As shown in Figure 11C, the MFIs recorded after bacterial incubation with the soluble extracellular portion of the recombinant receptors CEACAM-1, Siglec-5 and Siglec-9 were statistically different from their controls (bacterial cells in the absence of the protein of interest but incubated with the corresponding antibodies). These data point out that in addition to CEACAM-1 binding, Mcat is able to also engage the inhibitory Siglecs receptors (Siglec-5 and Siglec-9). To examine if Mcat specifically binds to these human receptors to suppress ROS production, we challenged PMA-activated neutrophil-like cells with Mcat, which were

left untreated or pre-incubated with each recombinant human receptor. The intracellular ROS production was measured by flow cytometry at 2 hours post-infection using CellRox dye. As shown in Figure 11D, when Mcat was exposed to CEACAM1 or Siglec-5, the observed suppression of the intracellular ROS production by PMA-stimulated infected dHL-60 cells was only slightly abolished. Interestingly, the MFIs recorded after incubation with the inhibitory Siglec-9 receptor was similar to that recorded for the uninfected PMA-activated cells. These data indicate that blocking the cognate binding Siglec-9 partner avoids the specific binding responsible for the Mcat interference with ROS production by dHL-60 cells.

While the role of UspA1 as an adhesin capable of binding to CEACAM-1 is already well described (Brooks et al., 2008), binding to Siglecs is currently not well known. Among the different adhesins from Mcat (Ren and Pichichero, 2016), OmpCD is the only outer membrane protein capable of binding human mucins (Akimana and Lafontaine, 2007). As mucin glycoproteins are particularly enriched with sialic acids (Haines-Menges et al., 2015), we verified the possible interactions between this bacterial protein and human Siglec-5 and Siglec-9 receptors. The *ompCD* gene was cloned and expressed in *Escherichia coli* without its signal peptide and then the recombinant protein was purified through the His-tag at its N-terminus (see the list of primers used in this study Table S1). Biolayer interferometry (BLI) was used to monitor protein-protein interactions in real-time. Protein G-functionalized fiber optic biosensors were used to capture the Fc-Tag human receptors (2 μ g per reaction) and as analytes, we used 200 nM of Mcat OmpCD and two additional proteins as controls: His-tag meningococcal Factor H Binding Protein (fHBP) and the Protein D (PD) from NTHi. As it can be observed in the association phases in Figure 11E, negligible binding to the captured Siglecs was recorded for fHBP and PD. Association was observed only in the case of Mcat OmpCD for both human Siglec-5 and Siglec-9 receptors with the generation of stable complexes (see the dissociation phases). Therefore, we decided to perform competitive experiments to validate this result. As previously described, Mcat was incubated with 2 μ g of each Siglec-5 or Siglec-9 recombinant receptors with or without 200 nM of OmpCD or PD (as a negative control for the competition experiment). The binding of Siglecs to the bacteria was revealed by flow cytometry using antibodies specific to each recombinant receptor. As observed in Figure 11F, the recorded MFI obtained after the incubation with the recombinant receptors was reduced only when OmpCD protein was added, confirming BLI data and thus suggesting a previously unknown function of this porin.

A**B****C****D**

E



F

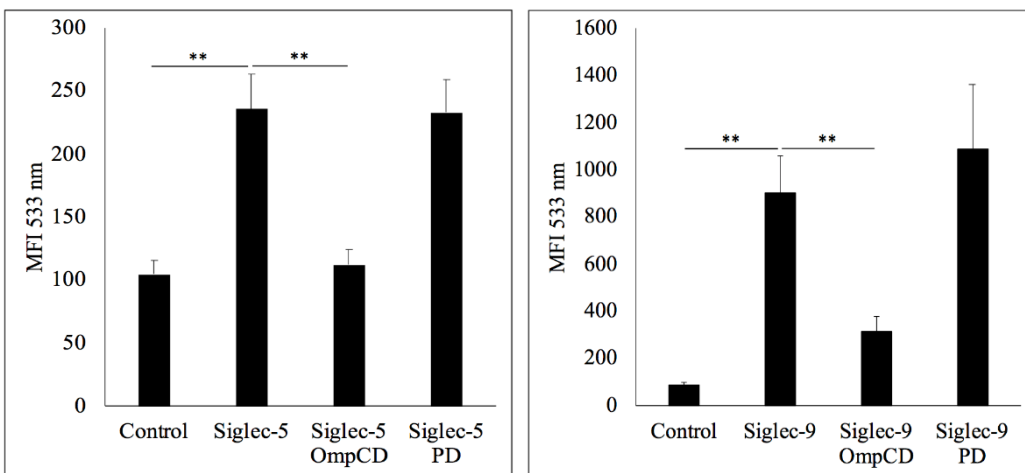


Figure 11. *M. catarrhalis* limits ROS production in a contact-dependent and phagocytosis-independent manner by possibly binding immunosuppressive receptors. (A) dHL-60 were infected or not by *M. catarrhalis* BBH18 strain (MOI 50) and the resulting supernatants were presented to naïve ROS-induced cells. (B) ROS-induced dHL60 cells were pre-incubated with cytochalasin D (phagocytosis inhibitor) and infected with *M. catarrhalis* BBH18 at MOI 50. (A and B) MFI at 633 nm from at least three independent experiments at the indicated time point after infection was

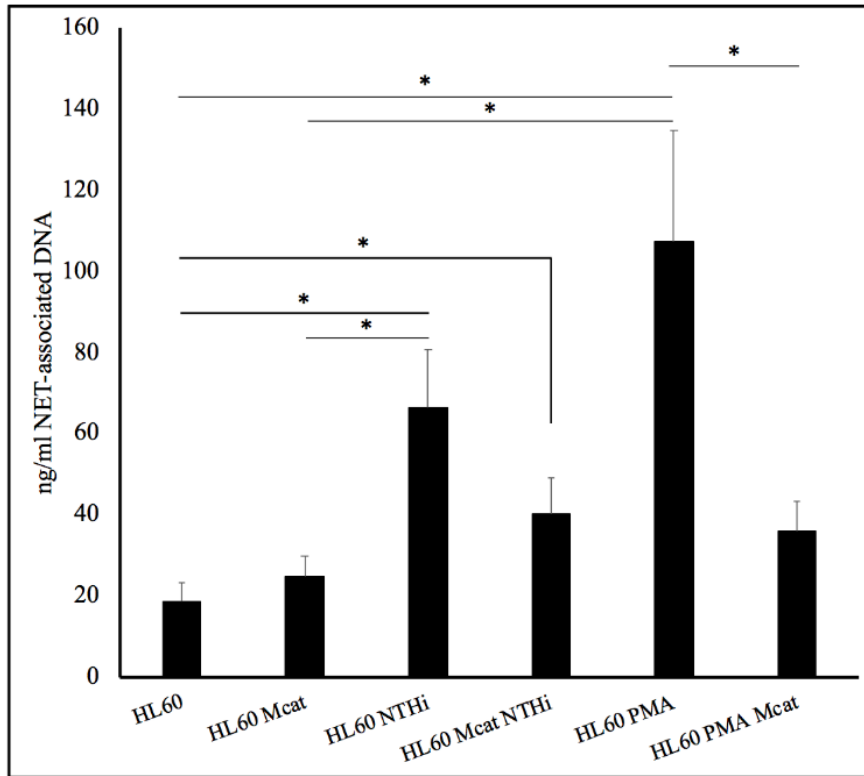
determined by flow cytometry. Bars represent means \pm SE. MFI, Mean fluorescence intensity. (C) *M. catarrhalis* was incubated or not (control) with 2 μ g of each human recombinant protein: CEACAM-1, Siglec-5 and Siglec-9. Antibodies raised against the recombinant proteins were used for detection by flow cytometry. MFI at 535 nm from at least three independent experiments. Bars represent means \pm SE. MFI, Mean fluorescence intensity. * $p < 0.05$. (D) *M. catarrhalis* was pre-incubated or not (control) with 200 nM of each human recombinant protein: CEACAM1, Siglec-5 and Siglec-9. dHL60 cells were stimulated for ROS production and infected with Mcat (control), Mcat_CEACAM1, Mcat_Siglec-5 or Mcat_Siglec-9 at MOI of 50. MFI at 633 nm from at least three independent experiments at 2 h post-infection was determined by flow cytometry. Bars represent means \pm SE. MFI, Mean fluorescence intensity. ** $p < 0.01$; *** $p < 0.001$. (E) Protein-protein interaction was revealed by BLI. Two μ g of Siglec-5 and Siglec-9 proteins were used as ligands and captured, *via* Fc-region, on the surface of the biosensors pre-coated with protein G and 200 nM of bacterial OmpCD, PD, and fHBP were used as analytes. The BLI results are shown as sensorgrams, in which the plot abscissae represent time in seconds [s] while ordinates represent the response [nm]. For each sensorgram, a blank subtraction is performed, by subtracting the blank signal from the response measured. A summary data of with ligands and analytes with the corresponding response [nm] is reported. (F) As a competition experiment, *M. catarrhalis* was incubated with 2 μ g of each Siglec-5 or Siglec-9 recombinant receptors with or without 200 nM of OmpCD or PD proteins. Antibodies raised against the human receptors were used for detection by flow cytometry. MFI at 535 nm from at least three independent experiments. Bars represent means \pm SE. MFI, Mean fluorescence intensity. ** $p < 0.01$.

4.4 NET generation is differently modulated by NTHi and Mcat

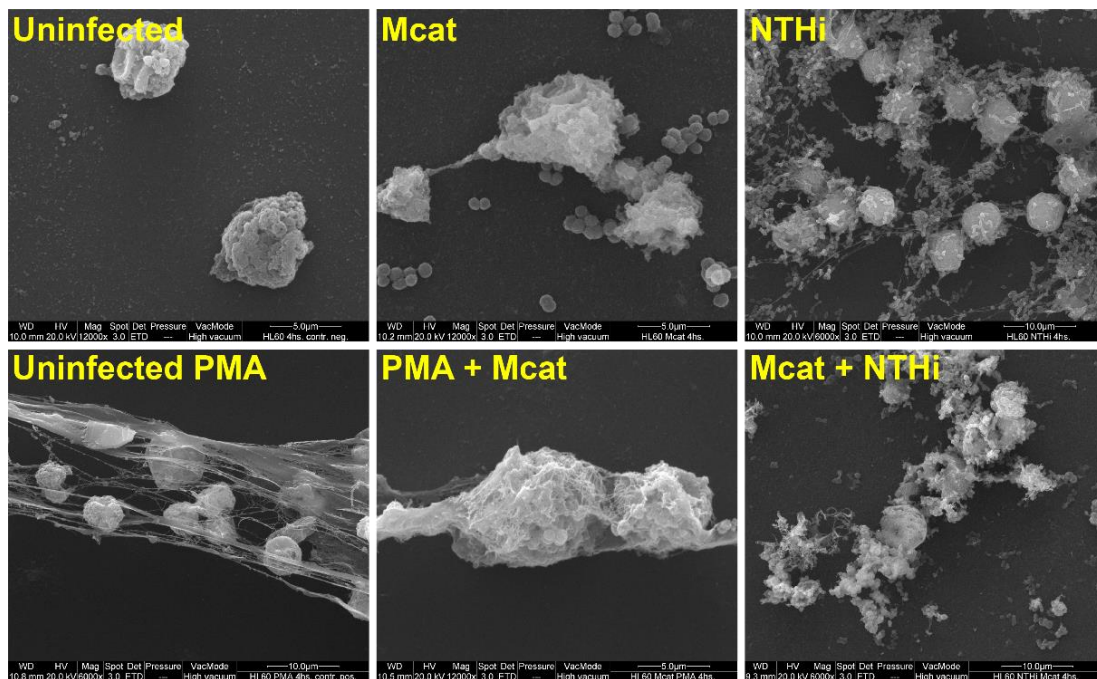
As NETs play a key role in chronic inflammation and lung tissue damages in COPD (Grabcanovic-Musija et al., 2015), the NET formation was investigated in cells infected with Mcat or NTHi individually at MOI of 50 and in their combination (MOI of 25, each bacterium), for 4 hours. As a positive control for NETosis, dHL-60 cells were also treated with PMA and subsequently left uninfected or challenged with Mcat (MOI=50). The extracellular DNA associated with NETosis was quantified, and these NET structures were visualized by confocal and electron microscopy. For the quantification, the supernatants of the samples were excluded to remove free/degraded NETs-DNA and DNA derived from necrotic cells. After treatment with micrococcal nuclease, the quantity of extracellular DNA in the resulting supernatants was measured using PicoGreen staining. We observed no significant differences in NETs-associated DNA of unstimulated cells or infected by Mcat (MOI 50) (18.7 and 24.7 ng/ml, respectively). By contrast, dHL-60 cells challenged with NTHi (MOI 50) or with PMA (positive control) resulted in high levels of NET-associated DNA (66.3 and 107.1 ng/ml, respectively), (Figure 12A). When co-infected by Mcat and NTHi, unstimulated cells released an intermediate amount of NET-associated DNA (40.3 ng/ml) compared to the single infections with Mcat or NTHi. Interestingly, the NETs-associated DNA of PMA-activated neutrophil-like cells infected by Mcat was almost three times lower compared to the positive control (35.9 ng/ml and 107.1 ng/ml, respectively) (Figure 12A). The same findings can be retrieved from the images of scanning electron microscopy (Figure 12B) and confocal microscopy (DNA and myeloperoxidase (MPO) are visualized in blue and green, respectively) (Figure 12C). As it is shown, networks of extracellular fibers made of DNA and MPO, one of the antimicrobial proteins that characterizes NET structures, were evident in PMA-treated dHL-60 cells. These web-like extracellular microbicidal structures were

also clearly visible in the case of NTHi single infection but partially rescued when the co-infecting Mcat was present. From the above data, we conclude that, unlike Mcat, NTHi induces more NETosis in infected unstimulated cells. Moreover, Mcat can dampen NET generation in PMA-activated cells or NTHi-infected dHL-60 cells.

A



B



C

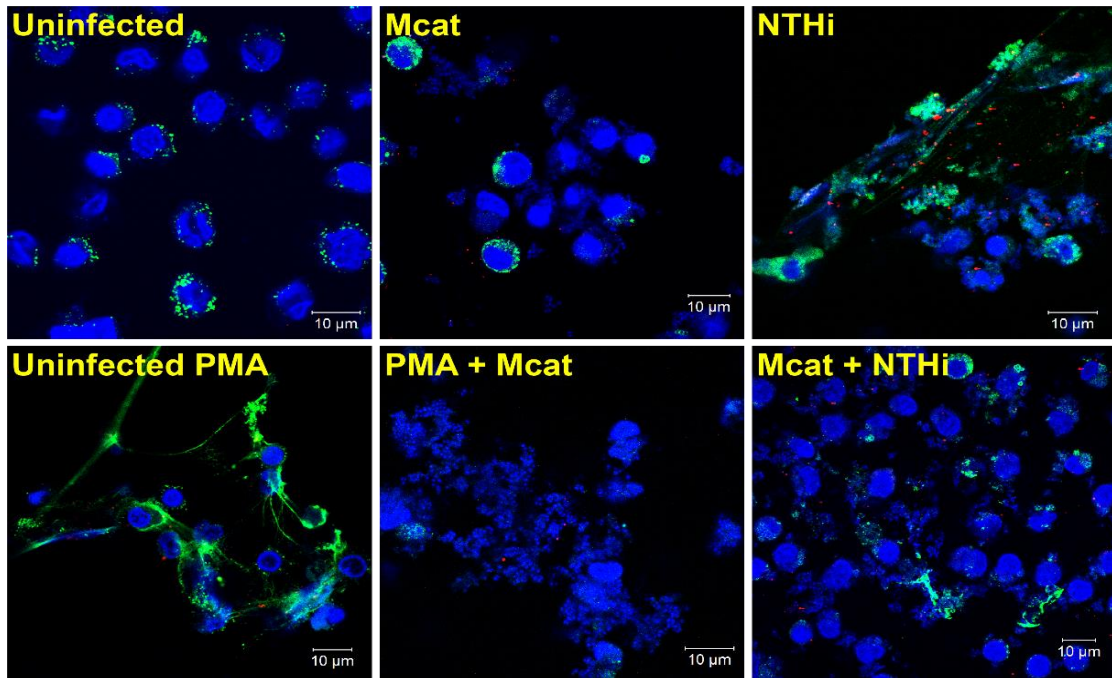


Figure 12. NET generation is differently modulated by NTHi and *M. catarrhalis* dHL-60 cells were left untreated, or either infected singly with *M. catarrhalis* (MOI 50) or NTHi (MOI 50), or with a combination of the two bacteria (MOI 25 each). dHL-60 were also treated with a known inducer of NETs (PMA) and infected or not with *M. catarrhalis* (MOI 50). The reaction was allowed to proceed for 4 h. (A) Samples were centrifuged, nuclease-treated and the amount of DNA in the supernatant was quantified using PicoGreen staining and the fluorescence was detected at 530 nm using a TECAN Infinite 200 plate reader. λ DNA at known concentrations was used as standard. Each sample was processed in triplicate to reduce intra-run variability. From a standard curve obtained by using known concentration of λ DNA, the ng/ml of NET-associated DNA were determined. The resulting graph is obtained from seven independent experiments. Bars represent means \pm SE. * $p < 0.05$. (B) Samples were fixed and analyzed by scanning electron microscopy. (C) dHL-60 cells were fixed with 4% paraformaldehyde and stained for DNA (DAPI, blue) or myeloperoxidase (MPO, green) The stained cells were analyzed by immunofluorescence microscopy. Scale bars, 10 μ m.

4.5 Mcat interferes with the autophagic pathway surviving intracellularly and reducing the killing of NTHi

Next, we focused on the responses of Mcat and NTHi to the autophagic pathway. To characterize these responses, PMA-activated neutrophil-like cells were left uninfected or challenged with Mcat or NTHi at MOI of 50 for 40 minutes. The non-interacting bacteria were washed away, and the growth of extracellular adherent bacteria was inhibited by adding gentamicin for 20 minutes. From this time on (1 h), samples were incubated for 3 additional hours in the presence of PMA (Figure 13A). By flow cytometry, the autophagic response was monitored at these two time points (1h and 4h) by staining dHL-60 cells for the lipidated form of the microtubule-associated protein light chain 3 (LC3-II), one ubiquitin-like conjugation systems essential in the entire autophagic pathway. As it can be observed from the MFIs in Figure 13B, the LC3-II expression level was 2.5-fold lower in Mcat-infected cells compared to the uninfected ones. By contrast, uninfected cells and NTHi-

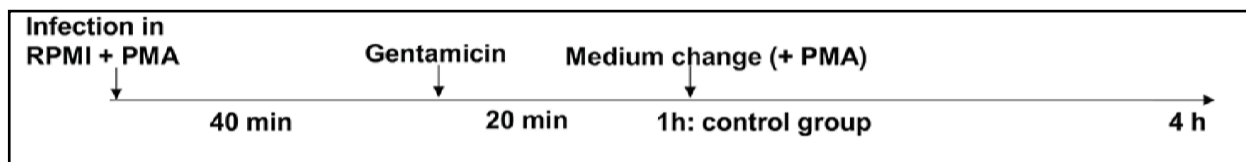
infected-cells showed similar expression levels of LC3-II (Figure 13B). These data indicate that Mcat can suppress the autophagic response in dHL-60 cells, while NTHi did not.

Transmission Electron Microscopy (TEM) was performed at the time points reported in Figure 13A and representative images are reported in Figure 13C. As it can be observed, at 1 h post-infection, uninfected PMA-activated cells showed intact membrane and progressive margination of chromatin beneath the nuclear envelope, suggesting the presence of early stages of apoptosis. Cytoplasmic vacuolization and different changes in mitochondrial morphology were observed. The increase in electron density (top left panels, yellow arrow), which may correspond to mitochondrial membrane potential changes (Pellegrini et al., 2007), is the most evident example. Interestingly, in some cases, elongation of mitochondria was appreciated (top left panel, white arrow), probably for maintenance of ATP production (Gomes et al., 2011), allowing the cell survival in oxidative environments (induced by PMA-addition). After three additional hours, the extensive accumulation of double-membraned cytoplasmic vesicles containing organelles or cellular debris (bottom left panel, yellow star) witnessed more prominent events of apoptosis and autophagy. At 1 h post-infection, Mcat was internalized in a single membrane vacuole, displaying a well-preserved ultrastructure. In the last time point, cells were packed with a higher number of bacteria present in larger vesicles. Despite the evident suffering state caused by PMA-addition, Mcat-infected and uninfected cells showed a very similar morphology as the host cells did not perceive the presence of this bacterium (see middle panels). Conversely, at 1 h post-infection by NTHi, a low number of bacteria were phagocytosed with dHL-60 cells showing condensation of internal mitochondrial cristae. In the last time point, NTHi-infected dHL-60 cells displayed marked phenomena of late stages of apoptosis (bottom right panel, white arrow) and autophagosomes containing cellular debris. The few phagocytosed NTHi were present in double-membraned autophagic vesicles (bottom right panel, yellow arrow), suggesting that neutrophil-like cells were active in the clearance of the infections caused by NTHi.

Further evaluation of the survival of internalized Mcat and NTHi and their interplays in dHL-60 cells was carried out by enumeration of the colony-forming units (CFU) by dilution plating on agar plates. By using the same experimental condition reported in Figure 13A, ROS-induced cells were infected with Mcat or NTHi at MOI of 50 (single infection, red and blue bars, respectively) or co-infected with both bacteria (MOI of 50 each bacterium, black and gray bars, respectively) (Figure 13D). The bacterial intracellular survival was investigated by dividing the CFU/ml recorded at 4 h by that obtained at 1 h (ratio 4 h/1 h) (Table T1). In the case of a single infection, Mcat overcame the antimicrobial effect of ROS, surviving over 4 h of infection. In fact, the number of bacterial cells slightly increased (Figure 13D, red bars). On the contrary, the viability of NTHi was dramatically reduced (Table T1, blue bars). In summary, the measured ratios 4 h/1 h were 1.5 and 0.2 for Mcat

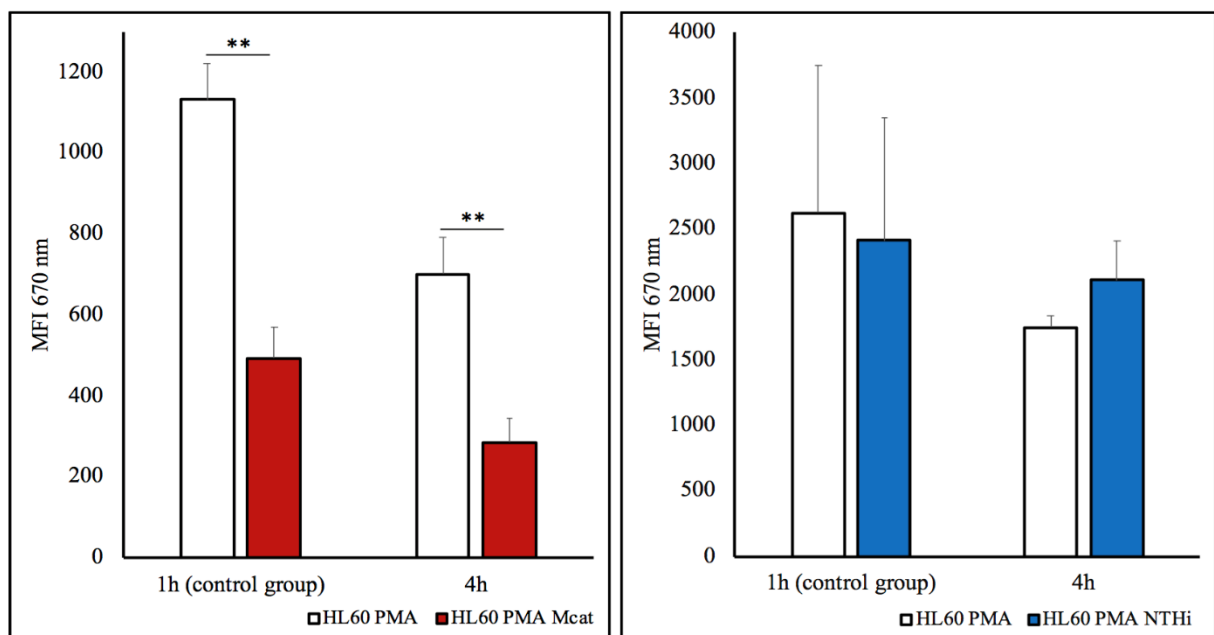
and NTHi, respectively (Table T1). These data indicate that NTHi is susceptible to ROS production, being efficiently killed by these innate immune cells. In the co- or single infections, the Mcat viability remained unchanged (Figure 13D, black and red bars, respectively), suggesting that NTHi had no influence on Mcat capability to interfere with the antimicrobial action of ROS. In fact, the observed CFU/ml and the related ratio 4 h/1 h were similar in the two experimental conditions (single and co-infections). Interestingly, in the co-infection system, a dramatic reduction in the viability of NTHi was not observed (Figure 13D, gray bars). The measured ratio of 4 h/1 h was 0.8 (Table T1), pointing out that the presence of Mcat reduced the killing of NTHi mediated by chemically activated neutrophil-like cells, thus providing an advantage of survival (ratio 4 h/1 h 0.8 and 0.2 in the co- and single infections, respectively), (Table T1). However, the strategies exploited by Mcat to survive or even duplicate after internalization and the ways it may affect NTHi uptake and its survival in an oxidative-like environment have to be fully elucidated.

A

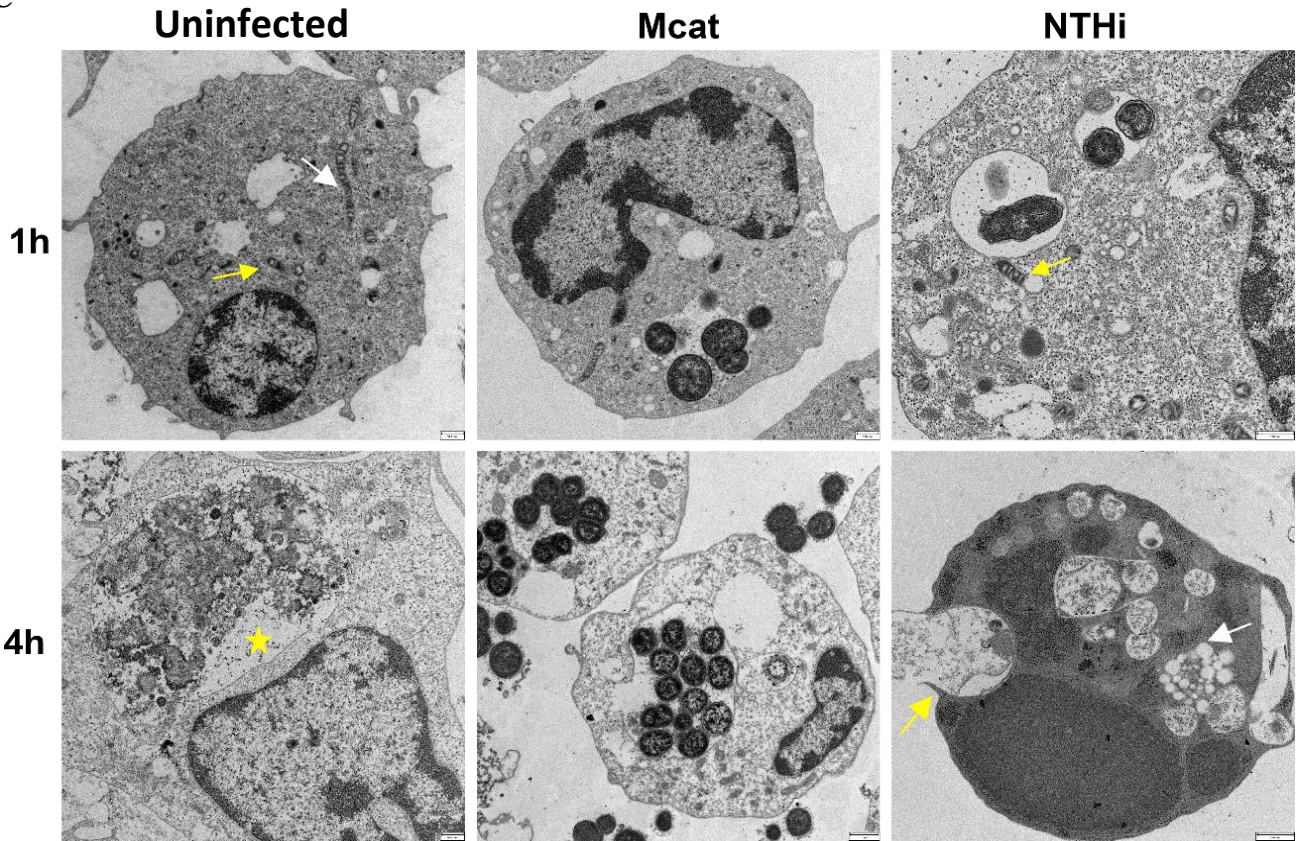


B

LC3-II



C



D

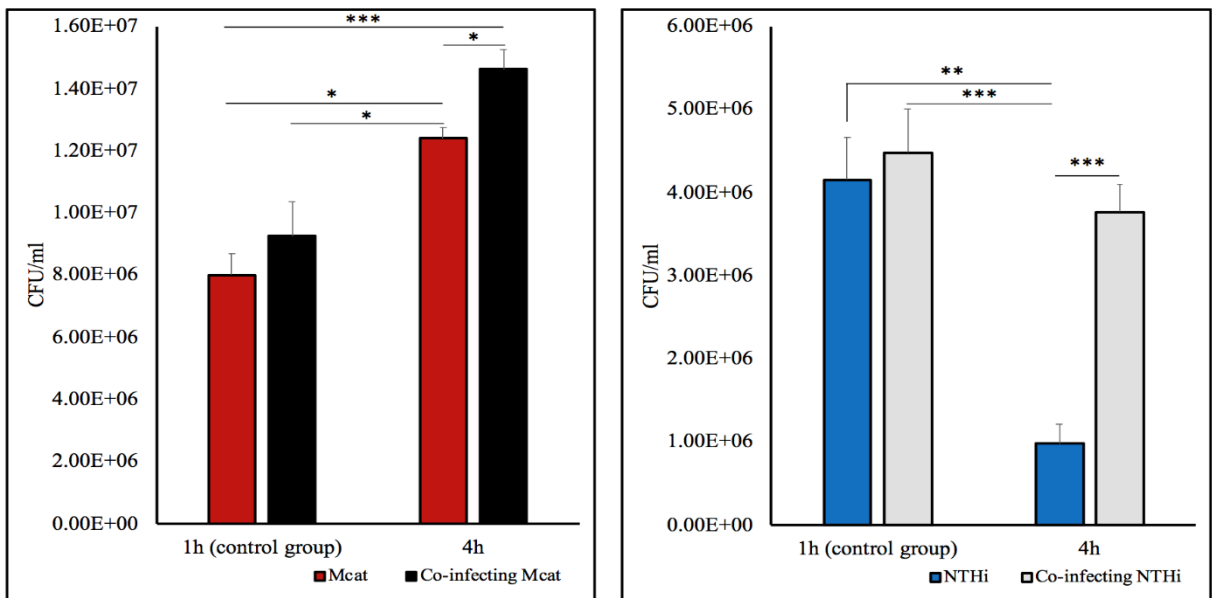


Figure 13. Mcat interferes with the autophagic pathway surviving intracellularly and reducing the killing of NTHi. ROS-stimulated dHL-60 cells were non-infected or incubated with *M. catarrhalis* or NTHi individually or in their combination at MOI 50 for 40 minutes. Then non adherent bacteria were washed out and gentamicin was added for 20 minutes to inhibit growth of extracellular bacteria. From this time (1 h, control group), samples were incubated for additional 3 hours (for a total of 4 h). (A) Schematic representation of the “autophagic response and intracellular survival assay”. (B) The autophagic response was monitored by flow cytometry using the LC3-II as a marker. The mean fluorescence intensity (MFI) at 670 nm were determined without performing gates. The resulting graph is obtained from four independent experiments. ROS-stimulated dHL-60 cells were non-infected (black bars) or incubated with *M. catarrhalis* (red bars) or NTHi (blue bars) Bars represent means \pm SE. * $p < 0.05$; ** $p < 0.01$. (C) Transmission electron

microscopy on uninfected ROS-induced dHL60 cells (left panels) and infected by non-opsonized *M. catarrhalis* at MOI 50 (middle panels) or by non-opsonized NTHi 658 at MOI 50 (right panels). Scale bars, 500 nm. (D) By using the protocol whose schematic representation is reported in panel (A), chemically-activated cells were infected by only *M. catarrhalis* (red bars) and NTHi (blue bars) at MOI 50 (single infection), or with both the bacteria (co-infection with MOI 50 each bacterium, black and gray bars). By dilution plating onto BHI or HAE2 plates, the number of colonies obtained per condition was calculated to plot CFU/ml and to determine the survival of *M. catarrhalis* and NTHi, respectively. Bars represent means \pm SE. MFI, Mean fluorescence intensity. * $p < 0.05$; ** $p < 0.01$; *** $p < 0.001$.

Table 1. Bacterial intracellular survival in dHL-60 cells.

ROS-induced dHL-60 cells			
	1 h (CFU/ml)	4 h (CFU/ml)	Ratio 4 h/ 1 h
Mcat	8.01E+06	1.24E+07	1.5
Co-infecting Mcat	9.26E+06	1.46E+07	1.6
NTHi	4.16E+06	9.88E+05	0.2
Co-infecting NTHi	4.49E+06	3.78E+06	0.8

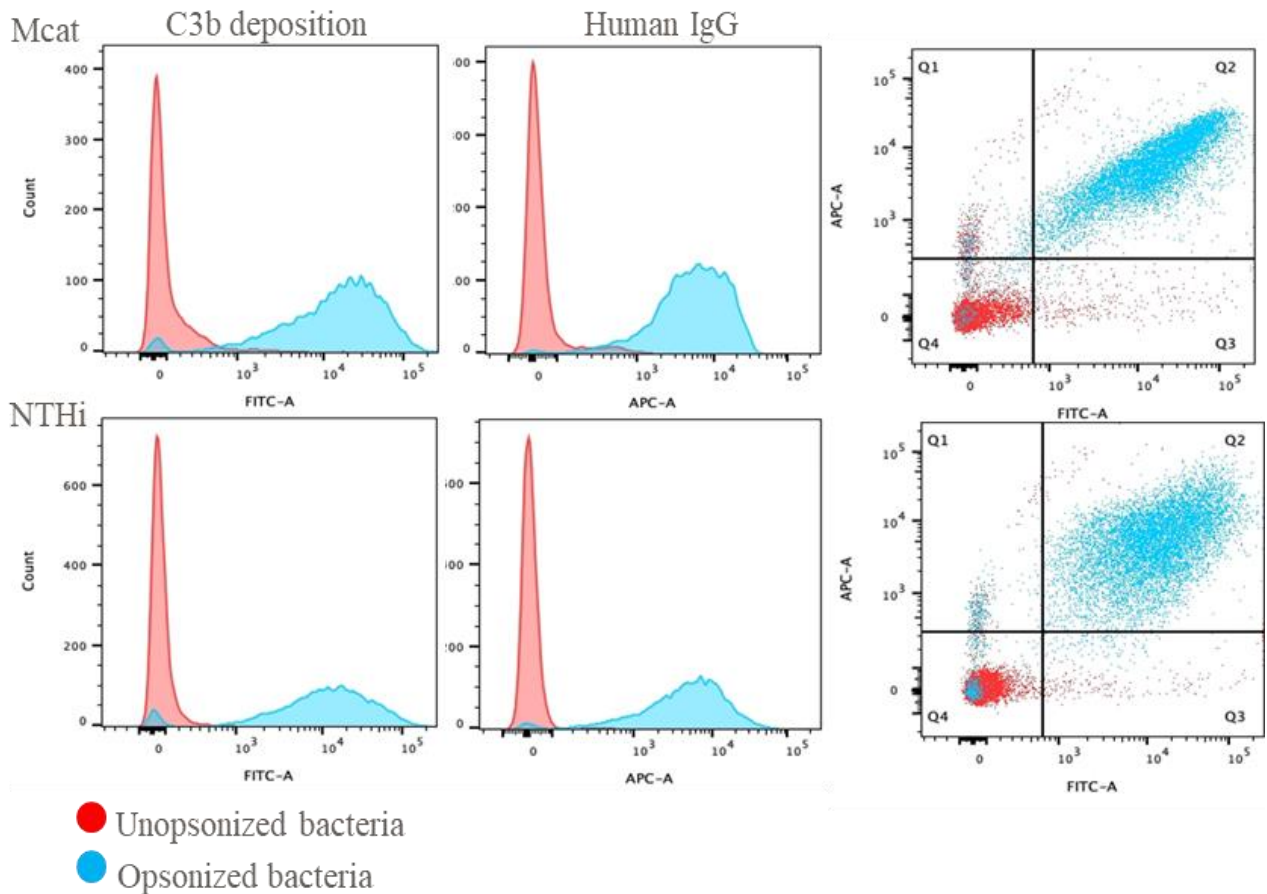
Table reporting the CFU/ml obtained at 1 h and 4 h post-infection for *M. catarrhalis* and NTHi both in single and co-infection. Bacterial intracellular survival was determined by dividing the CFU/ml obtained at 4 h to that recorded at 1 h (ratio 4 h/1 h).

4.6 Human opsonins increase Mcat and NTHi neutrophil uptake without affecting their ROS response

Upon entry of bacteria into the human host, the exposure to immune mediators (complement and immunoglobulins) coats to the bacterial surface leading to their opsonization. Within the complement cascade, the binding of C3b, an active complement component that is common to all the three pathways of complement activation, is fundamental for pathogen recognition by phagocytic cells or cell lysis through the formation of membrane attack complex (Lubbers et al., 2017, Noris and Remuzzi, 2013). In addition to the opsonin-independent internalization mediated by the CEACAM-3 receptor (Buntru et al., 2011), opsonization determines an enhanced neutrophil recognition and uptake of bacterial pathogens that are mediated by Fc γ receptors (Fc γ Rs) (Theprungsirikul et al., 2021). Moreover, the generation of the IgG immune complex has been shown to induce ROS production (García-García and Rosales, 2002). Hence, we investigated the effects of Mcat and NTHi opsonization on the bacterial uptake and intracellular ROS generation in dHL-60 cells. We pooled three human sera and used them as a source of complement at 10% (hereafter called normal human sera, NHS). By flow cytometry, we observed that more than 90% of the sera-treated Mcat and NTHi bacterial populations displayed on their surface not only C3b, but also human immunoglobulins (Figure 14A, APC-A+), with no reduction in bacterial viability (Figure 14B). By 2 h post-infection,

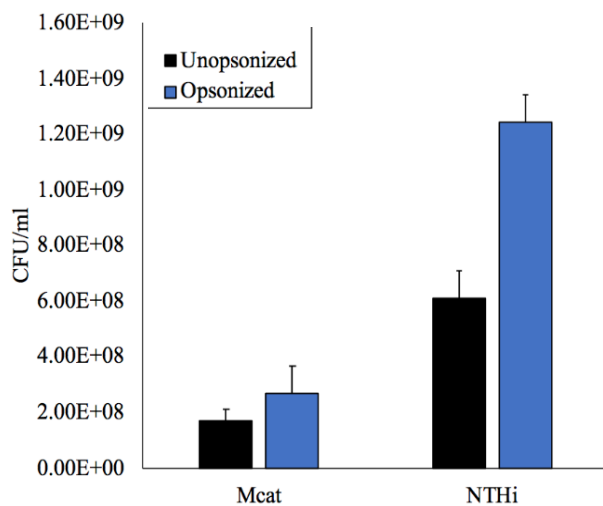
by comparing with unopsonized bacteria, opsonization significantly enhanced Mcat and NTHi uptake (3.6- and 2- fold increase, respectively) by neutrophil-like cells delineating the importance of complement factors and immunoglobulins in enhancing internalization (Figure 14C). As it is described above, intracellular ROS production was evaluated at 2 h post-infection. As it can be observed in Figure 14D, opsonized Mcat still elicited less ROS production in unstimulated dHL-60 cells compared to NTHi. Moreover, opsonized Mcat actively suppressed this response in PMA-activated dHL-60 cells while NTHi did not (Figure 14E). Curiously, for both opsonized Mcat and NTHi, the uptake by dHL-60 cells induced lower ROS production compared to their non-opsonized counterparts. Opsonins are thus fundamental for increasing Mcat and NTHi neutrophil internalization while only slightly affecting their response to ROS production by the host cells.

A

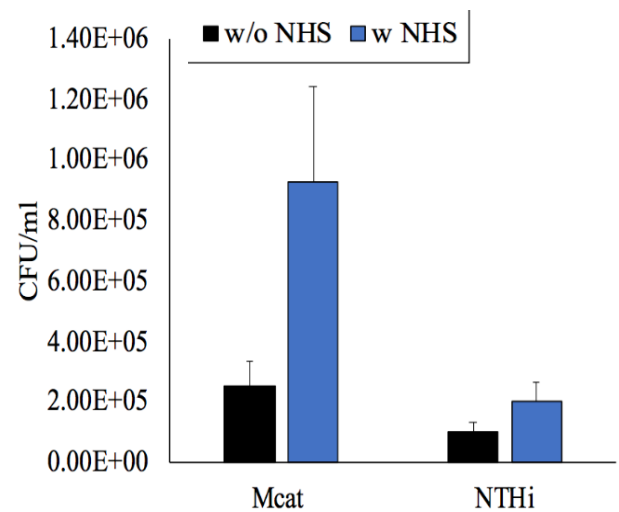


	FITC-A- APC-A+	FITC-A+ APC-A+	FITC-A+ APC-A-	FITC-A- APC-A-
Rep 1_Mcat	2,92%	0,93%	3,30%	92,85%
Rep 1_Mcat + 10% NHS	2,58%	93,50%	1,38%	2,54%
Rep 1_NTHi	0,97%	0,39%	1,14%	97,50%
Rep 1_NTHi + 10% NHS	1,41%	93,72%	1,63%	3,24%
Rep 2_Mcat	2,79%	0,95%	3,57%	92,51%
Rep 2_Mcat + 10% NHS	2,51%	94,90%	0,55%	2,06%
Rep 2_NTHi	1,21%	0,34%	1,08%	97,37%
Rep 2_NTHi + 10% NHS	2,22%	94,20%	1,77%	1,80%
Rep 3_Mcat	3,05%	0,86%	3,11%	92,98%
Rep 3_Mcat + 10% NHS	2,51%	94,40%	1,68%	2,62%
Rep 3_NTHi	0,89%	0,29%	1,08%	97,74%
Rep 3_NTHi + 10% NHS	2,51%	91,90%	1,68%	3,89%

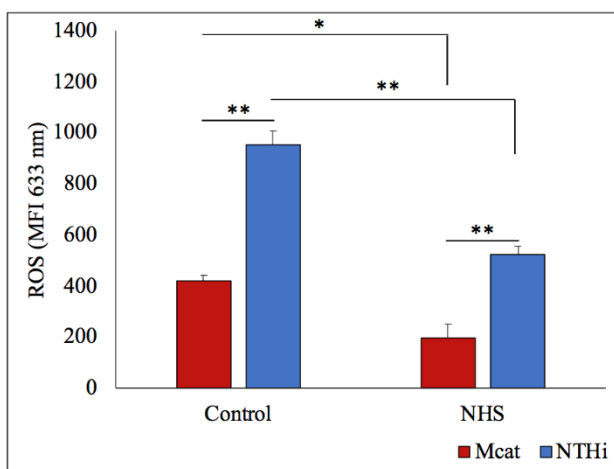
B



C



D



E

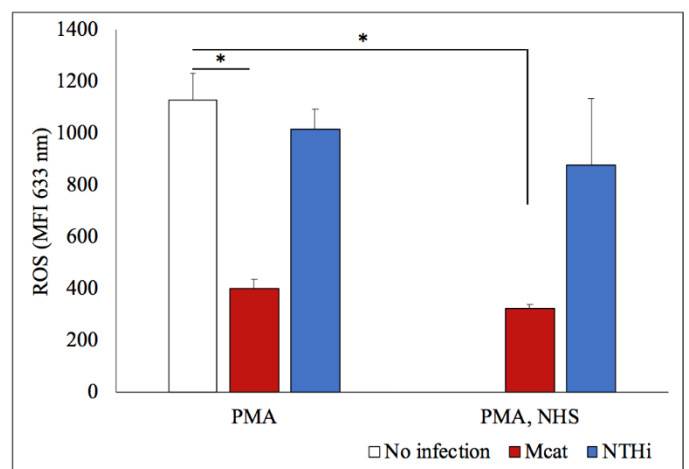


Figure 14. Human opsonins increase Mcat and NTHi neutrophil uptake without affecting their ROS response. Exponentially growing Mcat and NTHi bacteria were left unopsonized or treated with 10% of human sera,

hereafter called NHS. *M. catarrhalis* and NTHi were grown to mid-exponential phase and then treated or not with 10% of pooled human sera. (A) Flow cytometry was used to determine C3b and human IgG antibodies deposition on both, unopsonized (red signal) and opsonized (blue signal), Mcat (upper panels) and NTHi (bottom panels). A summary data of the percentage of bacteria binding to C3b (FITC+) and/or human IgG (APC+) across multiple replicate experiments was reported. (B) By dilution plating onto BHI or HAE2 plates, the number of colonies obtained per condition (w or w/o NHS) was calculated to plot CFU/ml and to determine the survival of *M. catarrhalis* and NTHi upon NHS exposure, respectively. (C) dHL-60 cells were challenged for 2 h with unopsonized or opsonized Mcat or NTHi at MOI 50. By dilution plating onto BHI or HAE2 plates, the number of colonies obtained per condition was calculated to plot CFU/ml and to determine the phagocytic uptake of *M. catarrhalis* and NTHi, respectively. (D) Non stimulated and € PMA-activated dHL60 cells were infected with *M. catarrhalis* BBH18 (red bars) or NTHi 658 (blue) at MOI 50 and ROS production at 2h post-infection was monitored using CellRox (intracellular ROS). MFI at 633 nm from at least three independent experiments at the indicated time point after infection was determined by flow cytometry. Bars represent means ± SE. MFI, Mean fluorescence intensity. *p < 0.05.

4.7 Mcat and NTHi behaviours in primary cells strongly reflect those observed in dHL-60 cells

Lastly, we verified if our main findings relate to human polymorphic nuclear leukocytes (PMNs), a more physiological condition. We challenged primary cells (PMA-activated or not) with unopsonized Mcat or NTHi (MOI 50) and, by flow cytometry, we measured the intracellular ROS production at 2 hours post-infection. Later time points were not analyzed as PMA strongly influenced the host cells viability. As shown in Figures 15A and 15B, NTHi elicited a stronger oxidative response in unstimulated PMNs and unlike Mcat, it was not able to interfere with PMA chemical activation of the host cells. Subsequently, the survival of phagocytosed bacteria and their interplays in human PMNs were evaluated by enumeration of CFU/ml. ROS-induced cells were infected with Mcat or NTHi individually at MOI 50 (red and gray spots, respectively) or with both bacteria, each at MOI 50 (co-infection, black and green spots for Mcat and NTHi, respectively) (Figure 15C). As it is shown in Table T2, the bacterial interplay was determined by dividing the CFU/ml in co-infection by that measured in single infection (ratio co/single infection). In a single infection, Mcat had proved to be a successful intracellular pathogen as more Mcat bacterial cells could survive compared to NTHi. In co-infection, the presence of Mcat strongly enhanced NTHi viability within chemically activated cells, thus providing a favorable replicative niche for NTHi (ratio co/single infection of 3.5), (Figure 15C and Table T2). NET structures were visualized by SEM (Figure 15D) and confocal microscopy (DNA, MPO and adherent, non-phagocytosed bacteria were in blue, green and red, respectively) (Figure 15E). The neutrophil extracellular traps were clearly visible both in PMA-activated cells and unstimulated cells infected by NTHi. In a single infection, NTHi was surrounded by these extracellular fibers but in co-infections, NETosis was by far lower. Interestingly, a lower amount of these microbicidal structures were present in the case of Mcat-infecting ROS-induced primary cells compared to Mcat-infecting non-stimulated neutrophils. Moreover, more grape-like structures of adherent bacteria and less internalization were present in the latter case. From the above data, we conclude that unlike Mcat, NTHi elicited more NETosis in infected cells and was not able to dampen

NET generation in PMA-stimulated or NTHi-infected PMNs. Therefore, the key findings obtained with dHL-60 cells were validated using primary cells, indicating that the observed phenotypes were not strictly related to the used cell line.

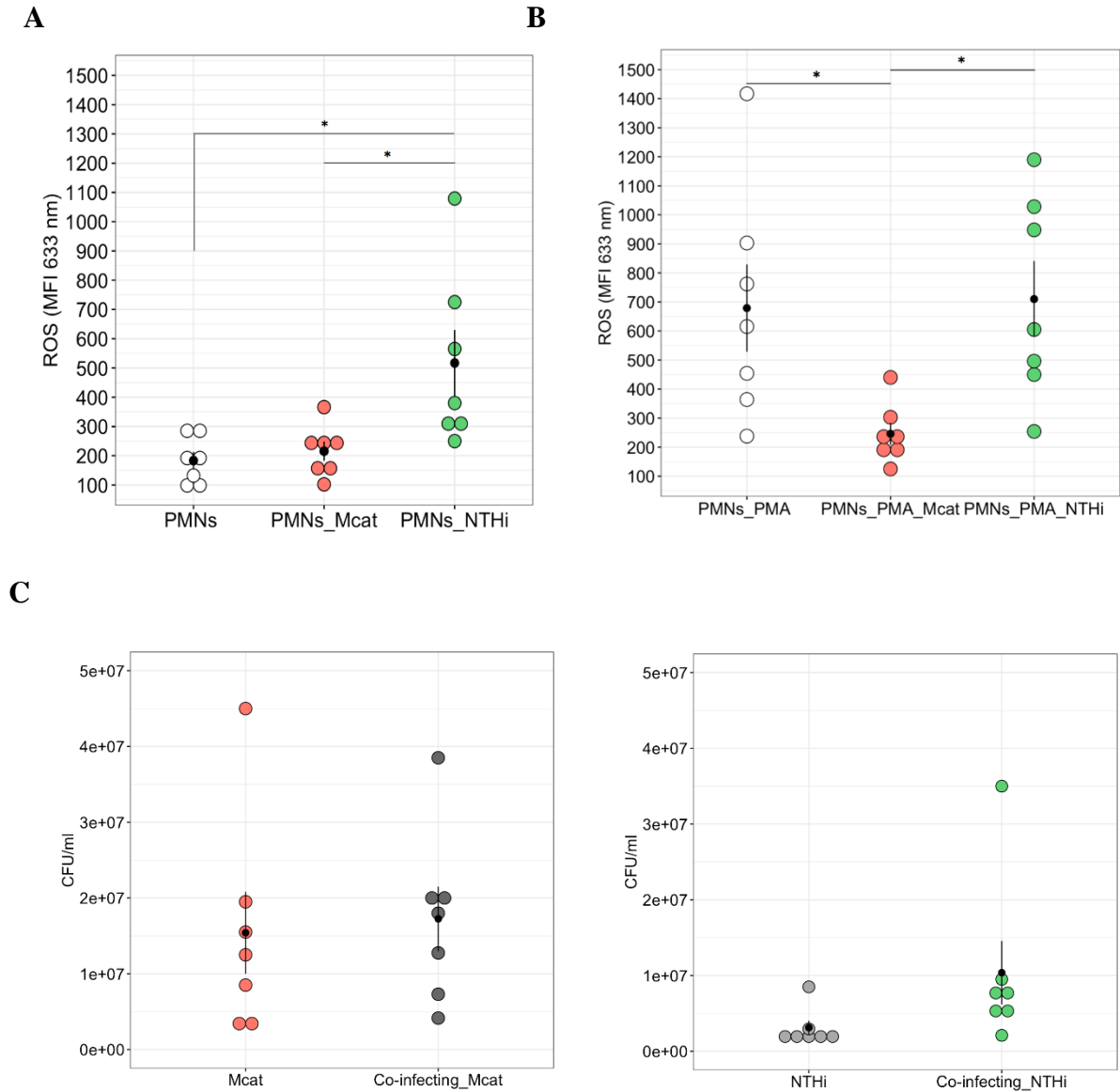


Table 2. Mcat and NTHi microbial interplays in primary cells

ROS-induced Primary cells, PMNs		
	2 h (CFU/ml)	Ratio co/single infection
Mcat	1.54E+07	
Co-infecting Mcat	1.72E+07	1.1
NTHi	3.13E+06	
Co-infecting NTHi	1.04E+07	3.3

Mcat and NTHi microbial interplay in primary cells. Table reporting the CFU/ml obtained at 2 h post-infection for *M. catarrhalis* and NTHi both in single and co-infection. The microbial interplay was determined by dividing the CFU/ml obtained in co-infection to that recorded in single infection (ratio co/single infection).

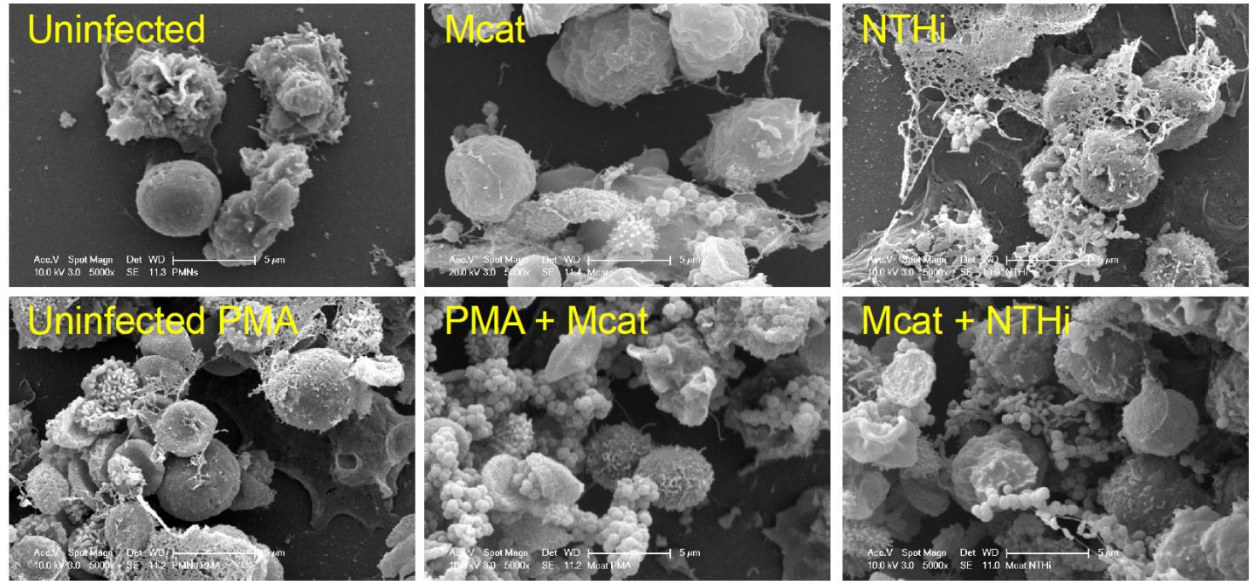
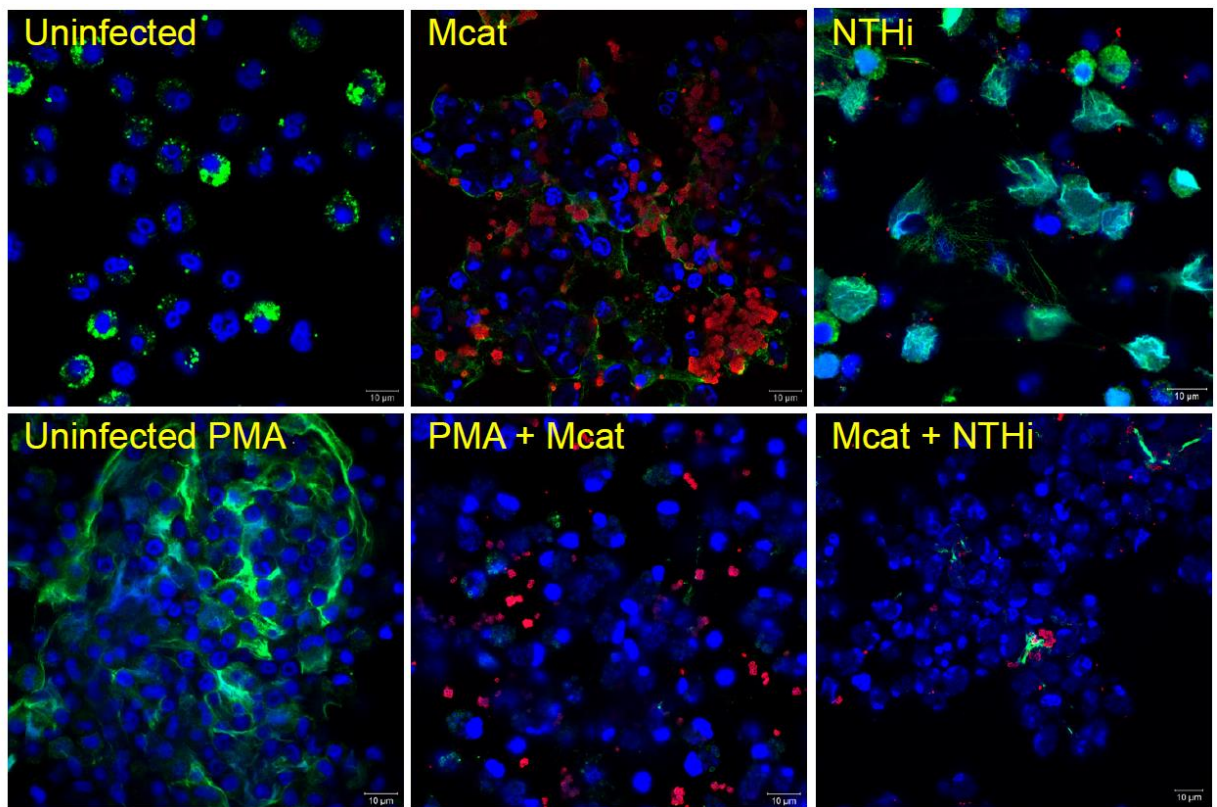
D**E**

Figure 15. Mcat and NTHi behaviors in primary cells strongly reflect those observed in dHL-60 cells PMNs (A) unstimulated or (B) PMA-activated were left uninfected (white spots) or infected with the *M. catarrhalis* BBH18 (red spots) or NTHi 658 (green spots) at MOI 50 and ROS production at 2 h post-infection was monitored using CellRox (intracellular ROS). MFI at 633 nm from seven donors was determined by flow cytometry. Bars represent means \pm SE. MFI, Mean fluorescence intensity. * $p < 0.05$. The MFI obtained for every single donor is represented by a spot. (C) PMNs were infected by only *M. catarrhalis* (red spots) or NTHi (gray spots) at MOI 50 (single infection), or with both the bacteria (co-infection with MOI 50 each bacterium, black and green spots, respectively). By dilution plating onto BHI or HAE2 plates, the number of colonies obtained per condition was calculated to plot CFU/ml and to determine the microbial interplay (ratio co/single infection) of *M. catarrhalis* and NTHi, respectively. Bars represent means \pm SE and the CFU/ml obtained for every single donor is represented by a spot. (D-E) Visualization of NET structures. Samples were fixed and analysed by scanning electron microscopy. (E) Samples were fixed and stained for DNA (blue), myeloperoxidase (green)

and adherent bacteria (red). Bacteria were detected by staining for UspA2 (rabbit polyclonal antibodies) and for whole bacteria for *M. catarrhalis* and NTHi, respectively. The stained cells were analyzed by immunofluorescence microscopy. Scale bars, 10 μ m.

5. DISCUSSION 1st part

The relationship between COPD and dysbiosis of the lung microbiome has been revealed in many studies describing a relevant increase in *M. catarrhalis* (Mcat) and nontypeable *H. influenzae* (NTHi) bacterial detection at exacerbation states (Mayhew, 2018). COPD is a progressive disease defined by neutrophilic inflammation, promoting excessive ROS generation and ROS-related responses, including neutrophil extracellular traps (NETs) and autophagy (Glasauer and Chandel, 2013). Even though growing evidence points out that the capabilities of surviving these responses are crucial bacterial virulence traits, this has not been extensively investigated in NTHi and Mcat pathogens. Here, the *in vitro* interactions of NTHi and Mcat with neutrophil-like cells were investigated. We showed that both bacteria are phagocytosed in an opsonin-independent manner. This finding is in agreement with the paper published by Schmitter *et al.* (2004). They demonstrated that granulocytes recognize these two human pathogens in an opsonin-independent manner *via* bacterial engagement to CEACAM3 receptor (Schmitter *et al.*, 2004). Nevertheless, in our study, it has been shown that the percentage of uninfected cells is by far higher in the case of NTHi infections and few bacterial cells are phagocytosed. By contrast, Mcat is rapidly internalized, is not killed and the number of internalized bacteria increases over time. We also found that both bacteria elicit significant levels of ROS compared to unstimulated cells. Our data support the findings of Heinrich *et al.* 2016, who got evidence that Mcat UspA1 engagement of human CEACAM3 receptor induces ROS generation (Heinrich *et al.*, 2016b) and those showing NTHi capable of promoting oxidative stress (Essilfie *et al.*, 2011) both in the lungs of BALB/c mice (King *et al.*, 2015) and in a tissue culture model (Kalograiaki *et al.*, 2016). However, in this work, we observed that the extent of the oxidative stress response elicited by Mcat was far lower than that of NTHi despite the higher uptake of Mcat by the dHL-60 cells. Additionally, as in COPD pathogenesis, neutrophils are defined aberrant due to the extremely high induction of ROS generation, phagocytosis, degranulation and NET production (Stockley *et al.*, 2013), the oxidative response was also evaluated in PMA chemically-activated cells. Here, we demonstrated for the first time that these neutrophil-like cells fail to respond to PMA chemical activation when infected by Mcat but not by NTHi. Therefore, contrary to other pathogens such as *S. aureus* (Beavers and Skaar, 2016) and in a similar way to group A *Streptococcus* (Uchiyama *et al.*, 2015), Mcat actively interferes with intracellular and extracellular oxidative stress response even when a strong stimulus such as PMA is present. Interestingly, in the presence of

opsonins (human antibodies and complement source), despite an expected relevant increase in bacterial uptake, the ability of Mcat to suppress ROS response was preserved, suggesting an opsonin-independent phenotype. We also confirmed these findings in primary neutrophils as, unlike NTHi, Mcat infection interferes with ROS production in PMA-activated PMNs. At the same time, no significant ROS was recorded after infection of non-stimulated PMNs.

Therefore, an in-depth investigation of the mechanisms exploited by Mcat to dampen ROS generation was pursued. It was shown that the reduction of the oxidative burst was phagocytosis-independent, contact-dependent and not due to the secretion of toxins or effector proteins. Similarly, it has been demonstrated that *Chlamydia* interferes with the PMA chemical activation of neutrophils. Nevertheless, in this case, the *Chlamydia* interference with ROS is mediated by the secreted protease-like activating factor (CPAF) that can cleave the formyl peptide receptor 2 (FPR2), an immunostimulating human receptor (Rajeeve et al., 2018). As direct contact of Mcat with neutrophil-like cells is required for the downregulation of ROS generation, we investigated the ability of Mcat to bind to different inhibitory receptors such as Sialic acid-binding immunoglobulin-type lectins (Siglecs), which can modulate oxidative stress responses (Schwarz et al., 2015). By engaging the neutrophils' inhibitory receptors Siglec-9 and Siglec-5, bacteria including *P. aeruginosa* and group B *Streptococcus* can impair the oxidative burst and NET responses (Carlin et al., 2009) (Khatua et al., 2012). Flow cytometric experiments revealed that besides CEACAM-1 binding, Mcat can engage both Siglec-5 and Siglec-9 inhibitory receptors, highlighting these as putative interactors leading to the observed suppression. However, only by blocking the cognate binding Siglec-9 partner avoids the specific binding responsible for the Mcat interference with ROS production by dHL-60 cells. As all the three receptors have an ITIM motif in their intracellular domain, conferring the ability to have an immunosuppressive role, we could only speculate on some possible explanations. Similar to what has been described for *N. gonorrhoeae* and *H. pylori*, the bacterial binding of CEACAM-1 does not abolish the activating signal of the CEACAM3 ITAM portion (Sarantis and Gray-Owen, 2012, Behrens et al., 2020). Siglec-5 ligand-binding domain is nearly identical to that of Siglec-14, which in turn is characterized by an activating ITAM-motif (Ali et al., 2014). Since neutrophils express both Siglec-14 and Siglec-5, there is the possibility that these function as paired Siglec receptors to balance immune responses (activating and repressing) in response to certain circumstances. Therefore, it would have been interesting to evaluate the specific contributions and the possible synergy of each of the three inhibitory receptors in the host cells during different temporal phases of Mcat infection.

Subsequently, we tried to identify the Mcat interactors of the neutrophils inhibitory receptors. Among the different adhesins from Mcat (Ren and Pichichero, 2016), OmpCD protein shows abundant surface-exposed epitopes and high conservation among different strains. OmpCD has

proved to be immunogenic, eliciting functional antibodies in mice and higher Mcat clearance from the lungs of challenged mice (Liu et al., 2007, Becker et al., 2007, Smidt et al., 2013). It also has adhesive properties, as it specifically binds to both human lung epithelial cells and importantly, to mucins (Akimana and Lafontaine, 2007) of different sources: salivary, nasopharyngeal, middle ear, and tracheobronchial mucins (Bernstein and Reddy, 2000). As mucins are particularly enriched with sialic acids (Haines-Menges et al., 2015), the possible interactions between this bacterial protein and human Siglec-5 and Siglec-9 receptors has been investigated. Results showed that OmpCD could bind Siglec immunosuppressive receptors, unravelling a previously unknown interaction and paving the way for better investigations on the structural features of the binding between these human receptors and Mcat OmpCD and the consequent signaling events.

Another immunological response that was investigated is NET formation. NETs represent a hallmark in COPD and are associated with ROS release (Wright et al., 2016). NET structures trap, neutralize and kill bacteria preventing their dissemination (Delgado-Rizo et al., 2017). As a matter of fact, bacterial pathogens with mutations in capsule genes (Wartha et al., 2007) or NET-degrading nucleases (Juneau et al., 2015) are defective in their ability to disseminate, enhancing their NET trapping *in vitro* (Papayannopoulos, 2018). Using both qualitative and quantitative approaches, we demonstrated that Mcat not only induces NETosis in infected cells to a lower extent compared to NTHi, but it can interfere with this response in PMA-activated cells and cells co-infected by NTHi. The latter has already been shown to elicit a strong oxidative burst and NETs responses (Kalograiaki et al., 2016) (King et al., 2015) and to exploit NETs for its survival in the middle ear (Juneau et al., 2011). It has recently been speculated that NTHi uses a phase variation mechanism to survive and/or evade within NETs (Robledo-Avila et al., 2020). Hence, it can be hypothesized that the predominant phase-variation occurring in the used NTHi strain promotes a prominent NET response, determining the significant killing of this bacterium. Similar to NTHi, the pore-forming toxin leukotoxin GH from *S. aureus* is known to drive NETosis (Malachowa et al., 2013). Furthermore, a recent intriguing study has revealed that through NET structures, neutrophils may cooperate with macrophages in the clearance of infections caused by *S. aureus* (Monteith et al., 2021). By examining the aforementioned examples in the bacterial responses to the NET formation, it would be interesting to analyze the role of Mcat nucleases and the cooperation between mature macrophages and neutrophils rather than isolated innate immune cells.

The last immunological response that was examined is autophagy, a homeostatic process that maintains cellular functions and is also exploited against microbes (a process referred to as xenophagy), (Levine and Kroemer, 2008, Jo et al., 2013). By controlling bacterial replication, autophagy plays a fundamental role in activating of both innate and adaptive immunity (Lamark et

al., 2009). Generally, successful intracellular pathogens antagonize both the signaling events that activate autophagic response as well as the trafficking events necessary for lysosomal delivery and degradation. This is the case of *M. tuberculosis* that interferes with phagolysosome biogenesis (Gutierrez et al., 2004) and whose LprE lipoprotein impairs the autophagic pathway to enhance bacterial survival within macrophages (Padhi et al., 2019). By contrary, medically important pathogens such as *Salmonella enterica* are degraded by xenophagy (Wild et al., 2011). Here, by the levels of expression of the LC3-II marker, it is shown that Mcat interferes with the autophagic pathway of dHL-60 cells while NTHi does not. These observations were supported by EM images. In fact, the number of Mcat bacteria increases over four hours of infection. In addition, the morphology of uninfected cells or Mcat-infected cells has been shown to be very similar, indicating that Mcat poorly influenced host viability. More prominent phenomena of apoptosis (as apoptotic bodies formation) were observed in the NTHi-infected cells despite a low number of internalized bacteria. We can hypothesize that Mcat may provide itself with an intracellular safe replicative niche where autophagy is inhibited, apoptosis is delayed, and phagolysosomes evaded. However, how Mcat survives within the host cells and antagonizes the autophagic pathway remains to be fully elucidated. We can only speculate that different strategies can be exploited: by interfering with the a) signaling pathways that induce autophagy and b) the membrane trafficking events responsible for lysosomal delivery or c) by directly targeting MAMs (mitochondria-associated endoplasmic reticulum (ER) membranes), the organelle where autophagosomes are generated (Escoll et al., 2016). Indeed, we have demonstrated that dHL-60 cells failed to clear Mcat infections, suggesting an obvious capability to subvert and exploit the host immune responses to facilitate its replicative life cycle. Hence, neutrophil-like cells are a target of Mcat infection, providing a safe replicative niche. By contrast, NTHi seems to be highly susceptible to the antimicrobial arsenal mounted by the host cells with ROS and likely NETosis and autophagy playing an important bactericidal effect. Another interesting observation is that, in PMA-stimulated neutrophil-like cells, Mcat provided a benefit of survival for NTHi, favoring its persistence within the host cells by protecting the co-infecting bacterium from the oxidative burst and NETs. Even if a unique time point was considered, Mcat-infecting PMNs dramatically reduced NTHi killing compared to a single infection (fold increase of 3.3). Curiously, all these microbial interplays resemble those occurring between *N. gonorrhoeae* and *C. trachomatis* in the urogenital tract in which the latter provides a safer niche for the co-infecting bacterium. Nevertheless, the mechanisms by which Mcat reprograms the host antimicrobial responses to survive and enhance NTHi internalization and viability have to be unraveled.

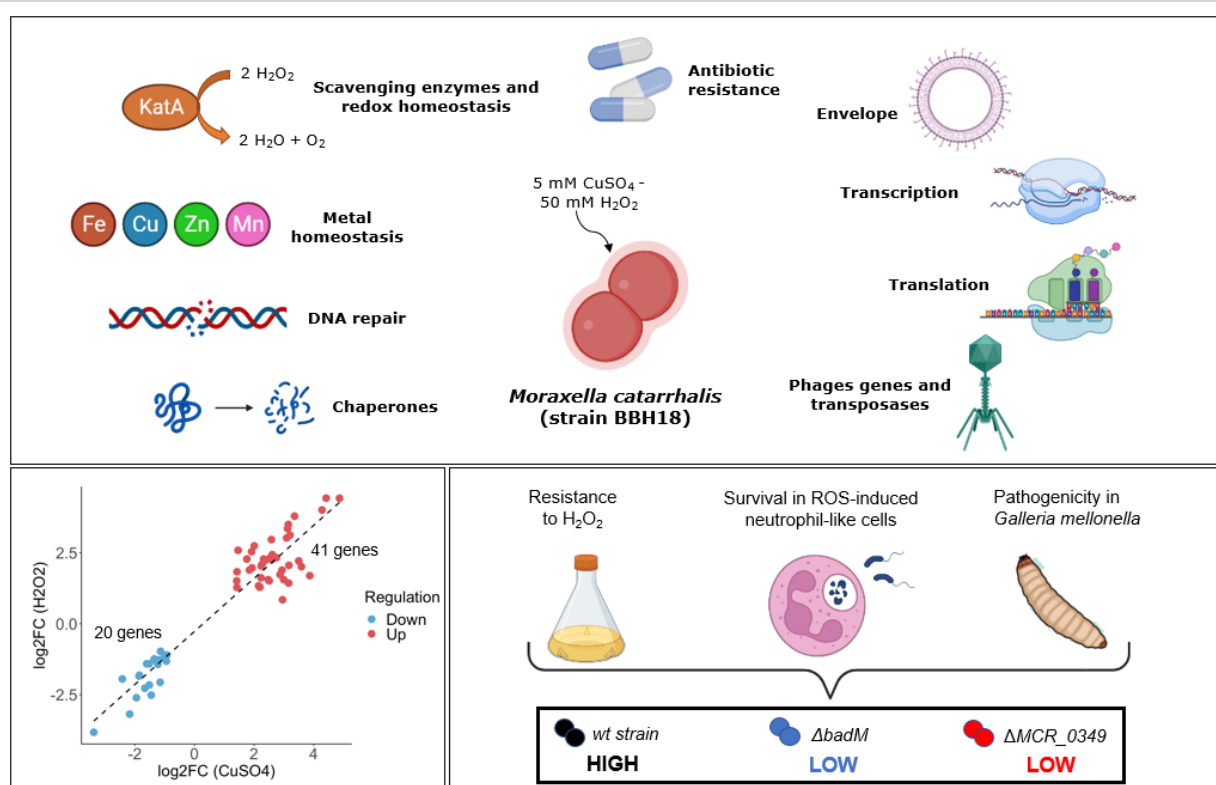
Altogether, we set up an *in vitro* model that mimics the oxidative environment that bacterial pathogens normally encounter within the infected tissues and provided a framework to improve the

understanding of how Mcat and NTHi cope with oxidative stress. Results have shown that Mcat impairs efficient innate immune responses by acting on different defenses such as ROS, phagocytic killing, NETosis and autophagy through an unknown contact-dependent mechanism. In co-infection, Mcat protects NTHi from the activated neutrophils' responses that may be active in the common anatomical niches. In fact, other studies have described synergies between these two human pathogens that colonize similar niches such as the nasopharynx and middle ears (Lee et al., 2020, Yamanaka et al., 2008). Interestingly, pneumococcus can produce millimolar amounts of hydrogen peroxide reducing the viability of competing bacteria. This is particularly true for NTHi (Johnson et al., 2015b, Wypych et al., 2019). By contrast, Mcat was shown to be highly resistant to this exogenous oxidative compound compared to the co-infecting pathogens *S. pneumoniae* and *H. influenzae* (Pericone et al., 2000, Hoopman et al., 2011), even if the underlying mechanisms are currently not well cleared. Moreover, Mcat outer membrane vesicles (OMV), enriched with complement resistance factors and beta-lactamase enzyme, act distally, favoring a safer niche for pathogens such as *S. pneumoniae* and NTHi. These bacteria colonize the same anatomical sites and which would otherwise be vulnerable to host innate immune factors and beta-lactam antibiotics (Schaar et al., 2011, Tan et al., 2007). To conclude, all the works done so far point out that even if initially considered a commensal, Mcat is a harmful co-pathogen (Barker et al., 2015, D'Anna et al., 2020). Thus, an in-depth understanding of the strategies that Mcat exploits to tackle the host innate immune responses and interplays with NTHi and *S. pneumoniae* in the human host cells, such as activated neutrophils, evaluating how they interact to influence each other could prompt prophylactic and therapeutic medical interventions for COPD and potentially, other diseases including acute otitis media.

6. BACKGROUND 2nd PART AND GRAPHICAL ABSTRACT

The second aim of the research in this thesis was to expand the knowledge of Mcat intrinsic resistance to exogenous oxidative stress. Therefore, RNA-Seq of exponentially growing Mcat exposed to sublethal amounts of H₂O₂ or CuSO₄ was performed. In both cases, we reported the highly significant regulations of known resistance mechanisms along with other pathways having less obvious associations with the oxidative stress response such as the glyoxylate metabolism and modulation of LOS and porins of the bacterial envelope. Comparing the two transcriptomes of Mcat treated with H₂O₂ or CuSO₄ a relevant overlap existing between the two transcriptional responses was unravelled. Finally, we selected ten genes to generate knock-out mutants that we validated in terms of sensitivity to H₂O₂ and tested for intracellular survival in ROS-induced neutrophil-like cells. Among them, the transcriptional regulator *badM* and *MCR_0349-MCR_0348* operon emerged as crucial in the response. Interestingly, the three genes are well conserved among different strains, suggesting their relevance for the oxidative stress response across different Mcat isolates. Moreover, *Galleria mellonella* has been used as a valuable *in vivo* infection model for Mcat pathogenesis with $\Delta badM$ and ΔMCR_0349 mutants showing reduced virulence. Thus, we identified new factors as essential in this complex response, improving our understanding of Mcat innate resistance to oxidative stress.

GRAPHICAL ABSTRACT



7. RESULTS 2nd part

7.1 Identification of a previously unknown overlap between Mcat transcriptional responses to H₂O₂ and CuSO₄

To investigate the global transcriptional response of Mcat exposed to H₂O₂ and CuSO₄, sublethal concentrations were previously determined to measure the maximal transcriptional response while not affecting bacterial viability. Briefly, RNA was harvested from exponentially growing bacteria that left untreated or treated with 50- or 5 mM of H₂O₂ and CuSO₄ for 15 minutes, respectively. From the MiSeq run, a high-quality data set was obtained with 1.5-3 million reads per sample. Following data processing, compared to untreated Mcat bacterial cells, 225 genes were called as differentially expressed (DE) by DeSeq2 as a consequence of H₂O₂ exposure (out of a total of 1720 predicted genes, ~ 13% by using an adjusted p-value ≤ 0.01). Among them, 128 and 97 genes emerged as up-regulated and down-regulated, respectively (Figure 16A). In the case of CuSO₄ treatment, a total of 140 DE genes were identified, of which 113 were found to be up-regulated and 27 down-regulated (~8%, adjusted p-value ≤ 0.01) (Figure 16A). As it is shown by the volcano plots (Figure 16A), the top 30 significantly DE genes upon H₂O₂ or CuSO₄ stimuli were similar in terms of both significance and regulation (e.g., the primary scavenger *ahpC* gene). Therefore, we sought to compare the two Mcat transcriptomes and interestingly, from the intersection of all Mcat DE genes after the two treatments, an overlap of 61 genes was identified (specifically 41 as commonly up-regulated and 20 down-regulated genes), (Figure 16B). Only the nuclease subunit *sbcC* gene appeared to be regulated in an opposite way in the two conditions (Figure 16D). The existence of a very similar transcriptional response mounted by this human pathogen upon exposure to H₂O₂ or CuSO₄ was revealed by correlating the log₂ fold changes for commonly DE genes. Indeed, a strong correlation (Pearson R² coefficient=0.9493) was observed (Figure 16D). Subsequently, we investigated whether the gene transcripts were enriched in specific biological processes. By using a hypergeometric test, among the DE genes, few statistically enriched KEGG pathways were identified (Figure 16C). Six pathways were enriched upon H₂O₂ treatment, in order of significance: “Lipopolysaccharide biosynthesis”, “Bacterial secretion system”, “Quorum sensing”, “Glyoxylate and decarboxylate metabolism”, “Lysine biosynthesis” and “Protein export”. The six pathways enriched upon CuSO₄ exposure were, in order of significance, the following: “Sulfur metabolism”, “Glyoxylate and decarboxylate metabolism”, “Selenocompound metabolism”, “RNA degradation”, “Monobactam biosynthesis” and “Nucleotide excision repair”. Interestingly, the “Glyoxylate and decarboxylate metabolism” was revealed as a KEGG-enriched pathway found in Mcat exposed to both stimuli. Nevertheless, as a high

portion of all DE genes was not categorized in any KEGG functional pathways, we performed a deeper analysis for these “uncategorized” genes by blast and study of existing literature. This led to the identification of 13 major functional categories encompassing many biological processes (Figure 16D). The most intriguing aspects emerging from the analysis of the 13 functional categories are disclosed in these six following sections.

1) Scavenging and redox genes are among the most significantly regulated genes: Approximately half of the most significant 30 DE genes upon H₂O₂ exposure belonged to scavenging and redox enzymes. Several genes such as the alkyl hydroperoxide reductases *ahpCF*, the catalase *kataA* and the thioredoxin *trx*, known members of the *oxyR* regulon, were among the top up-regulated genes in our analysis. Nevertheless, the gene expression of *oxyR* was not affected by H₂O₂, suggesting the existence of a translational or post-translational activation, and only slightly influenced after CuSO₄ treatment maybe representing a more stressful situation for the bacterium. Additionally, several uncharacterized genes emerged in this functional category. Among them, an operon composed of two poorly characterized redox genes, a putative nitroreductase (*MCR_0568*) and a NADPH dehydrogenase (*MCR_0569*), was found to be significantly up-regulated following H₂O₂ treatment.

2) Mcat modulates the expression of genes associated with damages of proteins and nucleic acids: ROS can damage proteins leading to their misfolding and altered intracellular redox (Imlay, 2013). Thus, chaperones are fundamental for protecting proteins in their conformation and refolding misfolded proteins. In particular, upon CuSO₄ exposure, the majority of the most significantly up-regulated genes specifically belonged to chaperones and folding catalysts, such as the chaperonins *groES* and *groEL* and the molecular chaperone *htpG*. As ROS can also damage nucleic acids, modulation in the expression of genes related to the base excision repair (BER) pathway and SOS response pathway, which elicits the UvrABC excision nuclease and the Rec recombinational machinery (Mullins et al., 2019), were observed.

3) The role of copper and iron homeostasis in Mcat oxidative response: Metal homeostasis is another crucial pathway that was highly involved in H₂O₂ and CuSO₄ responses. Interestingly, *MCR_1049* encoding for a copper-translocating P-type ATPase emerged as significantly regulated upon both stimuli, underlying the fact that copper homeostasis is important for Mcat resistance to oxidative stress. Furthermore, we observed high transcript levels for Fur, the global transcriptional regulator involved in maintaining iron homeostasis, and for the BadM/Rrf2 family transcriptional regulator (*MCR_0609*) that we found to be homologue to the *Neisseria spp* and *E. coli iscR* (Imlay, 2015). Two main categories of iron-associated genes were identified: one involved in iron transport (*tonB*, *exbB*, *exbD*, and *efeO*) and the other involved in the biosynthesis of Fe-S cluster-containing

enzyme centers (iron-sulfur cluster genes, including *hscB* and *iscSUA*). Moreover, many different operons involved in iron homeostasis and sulfur metabolisms were found to be modulated, such as the one of chelated iron ABC transporter *afeA* and *afeB*, and the sulfate ABC transporter permease protein genes *cysU* and *cysW*, indicating that iron homeostasis is also crucial for Mcat oxidative stress response.

4) Mcat exploits glyoxylate metabolism to tackle the oxidative stress: In response to both treatments, the Mcat general metabolism was also influenced, such as arginine and lysine biosynthesis. Furthermore, among the most significantly DE genes upon both stimuli, we observed the isocitrate lyase *aceA* and the malate synthase *aceB* belonging to the glyoxylate metabolism. This shunt, not present in all bacteria, represents an alternative pathway of the TCA cycle that lowers the production of oxidant NADH promoting the antioxidant NADPH generation (Van Acker and Coenye, 2017).

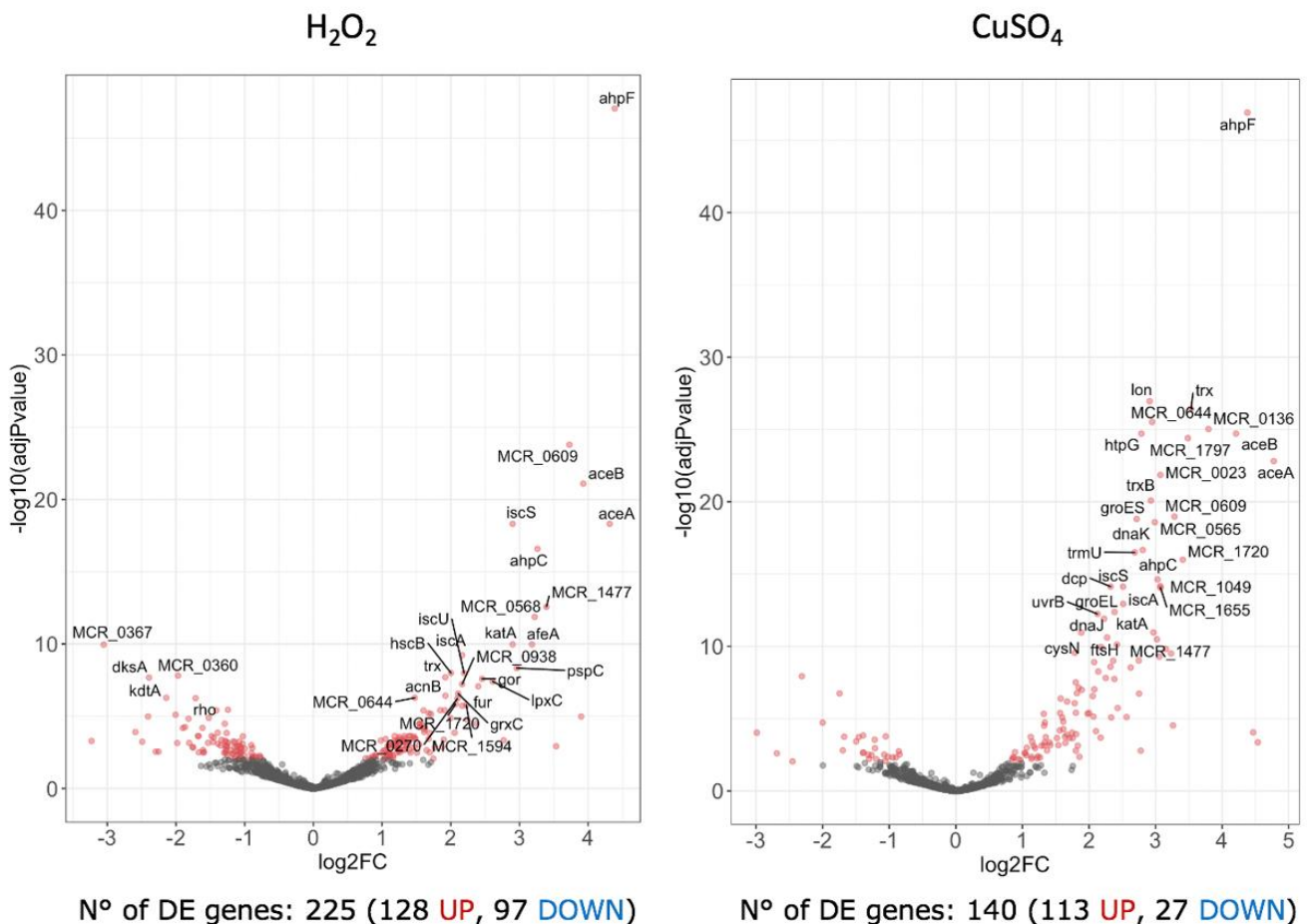
5) Mcat envelope rearrangements in response to ROS: Interestingly, we identified the regulation of various genes encoding for porins, LPS/LOS and peptidoglycan structures, revealing the occurrence of envelope rearrangements, accompanied by a modulation of the expression of genes associated with antibiotic resistance mechanisms. In particular, LPS biosynthesis emerged as the first significantly enriched KEGG-pathway upon H₂O₂ treatment. The up-regulated *lpxC* gene is known to catalyze the deacetylation of UDP-3-O-(acyl)-GlcNAc, which is the lipid A biosynthesis commitment step (Wang and Quinn, 2010). Curiously, many other genes that follow *lpxC* in the enzymatic cascade leading to LOS biosynthesis were downregulated. In this context, of note are the down-regulation of the lipid A disaccharide synthase *lpxB*, the UDP-3-O-[3-hydroxymyristoyl] glucosamine N-acyltransferase *lpxD*, the decanoyltransferase *lpxX*, the lipid A ethanolaminephosphotransferase (*MCR_1292*), the rare lipoprotein A family gene *rlpA*, the 3-deoxy-D-manno-octulosonic-acid transferase *kdtA* and the reductase *murB*. Up-regulation of genes putatively associated with antibiotic resistance, such as *ampD* and *glmM*, and down-regulation of the outer membrane porin M35 (*MCR_1247*), were also identified.

6) Mcat modulation of the transcriptional and translational machineries: Finally, we reported modulation of translation, phages, and transposases associated-genes. It is also recorded a lower transcript abundances of transcription-associated genes such as the RNA polymerase-binding protein *dksA*, the transcription elongation factor *greA* and the termination factor *rho*, indicating a possible formation of longer transcripts with regulatory roles in gene expression. In addition to the aforementioned *fur* and *badM*, treatment with H₂O₂ was associated with the induction of a number of regulators such as the putative stress-responsive regulator *pspC*, the poorly characterized small

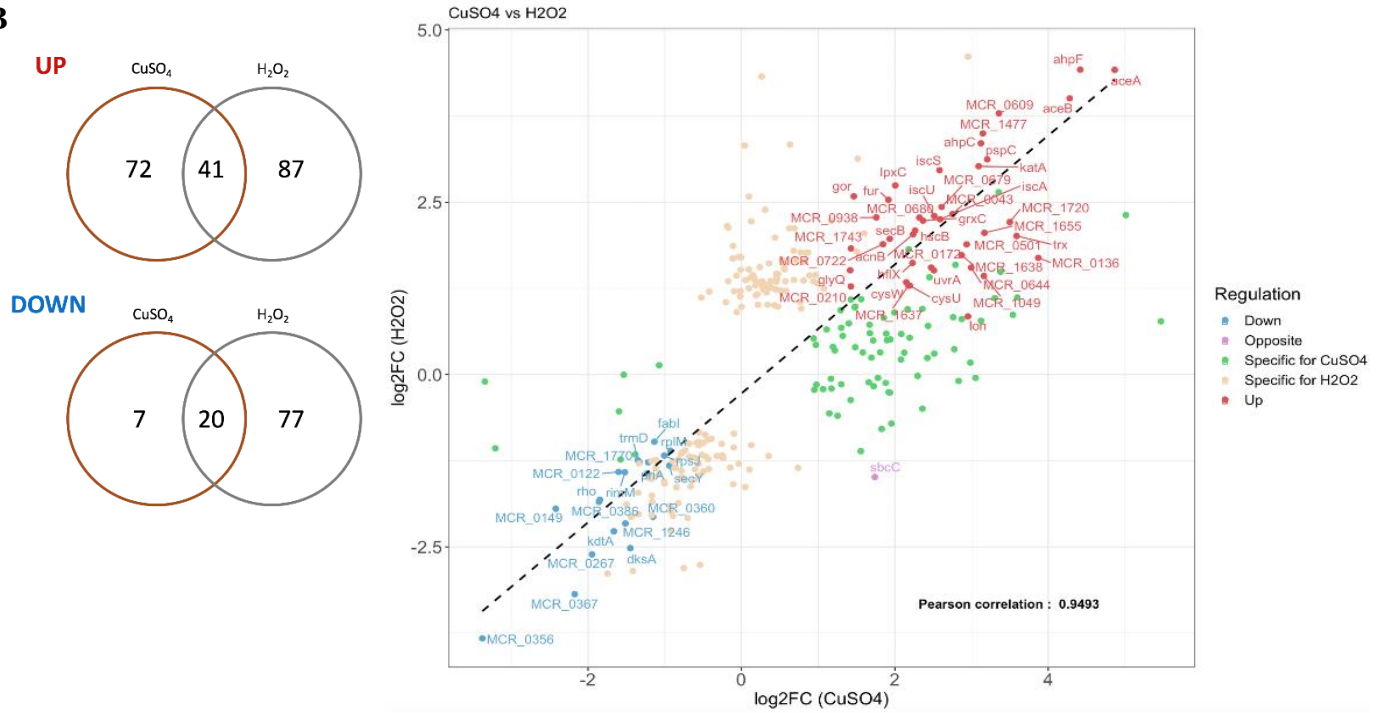
regulatory 6S RNA, the two-component system response regulator *ompR* and the one for the phosphate regulon *phoB*, suggesting a link between oxidative stress and phosphate starvation.

Validation of the RNA-Seq results were performed by qPCR on eight selected genes (*MCR_1049*, *lpxC*, *badM*, *fur*, *iscS*, *katA*, *MCR_1477* and *MCR_0644*). These were selected among the highly DE genes ones following both treatments and associated with different biological categories, obtaining a good correlation for the log₂ fold change values reported by the RNA-Seq and the qPCR analysis (Pearson R² coefficients equal to 0.73 and 0.64 for H₂O₂ and CuSO₄, respectively) (Figure 16E and Table T3). For the first time, the comparative analysis revealed that Mcat orchestrates a joint transcriptional response to H₂O₂ and CuSO₄ stimuli, modulating known genes linked with intrinsic resistance mechanisms and uncharacterized genes and pathways with less obvious involvement with the oxidative stress response.

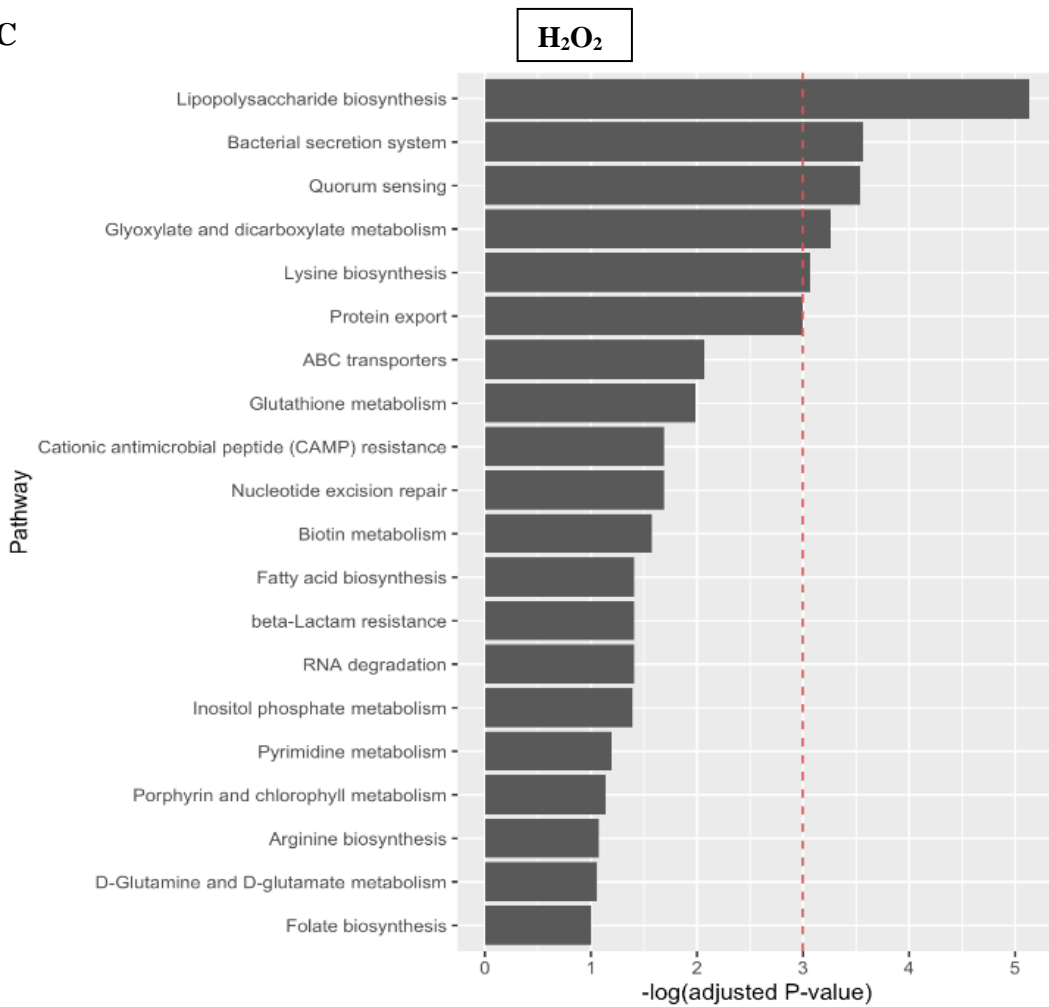
A

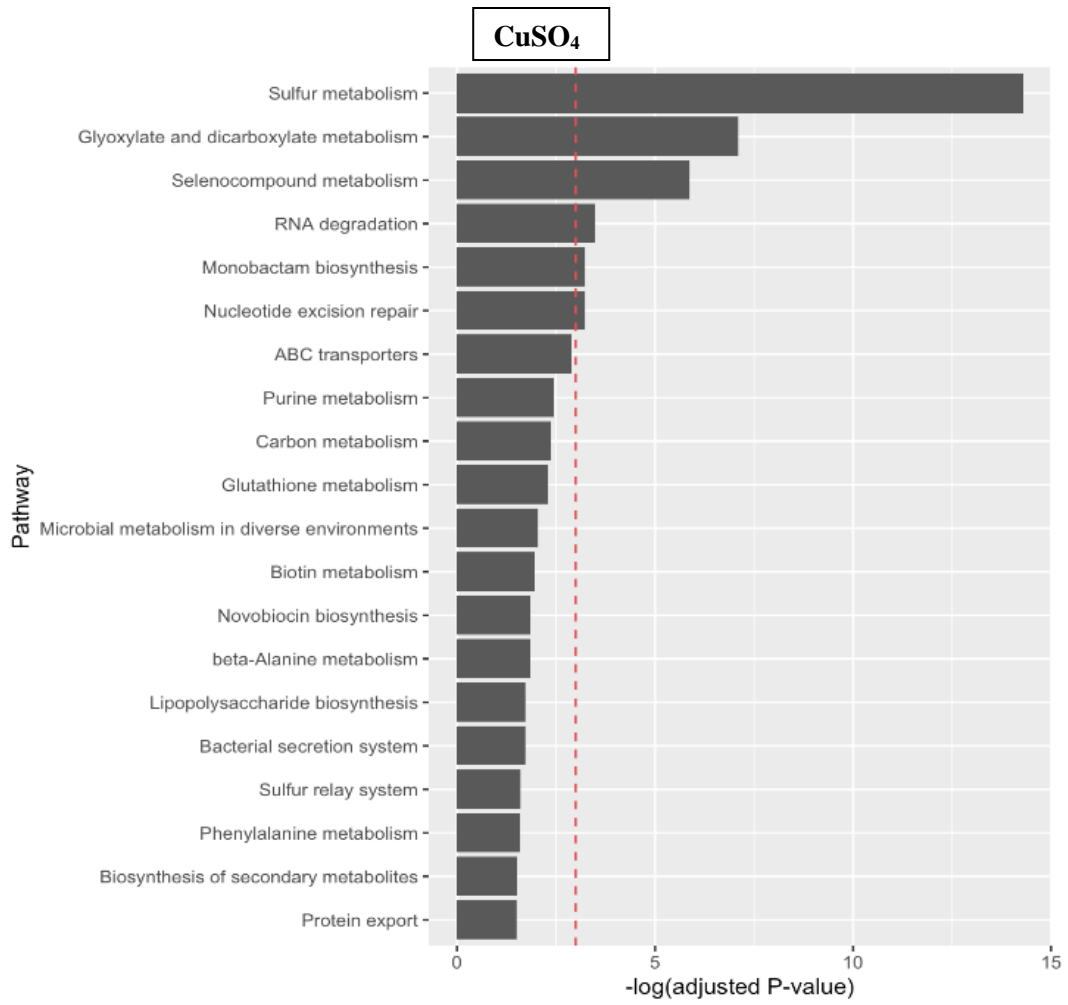


B

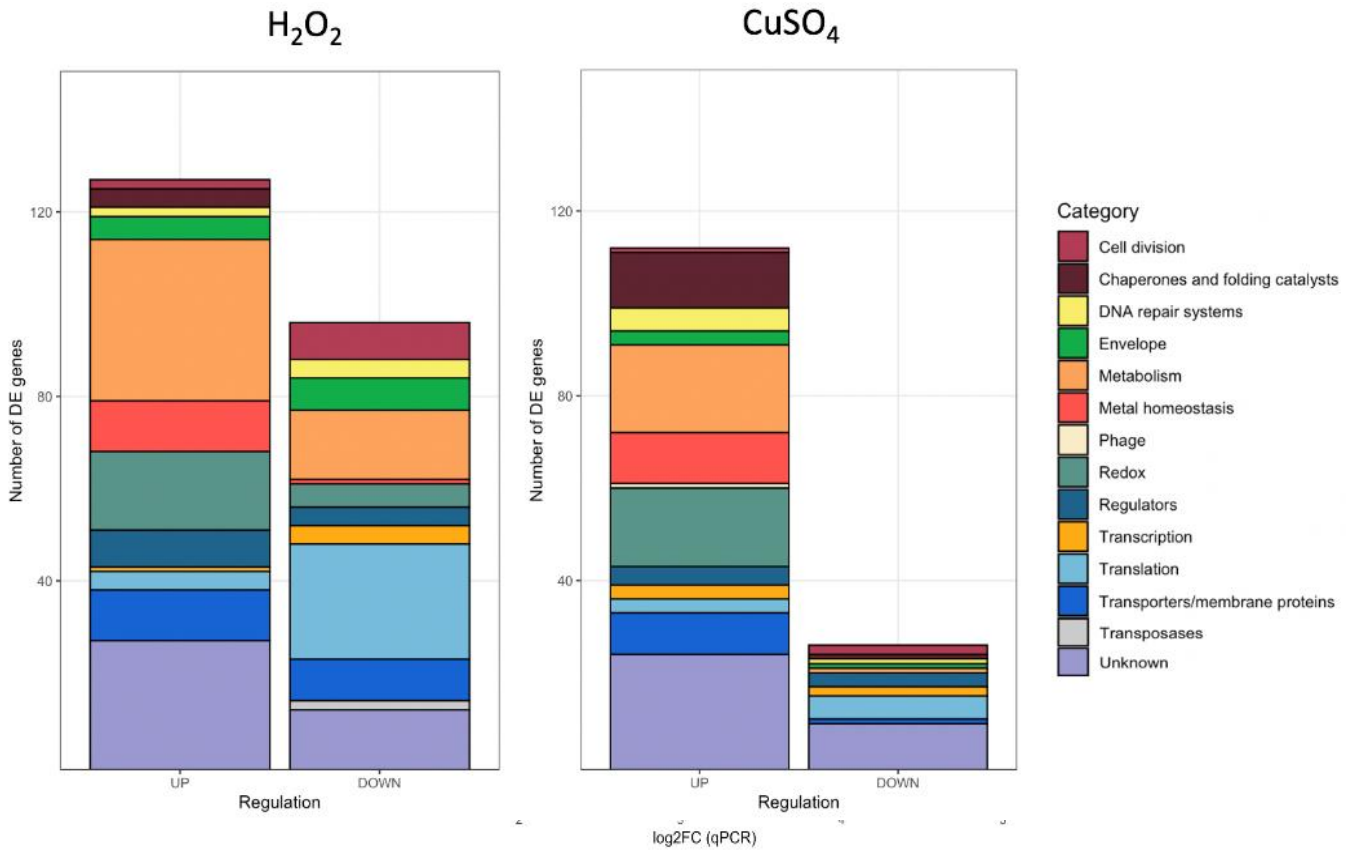


C

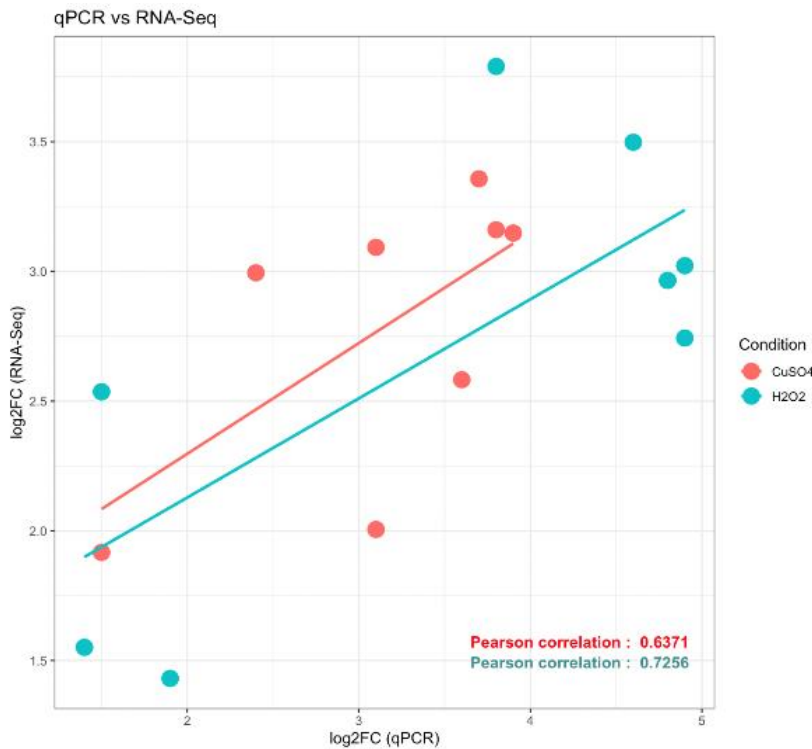




D



F



Gene	log2Fold	
	H ₂ O ₂	CuSO ₄
<i>MCR_1049</i>	1,9	3,8
<i>lpxC</i>	4,9	3,1
<i>badM</i>	3,8	3,7
<i>fur</i>	1,5	1,5
<i>iscS</i>	4,8	3,6
<i>katA</i>	4,9	3,1
<i>MCR_1477</i>	4,6	3,9
<i>MCR_0644</i>	1,4	2,4

Table T3. Table showing the RT-qPCR-log2Fold changes of 8 genes after H₂O₂

and CuSO₄ treatments: *MCR_1049*, *lpxC*, *badM*, *fur*, *iscS*, *katA*, *MCR_1477* and *MCR_0644*.

Figure 16. Identification of an unknown overlap between H₂O₂ and CuSO₄ Mcat transcriptional responses. RNA was extracted from at least three independent experiments in which *M. catarrhalis* BBH18 strain was grown in BHI at 37°C, 185 rpm to mid-exponential phase and then untreated or exposed for 15 min to H₂O₂ or CuSO₄ to a final concentration of 50 mM and 5 mM, respectively. **A)** The volcano plot combines the statistical significance (Adjusted p-value ≤ 0.01) with the magnitude of the change. The dots on the scatter plot denote an individual gene, with black dots indicating genes without significantly different transcript abundance between conditions, and red dots indicating genes with significant differences in transcript abundance in H₂O₂ and CuSO₄-treated *M. catarrhalis* BBH18 compared to untreated counterpart. **B)** Evaluation of the intersection H₂O₂ or CuSO₄-treated *M. catarrhalis* BBH18 transcriptomes showing the number of genes commonly DE and a plot showing the strong correlation between the log₂ fold changes of all DE genes in the two conditions, (Pearson R² coefficient=0.9493). **C)** The sets DE genes were tested for enrichment in specific functional KEGG pathways, using an adjusted p-values < 3%. **D)** All DE genes were broadly categorized according to H₂O₂ or CuSO₄ treatments and up- or down-regulation within 13 biological functions: cell division, chaperone and folding catalyst, DNA repair system, envelope, metabolism, metal homeostasis, oxidative/redox-genes, phage, regulators, transcription, translation, transporter/outer membrane proteins, transposase and unknown. Each bar represents the number of genes and each functional category is shown with a different color. **E)** RT-qPCR was performed on different biological replicates of those used for the RNA-Seq experiments. The validation of the RNA-seq results was carried out for a subset of 8 genes, selected for their relevance in DE-analysis and from different functional categories. RT-qPCR fold induction values was calculated using the 2^{ΔΔCT} method and plotted against RNA-Seq fold induction values, showing a good correlation (0.72 and 0.64 for H₂O₂ and CuSO₄ treatments, respectively).

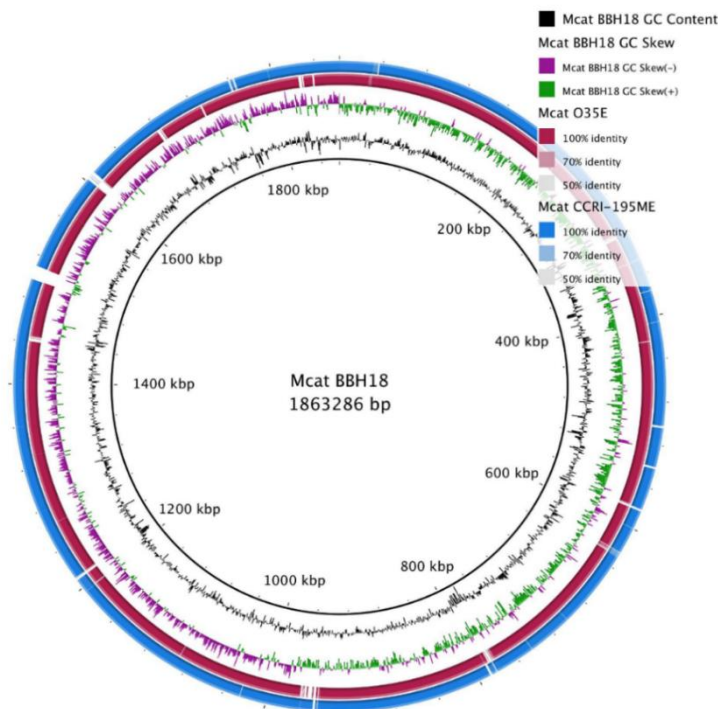
7.2 Co-expression network analysis, relevance in DE analysis and functional categories guide the selection of ten genes for functional characterization

From RNA-seq analyses, approximately 12-14% of the DE genes were not classified in any known major regulatory networks or functional pathways. To deduce their function, a co-expression network was built by Weighted Correlation Network Analysis (WGCNA), combining the data obtained for Mcat BBH18 with two other publicly available Mcat RNA-seq data sets on two strains: O35E (evaluation of the DE genes in Mcat exposed to continuous growth at 37 °C or 26 °C cold shock) and CCRI-195ME (evaluation of the epigenetically regulated genes by phase variation of the DNA methyltransferase ModM3) (Spaniol et al., 2013, Blakeway et al., 2019). This has been possible thanks to the high percentages of nucleotides identity between our laboratory strain and the other two strains (Figure 17A). From the resulting network, eight modules or communities of co-expressed genes associated with different putative biological functions were identified (Figure 17B). Most of the unknown DE genes belonged to modules called 2 (number of genes, n=311), 5 (n=102) and 7 (n=233). We further investigated the ten most highly connected genes present in the vicinity of the first significantly DE unknown genes *MCR_1477*, *MCR_0644* and *MCR_0349* of modules 2, 5 and 7, respectively (Figure 17C). *MCR_1477*, an orthologue of the peroxidase stress gene *yaaA*, was highly connected to the two enzymes (*aceAB*) of the glyoxylate cycle, the cell division gene *ftsW*, the translocase subunit *secY* and the gene encoding GTP-binding protein *typA*. Nevertheless, no homology with other bacterial genes was found for the *MCR_0644* and *MCR_0349* genes. *MCR_0644* was highly connected to the Fe/S biogenesis gene *nfu*, the thioredoxin *trx* gene and the putative stress-responsive transcriptional regulator *pspC*. The most interesting highly connected genes for *MCR_0349* were the acetolactate synthase large subunit *ilvB*, the family integral membrane protein MarC involved in antibiotic resistance (*MCR_0873*), the cytochrome c class I (*MCR_1594*), the D-isomer specific 2-hydroxyacid dehydrogenase (*MCR_0409*) and a polyisoprenoid-binding protein (*yceI* or *MCR_0657*), that has been shown to play crucial roles in respiratory electron transport, in controlling gene regulation and oxidative stress (Sisinni et al., 2010).

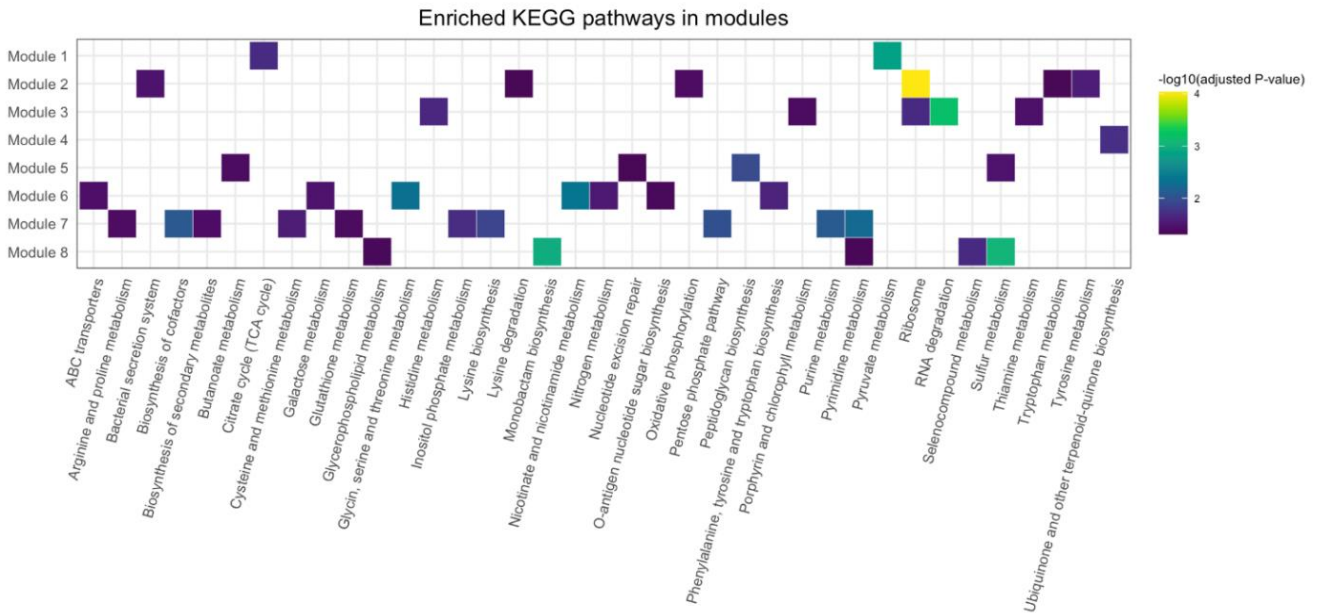
Together with the three unknown genes, seven up-regulated genes (*kataA*, *lpxC*, *cysP*, *afeA*, the K18829 antitoxin *vapB* or *MCR_1638*, *badM/rrf2* family transcriptional regulator and the copper-translocating P-type ATPase *MCR_1049*) were subsequently selected due to their significance, as commonly DE genes as a consequence of the two stimuli (H₂O₂ and CuSO₄) or known virulence factors (Table T4). 1) The *kataA* gene, known as a member of the *oxyR* regulon, encodes the enzyme responsible for the dismutation of H₂O₂ into O₂ and H₂O, leading to the detoxification of this type of ROS (Imlay, 2008). 2) The *lpxC* gene encodes an enzyme that catalyzes the deacetylation of UDP-3-

O-(acyl)-GlcNAc, the actual lipid A biosynthesis commitment step (Wang and Quinn, 2010). 3 and 4) The *cysP* and *afeA* genes encode conserved lipoproteins representing known nutritional virulence factors and whose deletions reduce the Mcat invasion of human respiratory epithelial cells. Moreover, they have been demonstrated to elicit potentially protective responses in the mouse pulmonary clearance model (Murphy et al., 2016, Murphy et al., 2017). 5) The putative *vap* gene was selected as an interesting target being recognized as a part of a toxin-antitoxin (TA) system and pathogenicity islands (PAI) important for bacterial adaptation to newly infected niches (Demidenok et al., 2014). Under stressful conditions, including oxidative stress, the labile antitoxin is degraded by either the Clp or Lon proteases (both UP-regulated in our RNA-seq analysis). The more stable toxin (usually an mRNA-specific RNase) promotes a dormant stage (bacteriostasis) that allows bacteria to face stress (persister cells formation) (Maisonneuve and Gerdes, 2014, Harms et al., 2018). 6) *badM* gene encodes an iron-sulfur cluster assembly regulator homolog, fundamental for bacterial defense against ROS (Imlay, 2015). Interestingly, this transcriptional regulator was present in module 2 and connected to the *MCR_1477* unknown gene. 7) *MCR_1049* is possibly a Cu¹⁺ exporter responsible for the efflux of copper ions from the cytoplasm into the periplasmic space, important for copper tolerance in bacteria (Ladomersky and Petris, 2015), a poorly studied mechanism in Mcat pathogenesis. The list of the ten selected genes with their relevance in DE analysis and their functions (putative or not) is reported in Table T4.

A



B



C

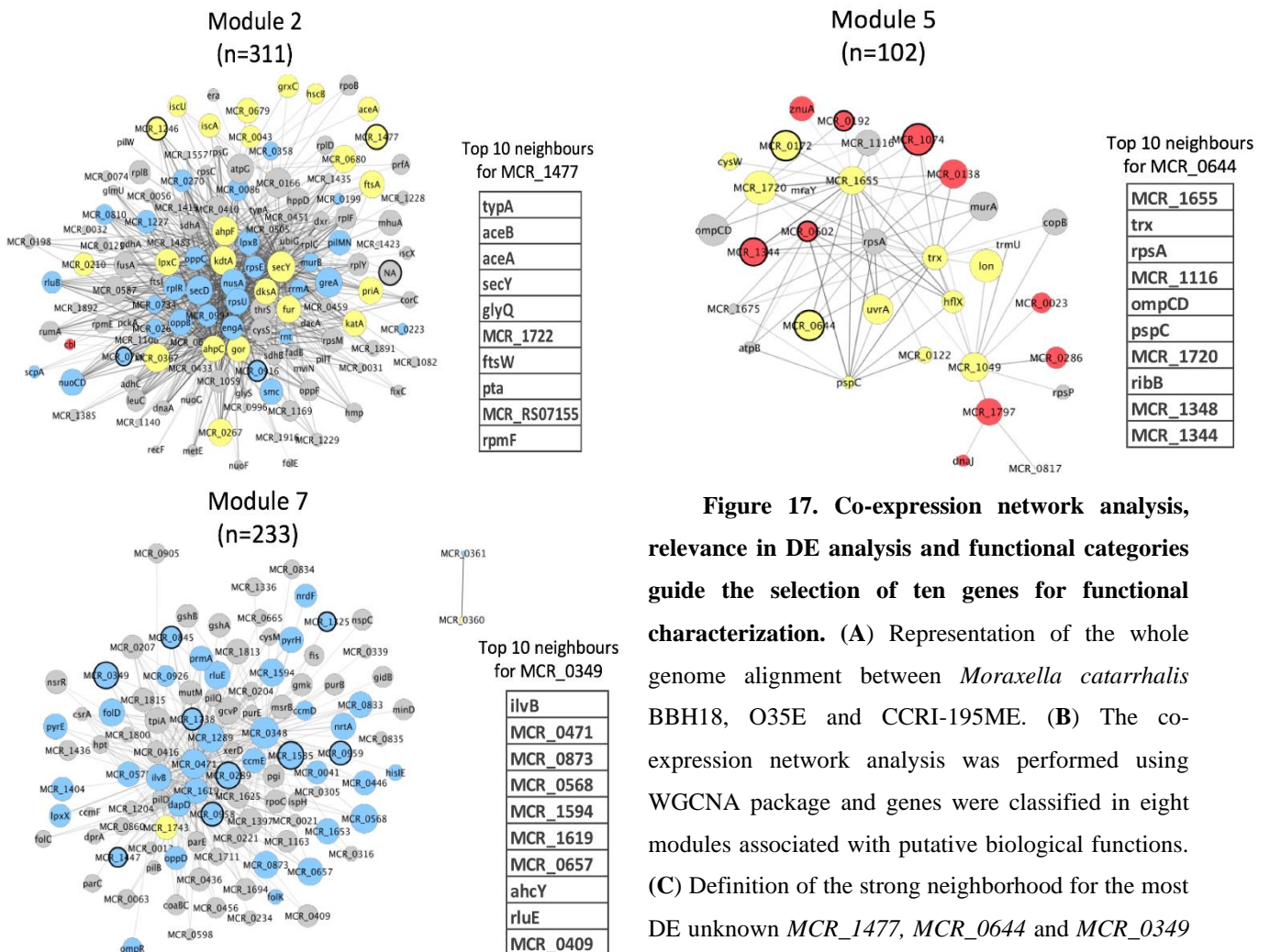


Figure 17. Co-expression network analysis, relevance in DE analysis and functional categories guide the selection of ten genes for functional characterization. (A) Representation of the whole genome alignment between *Moraxella catarrhalis* BBH18, O35E and CCRI-195ME. (B) The co-expression network analysis was performed using WGCNA package and genes were classified in eight modules associated with putative biological functions. (C) Definition of the strong neighborhood for the most DE unknown *MCR_1477*, *MCR_0644* and *MCR_0349* belonging to module 2, 5 and 7, respectively.

Table T4. List of selected genes

Upregulated gene	Relevance in DE analysis	Function
<i>katA</i>	Shared, top 30 CuSO ₄ , top 30 H ₂ O ₂	Enzyme catalyzing the dismutation of H ₂ O ₂
<i>lpxC</i>	Shared, top 30 H ₂ O ₂	Enzyme catalyzing the commitment step of lipid A biosynthesis
<i>cysP</i>	CuSO ₄ -specific	Lipoprotein binding sulfate ions, uptake of nutrients and important for intracellular survival in epithelial respiratory cells
<i>afeA</i>	H ₂ O ₂ -specific, top 30 H ₂ O ₂	Lipoprotein mediating the uptake of required trace cations, important for intracellular survival in epithelial respiratory cells
<i>MCR_1638</i>	Shared	Probably part of the Toxin-Antitoxin (TA) system inducing a dormant stage that allows bacteria to cope with stress
<i>badM</i>	Shared, top 30 CuSO ₄ , top 30 H ₂ O ₂	Iron-sulfur cluster assembly regulator homolog
<i>MCR_1049</i>	Shared, top 10 CuSO ₄ , top 10 H ₂ O ₂	Cu ¹⁺ exporting ATPase maybe localized in the inner membrane like <i>copA</i> from <i>E.coli/Salmonella</i>
<i>MCR_1477</i>	Top 10 H ₂ O ₂	Unknown gene, orthologue of the peroxidase stress protein YaaA, probably associated with ribosome and tyrosine metabolism
<i>MCR_0644</i>	Shared, Top 10 CuSO ₄ and H ₂ O ₂ ,	Unknown gene, probably associated with peptidoglycan biosynthesis
<i>MCR_0349</i>	37 th H ₂ O ₂	Unknown gene, probably associated with purine and pyrimidine metabolisms, cofactors, lysine and pentose phosphate biosynthesis

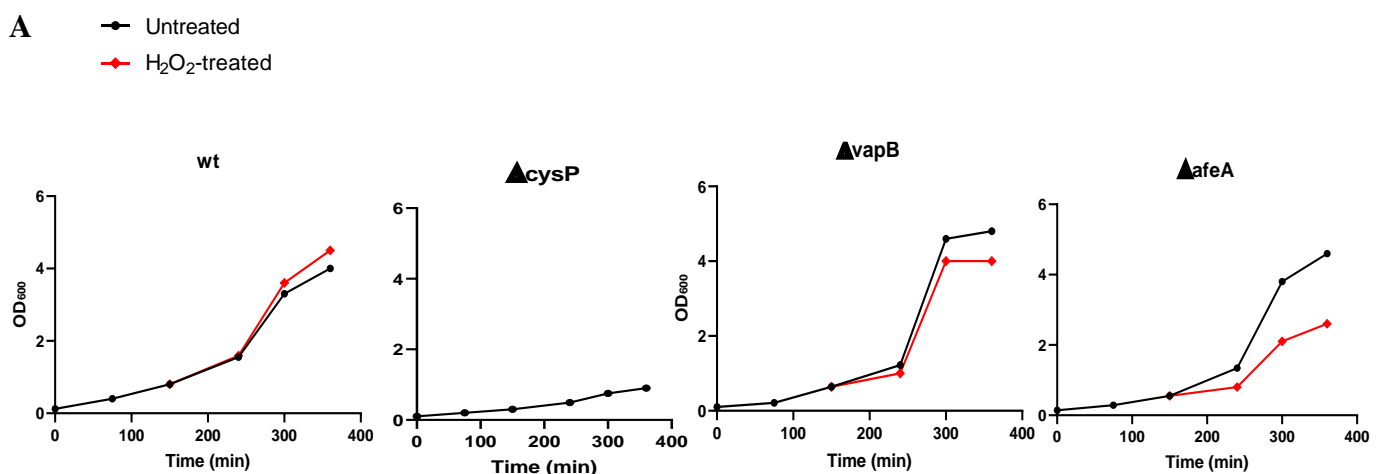
7.3 *badM* transcriptional regulator and *MCR_0349* unknown genes emerged as fundamental factors for Mcat resistance to oxidative stress

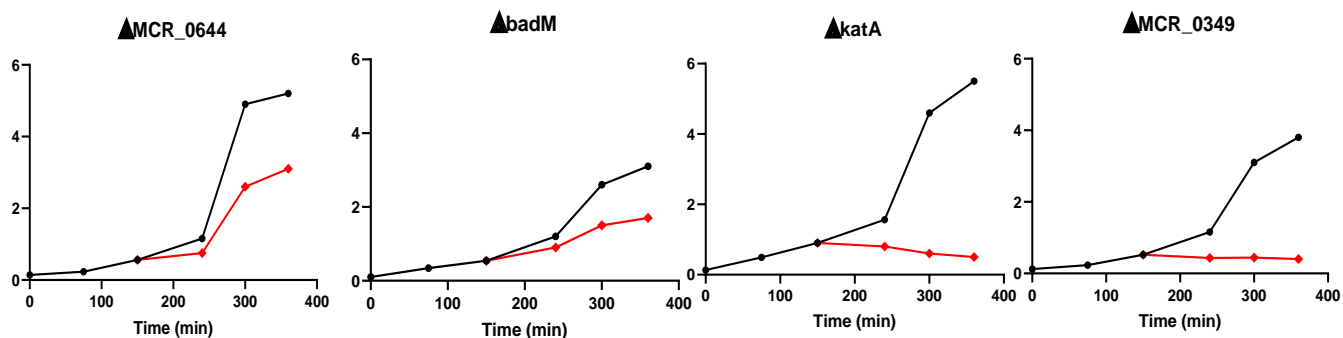
Functional characterization of the ten selected genes was carried out through the generation of knock-out (KO) mutants (Table T4). Directed gene deletion mutants of Mcat BBH18 were achieved by allelic exchange of the gene of interest with a kanamycin resistance cassette. Among them, deletion of *MCR_1477*, *MCR_1049* and *lpxC* genes was not obtained because of technical difficulties (*MCR_1477* and *MCR_1049*) or the loss of Mcat viability (*lpxC*). First, the sensitivity to hydrogen peroxide was determined. Early-exponentially growing bacteria (ca. 0.5 OD₆₀₀) were left untreated (Figure 18A, black lines) or exposed to H₂O₂ (Figure 18A, red lines). As it is shown in the *in vitro* growth curves of the seven mutants, *cysP* deletion negatively affected Mcat viability, suggesting that *cysP* is required for bacterial growth. The remaining KO mutants showed wild-type growth characteristics in the BHI medium. In the presence of H₂O₂, the deletion of *katA* and *MCR_0349* genes revealed the highest sensitivity to H₂O₂ while the growth of Δ *MCR_0644*, Δ *afeA* and Δ *badM* mutants was only partially influenced. Compared to the wt strain, no differences were observed for the Δ *vapB* mutant (Figure 18A).

We further evaluated the survival of phagocytosed BBH18 wt and deletion mutant strains in the human HL-60 cell line differentiated into neutrophil-like cells (dHL-60) and chemically activated *in vitro* with Phorbol 12-Myristate 13-Acetate (PMA) treatment, to promote a strong activation of the oxidative burst response. ROS-induced dHL-60 cells were left uninfected or incubated with different Mcat strains at MOI of 50 for 40 minutes. Non-interacting bacteria were washed away, and gentamicin antibiotic was added for 20 minutes to kill extracellular bacteria. From this time on (1 h, red bars), an incubation for additional 2 hours was carried out (for a total of 3 h, black bars) in the presence of PMA (Figure 18B). The intracellular survival of Mcat was determined by dividing the CFU/ml recorded at 3 h by that obtained at 1 h (ratio 3 h/1 h), as it is shown in Table T5. Mcat *wt*, Δ *vapB*, Δ *afeA* and Δ *MCR_0644* strains overcame the antimicrobial responses mounted by ROS-induced dHL-60 cells, surviving over 3 h post-infection. By contrast, Δ *katA*, Δ *MCR_0349* and Δ *badM* mutants were efficiently killed by these innate immune cells, suggesting a significantly enhanced susceptibility to ROS compared to the wt strain (Figure 18B). Therefore, besides the well-characterized *katA* gene, *badM* and *MCR_0349* have proved to play a pivotal role in Mcat resistance to oxidative stress.

To examine if the observed phenotypes were actually due to the specific gene deletions, pWW115 plasmid was exploited to generate Δ *badM* and Δ *MCR_0349* genetically complemented mutants. The structures of both *badM* and *MCR_0349* gene clusters are here represented (Figure

18C). The *badM* gene is located upstream of *iscSUA*, *hscBA* and *fdx*, analogously to the ortholog *iscR* regulator from *Neisseria spp* and *E. coli* (Santos et al., 2015). The *MCR_0349* gene is predicted to be co-transcribed with the neighbor gene *MCR_0348* (encoding an endoribonuclease), from which is spaced of only 10 nt. *badM*, *MCR_0349* and *MCR_0348* genes were additionally analyzed for their conservation among the 12 NCBI available Mcat strains. As it can be observed in Table T6, the three genes are widely conserved. To genetically complement $\Delta badM$ and ΔMCR_0349 mutants, the pWW115 plasmid carrying ca. 200 bp upstream region and the gene's coding sequence (CDS) were used. In the case of ΔMCR_0349 mutant, a second complementing strain was created by also including the 10 nt intergenic region and the CDS of the *MCR_0348* neighbor gene (double complemented). The empty plasmid was used as a control to transform the wt strain. The resulting four complemented strains were investigated for both resistance to H₂O₂ and intracellular survival in ROS-induced dHL-60 cells (Figures 18D and 18E, and Table T7). Importantly, growth of the complemented $\Delta badM$ mutant under oxidative stress conditions and its survival after internalization in PMA-activated neutrophil-like cells were restored to wt levels, underlying that the obtained phenotypes were actually the result of the gene deletion. Compared to the ΔMCR_0349 mutant, the single complementing strain displayed similar growth defects when exposed to H₂O₂ and the inability to tackle the dHL-60 cell's antimicrobial arsenal. By contrast, the double complemented strain showed similar wild-type growth phenotypes. These data suggest that *MCR_0349* mutation is polar on *MCR_0348* and the expression of *MCR_0348* is necessary to complement the phenotype. Hence, through genetic complementation, it has been demonstrated that the enhanced susceptibility to H₂O₂ and to killing by neutrophil-like cells were the results of *badM* and *MCR_0349* gene deletions and not due to unspecific effects.





B

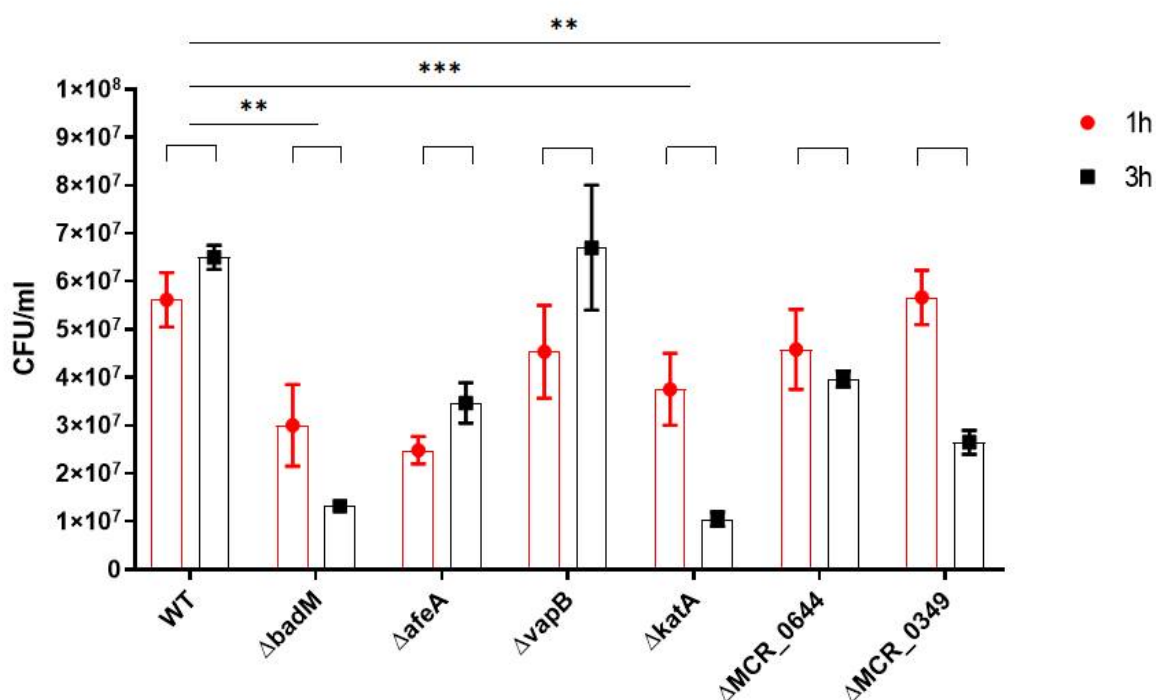


Table T5. Intracellular survival of deletion mutants in dHL-60 cells. Table reporting the CFU/ml obtained at 1 h and 3 h post-infection. Bacterial intracellular survival was determined by dividing the CFU/ml obtained at 3 h to that recorded at 1 h (ratio 3 h/1 h).

Strains	1 h	3 h	ratio 3 h/ 1h
Wt	5,62E+07	6,50E+07	1.16
$\Delta badM$	3,00E+07	1,32E+07	0.44
$\Delta afeA$	2,48E+07	3,47E+07	1.40
$\Delta vapB$	4,53E+07	6,70E+07	1.48
$\Delta katA$	3,75E+07	1,05E+07	0.28
ΔMCR_0644	4,58E+07	3,97E+07	0.87
ΔMCR_0349	5,67E+07	2,65E+07	0.47

C

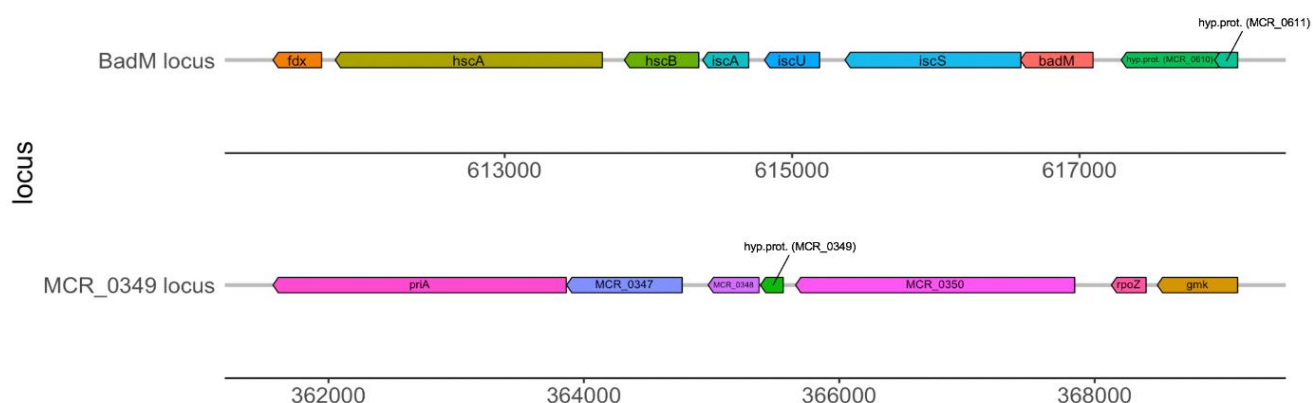
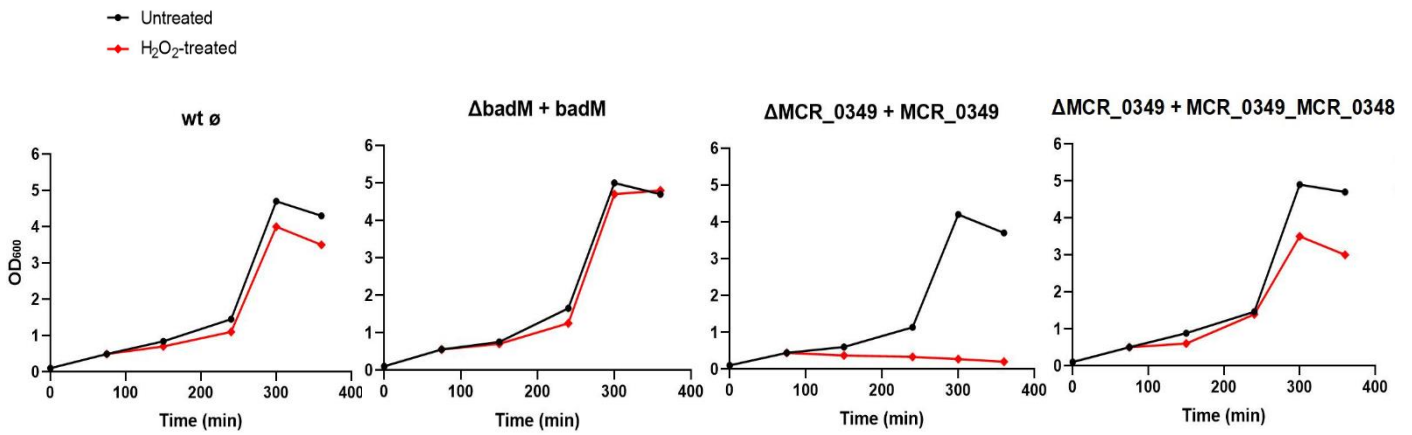


Table 6. % of nt coverage and identity of *badM*, *MCR_0349* and *MCR_0348* genes across twelve strains.

Strains	<i>badM</i> (<i>MCR_0609</i>)		<i>MCR_0349</i>		<i>MCR_0348</i>	
	% Coverage	% Identity	% Coverage	% Identity	% Coverage	% Identity
12P80B1	100.00	100.00	100.00	100.00	95.00	100.00
103P14B1	100.00	100.00	100.00	98.31	95.00	100.00
7169	100.00	100.00	100.00	100.00	95.00	99.21
46P47B1	100.00	100.00	100.00	100.00	95.00	100.00
B496	100.00	100.00	100.00	100.00	95.00	99.21
BC1	100.00	100.00	100.00	100.00	95.00	99.21
B502	100.00	100.00	100.00	100.00	95.00	100.00
BC7	100.00	100.00	100.00	100.00	95.00	100.00
B503	100.00	100.00	100.00	100.00	95.00	100.00
BC8	100.00	100.00	100.00	100.00	95.00	100.00
B507	100.00	100.00	100.00	100.00	95.00	99.21
CO72	100.00	100.00	100.00	100.00	95.00	99.21

D



E

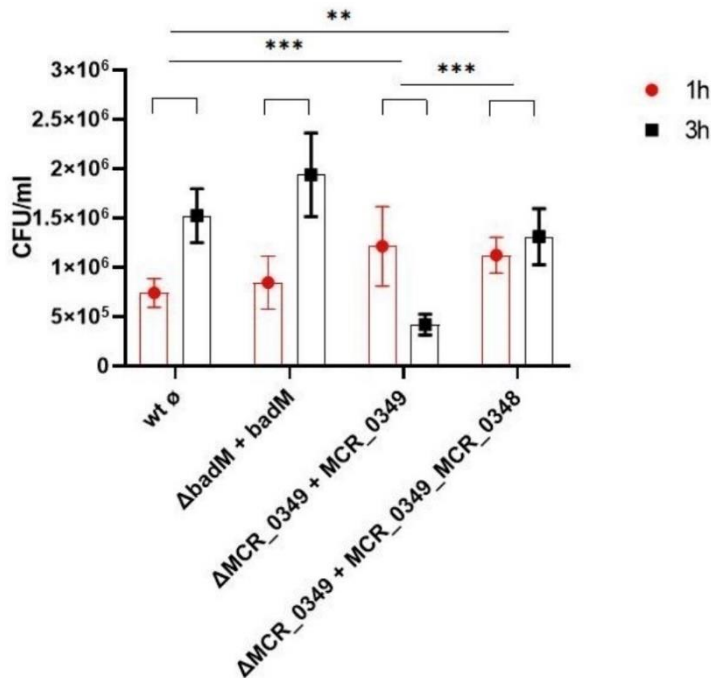


Figure 18. *badM* transcriptional regulator and *MCR_0349* unknown genes emerged as fundamental factors for Mcat resistance to oxidative stress.

(A) *M. catarrhalis* BBH18 wt, $\Delta cysP$, $\Delta badM$, $\Delta afeA$, $\Delta vapB$, $\Delta kata$, ΔMCR_{0644} and ΔMCR_{0349} were grown to mid-exponential phase and left untreated (black lines) or treated with 50 mM of H_2O_2 (red lines). Measurements of OD_{600} were recorded over time. (B) ROS-stimulated dHL-60 cells were incubated with *M. catarrhalis* wt and mutant strains were at MOI 50 for 40 minutes. Then non adherent bacteria were washed out and gentamicin was added for 20 minutes to inhibit growth of extracellular bacteria. From this time (1 h, red bars), samples were incubated for additional 2 hours (for a total of 3 h, black bars). By dilution plating onto BHI or HAE2 plates, the number of colonies obtained per condition was calculated to plot CFU/ml. Bars represent means \pm SE. ** $p < 0.01$; *** $p < 0.001$. (C) Schematic representation of *badM* and *MCR_0349* gene clusters. **D** and **E**) *M. catarrhalis* BBH18, wt + empty pWW115, $\Delta badM$ + pWW115_ *badM*, ΔMCR_{0349} + pWW115_ *MCR_0349* and ΔMCR_{0349} + pWW115_ *MCR_0349-MCR_0348* strains were evaluated exactly as reported in A and B, respectively.

Table 7. Intracellular survival of complementant strains in dHL-60 cells.

Strain	1 h	3 h	ratio 3 h/ 1h
wt ϕ	1,06E+06	1,99E+06	1.9
$\Delta badM + badM$	1,48E+06	2,60E+06	1.8
$\Delta MCR_0349 + MCR_0349$	1,45E+06	4,25E+05	0.3
$\Delta MCR_0349 + MCR_0349_MCR_0348$	1,34E+06	1,44E+06	1.1

Table reporting the CFU/ml obtained at 1 h and 3 h post-infection. Bacterial intracellular survival was determined by dividing the CFU/ml obtained at 3 h to that recorded at 1 h (ratio 3 h/1 h).

7.4 $\Delta badM$ and ΔMCR_0349 mutants are less virulent in *Galleria mellonella* larvae, a valuable *in vivo* model for Mcat

We then decided to study our mutants in *in vivo* multicellular systems. We decided to explore the invertebrate *Galleria mellonella in vivo* model as its innate immune response retains remarkable similarities with the human one. In fact, once phagocytosed, pathogens are killed mainly by the oxidative burst (Pereira et al., 2020). After having identified the infecting dose, $2 \cdot 10^7$ of wt, $\Delta badM$, or ΔMCR_0349 Mcat bacterial cells were injected into *G. mellonella larvae*. As a control, *larvae* were injected with the buffer only to detect any potentially lethal effects due to the physical injection procedures. Twenty *larvae* were infected with each strain, and these were evaluated at 0-, 24-, 48-, 72- and 144 h post-infection at 37 °C. According to the Health Index Score (see supplementary materials), *G. mellonella* was analyzed for its survival (alive or dead), melanization (how much *larvae* differed from the healthy creamy color: beige or brown *larvae* showing dots or tail/line, or completely black *larvae*) and activity (minimal movement, only upon stimulation or no movement at all). The higher the percentages, the healthier the *larvae* (results are presented in Table T8). As it can be observed in Figure 19, the percentages of survival, melanization and activity of *G. mellonella* infected with Mcat wt strain (black lines) were significantly lower than that recorded in *larvae* infected with both mutant strains, prompting for *badM* (blue lines) and *MCR_0349* (red lines) as pivotal virulence factors for the bacterial pathogenesis.

Table T8.

Strain	% of Survival					% Melanization					% of Activity				
	0 h	24 h	48 h	72 h	144 h	0 h	24 h	48 h	72 h	144 h	0 h	24 h	48 h	72 h	144 h
wt	100,0	81,0	67,0	46,0	8,9	100,0	58,8	46,0	29,8	5,6	100,0	73,7	51,3	38,7	6,7
<i>AbadM</i>	100,0	97,0	89,0	81,0	62,7	100,0	84,5	77,5	65,0	47,7	100,0	93,3	82,7	72,7	59,6
<i>ΔMCR_0349</i>	100,0	99,0	89,0	84,0	63,5	100,0	82,5	74,5	59,5	47,4	100,0	93,7	78,7	75,7	55,0

Percentages of survival, melanization and activity of larvae infected with *M. catarrhalis* wt, *AbadM* and *ΔMCR_0349* strain compared to the control group.

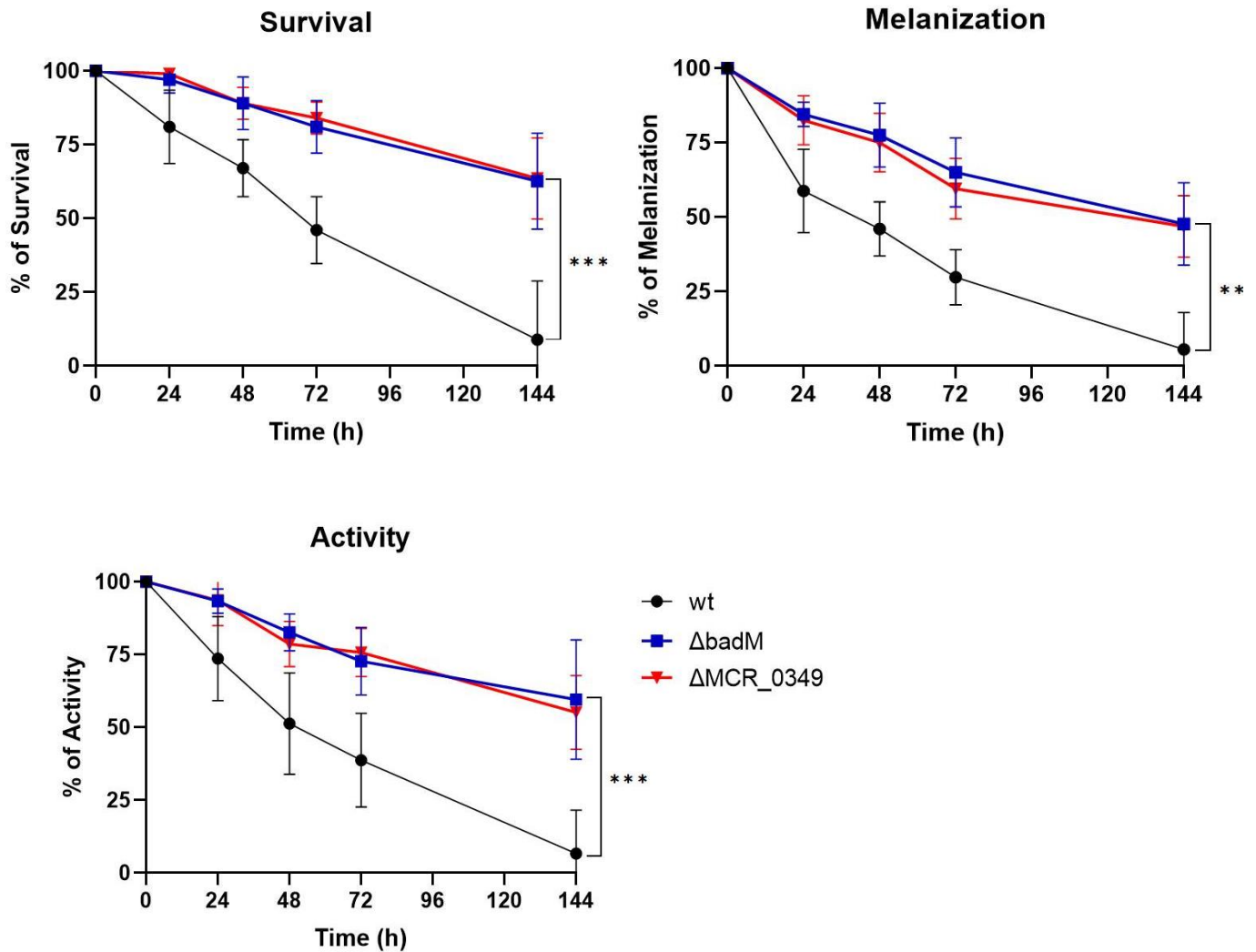


Figure 19. *AbadM* and *ΔMCR_0349* mutants are less virulent in *Galleria mellonella* larvae, a valuable *in vivo* model for *Mcat*. *M. catarrhalis* wt (black lines), *AbadM* (blue lines), or *ΔMCR_0349* (red lines) strains were grown to mid exponential phase and the corresponding 2×10^7 bacteria/ $10 \mu\text{l}$ was used to infect *G. mellonella*. The control group was injected with $10 \mu\text{l}$ 10 mM MgSO_4 only and used as reference. Following the injections, larvae were incubated at 37°C , $5\% \text{ CO}_2$ for six days (24-, 48-, 72- and 144 h) to allow the progression of *Mcat* infection. According to the Health Index Score, larvae were monitored for their survival (dead or alive), melanization (black, brown or creamy-colored larvae in the absence or presence of <3 or >3 spots) and activity (no movement, minimal movement or upon stimulation). For each strain, 5 independent repeats were carried out. Bars represent means \pm SE. *** $p < 0.00$

8. DISCUSSION

Oxidative stress is an important hallmark among the factors that depict COPD pathogenesis (Choudhury and MacNee, 2017, Jaroenpool et al., 2016). Different Mcat isolates are more resistant to H₂O₂ than either *H. influenzae* or *S. pneumoniae* (Pericone et al., 2000), and OxyR was identified as a crucial bacterial transcriptional regulator involved in response to the oxidative stress (Chiang and Schellhorn, 2012, Hoopman et al., 2011) (Jo et al., 2015). Moreover, by using HL-60 human cell line as *in vitro* model and neutrophils isolated from whole blood, we have recently demonstrated that Mcat is a successful intracellular pathogen that actively interferes with ROS and other ROS-related responses. These considerable innate resistance levels to oxidative stress could reflect the anatomical niches in which Mcat typically resides, including the nasopharyngeal mucosa and the lungs. In addition to genes that are well-characterized established bacterial factors for the oxidative stress response, it is plausible that Mcat encodes additional effectors to tackle this insult. Still, the underlying mechanisms are not yet clarified.

Therefore, an RNA-seq experiment was carried out to understand better the global transcriptional response to both H₂O₂ and CuSO₄ as stimuli that mimic *in vitro* the oxidative burst. H₂O₂ represents one of the leading ROS experienced by pathogens during infections and one of the most used stimuli for the study of the oxidative response because of its highest stability compared to any other ROS and its properties to cross and diffuse rapidly through the cell membranes (Kim et al., 2019). Even if not obvious as H₂O₂, copper is crucial in controlling infections. In phagocytes, Cu acts as a component of the antimicrobial arsenal being delivered into the phagolysosome to eradicate engulfed bacteria (White et al., 2009). The antimicrobial activities of copper are multifaceted: hydroxyl radicals generation *via* the Fenton and Haber-Weiss reactions (Ladomersky and Petris, 2015), targeting of enzymes with solvent-exposed [Fe-S] clusters (Besold et al., 2016) and mismetallation competing with all other transition metal ions from key biosynthetic enzymes (Begg, 2019). Differently from H₂O₂, a low number of transcriptional studies exists on human pathogens exposed to copper (an example is provided by *P. aeruginosa* (Quintana et al., 2017)), despite the fact that copper efflux genes have been identified as key virulence factors for successful intracellular bacteria such as *Vibrio spp.* (Vanhove et al., 2016), *M. tuberculosis* (Shi et al., 2014), *S. pneumoniae* (Johnson et al., 2015a) and *P. aeruginosa* (Schwan et al., 2005).

From the RNA-seq analysis, compared to non-treated bacteria, out of a total of 1720 predicted genes, 225- and 140, DE genes emerged following H₂O₂ and CuSO₄ exposure, respectively. Interestingly, comparing the two transcriptomes, 61 commonly regulated genes were identified with

a high correlation in log₂ fold changes, indicating that Mcat exploits similar strategies to cope with the damages triggered by the two treatments. Moreover, this finding could suggest the relevance of copper homeostasis for Mcat resistance to oxidative stress. Interestingly, the glyoxylate metabolism, which is not owned by all bacterial pathogens, was reported as one of the top pathways significantly enriched upon both treatments. This metabolic change promotes the reduction of oxidant production and the enhancement of antioxidants formation (Van Acker and Coenye, 2017). In *P. aeruginosa*, this shunt is elicited by ROS (Riquelme and Prince, 2020), and in *Burkholderia cenocepacia* upon treatment with tobramycin, an aminoglycoside antibiotic (Van Acker et al., 2013). Indeed, oxidative stress and antibiotic resistance were possibly linked in Mcat transcriptional response along with modulation of LOS and porins of the bacterial envelope in our experimental conditions. These kinds of rearrangements enable bacteria to grow and survive the phagocytic attack and are important sites of mutations for harboring antimicrobial resistance (Riquelme et al., 2018). In this context, the LPS biosynthesis emerged as the first enriched pathway upon H₂O₂ exposure, and from the identified DE genes, it was as if Mcat impaired the lipid A biosynthetic pathway as a strategy to counteract the oxidative stress. To date, only two other Gram-negative bacteria, *N. meningitidis* and *A. baumannii* have been shown to be able to survive after lipid A inactivation (Maldonado et al., 2016). Genes globally affecting gene expression were also identified, as reported by the downregulation of elongation factors, presumably leading to longer transcripts with putative regulatory properties. The non-coding 6SRNA *ssrS*, *ompR* and *phoB-phoR* two-component systems from Mcat emerged as DE as a consequence to the oxidative stress, similar to what has been described to other bacterial species. The 6S sRNA has been reported to play a pivotal role in bacterial intracellular survival within the host for *L. pneumophila* and *S. enterica* (Faucher et al., 2010, Ren et al., 2017). The regulator *ompR* has been primarily implicated in the oxidative stress response in *Rhodobacter sphaeroides* (Zhao et al., 2019), and acidic and osmotic stresses in *E. coli* and *S. typhimurium* (Chakraborty and Kenney, 2018). The PhoB-PhoR two-component system, which senses phosphate starvation, is involved in regulating oxidative resistance genes as it has been already described for *V. cholerae* 01 (Goulart et al., 2016) and *E. coli* (Iwadate and Kato, 2017). Genes associated with translation exhibited decreased transcript abundance likely suggesting a reduction in growth, and a subset of cryptic prophage and transposase genes were modulated upon both stimuli.

Among the seven deletion mutants, only *ΔbadM* and *ΔMCR_0349* mutants displayed a significant decrease in viability upon H₂O₂ treatment and survival in ROS-induced dHL-60 cells. Mcat *badM* is a homologue of *iscR*, a known global iron-sulphur [Fe-S] cluster assembly transcription factor (Santos et al., 2015). Curiously, similar to *P. aeruginosa* PAO1 (Romsang et al., 2014), Mcat

BBH18 (our laboratory strain) genome contains a homologue of the *isc* operon but is devoid of a *suf* (Sulphur formation) operon, another important bacterial [Fe-S] biosynthetic systems (Santos et al., 2015). *iscR* has been demonstrated to play fundamental roles not only for iron homeostasis but also for the resistance to oxidants in *P. aeruginosa* (Romsang et al., 2014), for the biosynthesis of capsular polysaccharide in *K.pneumoniae* (Wu et al., 2014) and for the synthesis of colonization factor antigen I fimbriae in Enterotoxigenic *E. coli* (Haines et al., 2015). A recent work reported that *N. gonorrhoeae* exposed to a sublethal dose of H₂O₂ showed a high transcript abundance of *iscR* (Quillin and Seifert, 2018). In Mcat, *badM* is a crucial regulator found to be differentially expressed in biofilm-like condition (Hoopman et al., 2011), in the interplay with epithelial cells of the human respiratory tract (de Vries et al., 2013) and this thesis, similarly to what has been revealed for *N. gonorrhoeae*, also in oxidative stress responses, highlighting a pivotal role of this regulator in the virulence across multiple bacterial species. While the *iscR* homologue was found to be important for the pathogenesis of other bacterial species, *MCR_0349* is a unique effector of *M. catarrhalis* spp. *MCR_0349* is a small gene of 180 nt only that maps into a genomic region, including genes involved in DNA repair systems, metal homeostasis, and fimbrial biogenesis. *MCR_0348* neighbor gene is predicted to encode an endoribonuclease and, along with *MCR_0349*, has been shown to be fundamental for Mcat oxidative stress response. Indeed, only the double complemented strain of Δ *MCR_0349* mutant exhibited near wild-type phenotypes. Interestingly, regulation at the post-transcriptional level (like that of endoribonuclease) plays a crucial role in the adaptation of pathogens to environmental changes. In *P. aeruginosa*, it has been recently reported that the endoribonuclease Δ *ybeY* mutant is more susceptible to H₂O₂ and the killing mediated by neutrophils compared to the corresponding wt strain (Xia et al., 2020), similarly to what we observed for the Δ *MCR_0349* mutant. Moreover, high conservation of *badM*, *MCR_0349* and *MCR_0348* genes was observed among the thirteen NCBI available Mcat strains. Therefore, we can assume that their role is not restricted to the strain used in this study, but they are presumably part of a well-preserved mechanism exploited by Mcat to resist oxidative stress-mediated killing.

For the first time, the virulence of Mcat wt, Δ *badM*, and Δ *MCR_0349* strains were also investigated in the *G. mellonella* experimental infection model. Although invertebrates have diverged from vertebrates about 500 million years ago and are devoid of an adaptive immune response, their phagocytic cells, named hemocytes, are capable to phagocytose and kill pathogens, mainly through the oxidative burst, in a process very similar to that of vertebrates (Browne et al., 2013). Here, we demonstrated for the first time, that *G. mellonella* can be used as a valuable *in vivo* model to examine Mcat infection by monitoring the immune responses over several days. Interestingly, the survival of *G. mellonella* larvae infected with the *badM* and *MCR_0349* mutant strains was significantly higher

than those infected with the wt strain, indicating that these are important virulence genes for the Mcat *in vivo* pathogenesis.

To conclude, the ability to fine-tune the expression of genes encoding effectors involved in oxidative stress resistance is likely the result of a necessity for Mcat to respond to the rapidly changing environment during infections. Why Mcat is more resistant to H₂O₂-mediated killing compared to other pathogens that colonize the same anatomical sites, such as the nasopharynx, was not apparent. Here, we provided a comprehensive picture of Mcat transcriptomes in response to stimuli mimicking the oxidative environment, unravelling a previously unidentified common transcriptional program following H₂O₂ and CuSO₄ treatments. We ascertained new crucial factors for this pathogen's response, all of which are well conserved among different isolates of Mcat. Finally, we have established a novel *in vivo* Mcat infection model using the invertebrate *Galleria mellonella* and observed that deletion mutants of genes implicated in oxidative stress resistance exhibited reduced virulence. To conclude, another piece is added to the complex puzzle of Mcat's innate resistance to ROS improving our understanding of the strategies exploited by this harmful human pathogen to colonize and persist within the respiratory tracts.

9. MATERIALS AND METHODS

9.1 Cell culture and differentiation

The human promyelocytic cell line HL-60 (ATCC CCL-240) was maintained in RPMI 1640 medium, GlutaMAX supplement (ThermoFisher) supplemented with 10% fetal bovine serum (FBS, ThermoFisher) at 37°C and 5% CO₂ between 2.0×10^5 and 1×10^6 cells/ml. 4×10^5 cells/ml were differentiated with 100 mM with N, N-dimethylformamide (DMF, Sigma). HL-60 cells are differentiated into granulocytes by 4-5 days of treatment and are ready to be used as phagocytes with a typical yield of $8-12 \times 10^5$ cells/ml. For all host-pathogen interactions studies, RPMI 1640 Medium, no phenol red (ThermoFisher) with 2% of FBS was used. When desired, differentiated cells were stimulated for ROS production by using 10 µg/ml of phorbol 1-myristate 13-acetate (PMA, Sigma). When stated, 10 µg/mL cytochalasin D (Sigma) was used to inhibit phagocytosis. Permeabilization buffer containing PBS + 0.2% saponin with or without 2% BSA was used for phagocytosis, NET, autophagic studies and bacterial survival evaluation.

9.2 Bacterial Strains and Cultures

The experiments were performed using these Gram-negative bacteria: *Moraxella catarrhalis* BBH18 (GenBank assembly accession: GCA_000092265.1) a seroresistant-lineage strain isolated from a sputum isolate from a COPD patient during an exacerbation and a clinical isolates and Nontypeable *Haemophilus influenzae* NTHi 658 coming from AERIS Study (Study ID: EPI-HIP 001 BOD UK). *M. catarrhalis* was grown in Brain-Heart Infusion Broth (BHI) agar plates at 37 °C with 5% CO₂. The complete list of *M. catarrhalis* deletion mutants and complementant strains used in this study is reported in supplementary S1. BHI was used as fluid growth medium at 37 °C, 185 rpm with 5% CO₂. NTHi was grown on chocolate Haemophilus 2 agar (HAE2, BioMerieux) at 37°C with 5% CO₂. Brain-heart infusion (BHI) broth (Difco Laboratories) supplemented with 10 µg/mL each of haemin (Sigma) and nicotinamide adenine dinucleotide (NAD, Sigma) was used as fluid growth medium. Bacteria concentration was determined by both measuring O.D. at 600 nm and colony forming units (CFU) by dilution plating. 0.5 O.D.₆₀₀ has proved to be equivalent to 2×10^8 CFU /mL for BBH18 while 6×10^8 CFU/ml for NTHi 658. For all host-pathogen interactions studies, viable and exponentially-growing bacterial cells were used. When necessary, kanamycin and spectinomycin were added at a concentration of 30 µg/ml.

9.3 Phagocytosis Studies by FACS

PMA-stimulated dHL-60 (1×10^6) were treated with 10 µg/mL cytochalasin D (Sigma) (for bacterial adhesion) or left untreated (total bacteria-dHL-60 interaction). They were infected with 5×10^7 CFU (MOI 50) of *M. catarrhalis* or NTHi bacterial cells for 20, 45 and 75 min in RPMI 1640 (no phenol red) + 2% FBS medium and incubated at 37°C in the presence of 5% CO₂. After incubation, samples were fixed with 4% (v/v) formaldehyde (Sigma) for 1 h and *M. catarrhalis* and NTHi bacteria were detected by staining for UspA2 or whole cell, respectively (rabbit polyclonal antibodies diluted 1:1000 in permeabilization buffer). Samples were incubated for 20-30 min at RT in the dark with 100 µL of permeabilization buffer containing a secondary rabbit anti-mouse immunoglobulin G (whole molecule) Alexa fluor 633-conjugated (Invitrogen) diluted 1:500. After two washes with PBS, dHL-60 were evaluated by flow cytometry and expressed as the percentage of Alexa Fluor 647 positive cells (untreated samples) or the percentage of cells with bacteria attached (cytochalasin D). The percentage of phagocytosis was calculated subtracting the percentage of adhesion to the total interaction. All data were collected using a BD FACS CANTO II (BD Bioscience) by acquiring 100,000 events, and the data analysed using the FlowJo software (v.8.6, TreeStar Inc)

9.4 Reactive Oxygen Species Detection

Intracellular ROS with CellRox Deep red flow cytometric analysis and Extracellular ROS with a Luminol-dependent chemiluminescence (LDCL) assay

Differentiated HL-60 cells resuspended in phenol red free RPMI 1640 containing 2% FBS. Untreated and 10 µg/mL PMA-treated dHL-60 cells represented negative and positive controls for ROS production, respectively. Cells were also infected by *M. catarrhalis* or NTHi bacterial cells at different MOI.

For intracellular ROS, CellROX Deep Red Reagent (ThermoFisher) was added at a final concentration of 5 µM to differentiated cells (1×10^6 /reaction) and incubate for 30 minutes at 37°C. dHL-60 cells were infected or not with *M. catarrhalis* or NTHi bacterial cells at MOI 50. At the time points indicated in the figure legends, samples were fixed with 4% (v/v) formaldehyde (Sigma) for 1 h and subsequently, the mean fluorescence intensity (MFI) at 633 nm was determined after having performed gates on viability (LIVE/DEAD Fixable Aqua Dead Cell Stain, 1:1000, ThermoFisher), morphology and non-aggregated cells. All data were collected using a BD FACS CANTO II (BD Bioscience) by acquiring 100,000 events, and the data analysed using the Flow-Jo software (v.8.6, TreeStar Inc). For extracellular ROS, 2 mM luminol (Sigma) was used to monitor the kinetics of the oxidative stress response. Approximately 5×10^4 cells in 90 µL were seeded into a black flat 96-well microplate (costar) and infected or not with bacteria at a MOI 12, 25, 50 and 100. Luminescence was read in a TECAN Infinite 200 plate reader with settings of: 1,000-ms integration, reading every 3 min for 2 h at 37°C.

To verify if bacteria-cells contacts or secreted bacterial products were required, dHL-60 cells were infected with *M. catarrhalis* at a MOI of 50 for 45 min in white RPMI or bacteria were simply grown until mid-exponential phase in BHI medium, respectively. The resulting supernatants were collected, passed through a 0.2 µm syringe filter and subsequently added to PMA-stimulated naïve cells. To examine whether bacterial internalization was needed, dHL-60 cells were pre-exposed to 10 µg/ml cytochalasin D (Sigma) for 15 min to inhibit phagocytosis.

9.5 Flow cytometric analysis of *M. catarrhalis* engagement of human recombinant receptors CEACAM-1, Siglec-5 and Siglec-9

1×10^7 exponentially-growing *M. catarrhalis* bacterial cells were resuspended in PBS and incubated or not (naïve bacterial cells), overnight at 4 °C, with 2 µg of each human recombinant protein (VWR): CEACAM-1 (as positive control), Siglec-5 and Siglec-9 inhibitory receptors. For

competitive experiments, 200 nM of Mcat OmpCD or NTHi PD proteins was added. Samples were fixed with 4% (v/v) formaldehyde (Sigma) for 1 h and subsequently incubated for 1 h with rabbit antibodies specific to each recombinant receptor (rabbit anti-CEACAM1, anti-Siglec-5 and anti-Siglec-9; ThermoFisher) diluted 1:500 in PBS. Samples were incubated for 20-30 min at RT in the dark with PBS containing a secondary goat anti-rabbit immunoglobulin G (whole molecule) Alexa fluor 488-conjugated (ThermoFisher) diluted 1:500. After two washes with PBS, binding of these soluble proteins to the bacteria was revealed by flow cytometry. All data were collected using a BD FACS CANTO II (BD Bioscience) by acquiring 100,000 events, and the data analysed using the Flow-Jo software (v.8.6, TreeStar Inc).

9.6 Recombinant OmpCD preparation

The genomic DNA of *M. catarrhalis* BBH18 was used as templates for amplifying the coding region corresponding to the mature portion of OmpCD (without its signal peptide) and cloned into the pET15b vector (Novagen) using the polymerase incomplete primer extension (PIPE) method (Klock et al., 2008). All the unpurified PCR products (V-PCR and I-PCR) were used to directly transform chemically competent Stellar cells (Takara Bio). The screening of positive clones was performed by colony PCR and subsequently verified by sequencing. All expression experiments were performed using the and T7 express Iq LysY (New England Biolabs) *E. coli* strain. For protein expression and purification, one single colony of T7 express LysY/Iq *E. coli* strain expressing Mcat OmpCD was inoculated in LB plus ampicillin and grown overnight at 37°C, diluted in fresh LB medium and grown at 37 °C to an OD600 of 0.5-0.8. Protein over-expression was induced by the addition of 1 mM isopropyl-1-thio-β-D-galactopyranoside (IPTG, Sigma) for 3 hours. *E. coli* cells were lysed by cell lytic express (Sigma-Aldrich). The bacterial lysate was centrifuged at 9000 rpm for 30 min. The total and soluble fractions were treated with Loading dye NuPage LDS Sample Buffer 4X (Thermo Scientific) and DTT 10X NuPage Reducing Agent (Thermo Scientific) and denatured at 95°C for 5 minutes. Protein extracts were separated by SDS-PAGE on NuPAGE Novex 4-12% Bis-Tris Protein Gels in MES 1X (Thermo Scientific). Novex Sharp Pre-Stained Protein Standard (Thermo Scientific) was used as a molecular weight marker. Protein expression was evaluated by Western blot analysis. Protein extracts were transferred onto nitrocellulose membrane using an iBlot Dry Blotting System (Thermo Scientific). Membranes were saturated for 1 hour at room temperature with PBS containing 0.05% (v/v) Tween 20 (Sigma) and 10% (w/v) milk Blotting-Grade Blocker (Biorad). Membranes were incubated at room temperature for one hour with mouse monoclonal anti 6 His-tag antibody HRP-conjugated (Sigma), diluted 1:1000 in PBS with 1% (v/v) Tween 20 (Sigma)

and 1% milk. The Biorad OPTI-4CN substrate kit was used according to the manufacturer's instructions. The recombinant protein from the soluble fraction was purified by immobilized metal ion chromatography using nickel-nitrilotriacetic acid (Ni-NTA) agarose resin (Qiagen, Germantown, MD, USA), according to the manufacturer's instruction. Purity was checked by SDS-PAGE electrophoresis staining with Coomassie blue and protein concentration was determined using a nanodrop spectrophotometer (Thermo Scientific). Nanoscale Differential Scanning Fluorometry (nanoDSF) was used to evaluate the folding and the stability of the purified OmpCD recombinant protein. Real-time simultaneous monitoring of the Intrinsic Tryptophan Fluorescence ITF at 330 nm and 350 nm during the conversion of was carried out in a Prometheus NT.48 instrument from NanoTemper Technologies with an excitation wavelength of 280 nm. Capillaries were filled with 10 μ l of a suspension of OmpCD (1.2 mg/ml in PBS), placed into the sample holder and the temperature was increased from 25 to 95°C at a ramp rate of 1°C/min. The ratio of the recorded emission intensities (Em_{350nm}/Em_{330nm}) was plotted as a function of the temperature.

9.7 Biolayer interferometry (BLI)

The experiments were performed using the “dip and read” format. The eight biosensors were dipped into reagents prepared in the 96-well plate. Siglec-5 and Siglec-9 proteins were used as ligands and captured, *via* Fc-region, on the surface of the biosensors pre-coated with protein G; they were diluted in PBS 1X to reach the final concentration of 2 μ g per well, while the proteins OMP CD, PD, Hla-CP5 and 741 v2.77 were used as analytes and diluted in PBS 1X to reach the final concentration of 200 nM. The analysis consists of six steps: 1) baseline (100 sec, 1000 rpm): sensor check of biosensors in PBS 1X; 2) loading (300 sec, 1000 rpm): capture of Siglec proteins on the surface of biosensors; 3) baseline 2 (30 sec, 1000 rpm): wash of biosensors in PBS 1X; 4) association (500 sec, 1000 rpm): binding between Siglecs captured on the biosensors surface and the analyte proteins in solution; 5) dissociation (200 sec, 1000 rpm): dissociation of the Siglec-protein complex by dipping the biosensors into PBS 1X alone; 6) regeneration (30 sec, 1000 rpm): regeneration of the biosensors surface using the 0.23% formic acid, pH 2.35 solution. The experiments are performed using the Octet Qke instrument (Sartorius), the Data Acquisition 12.0 is used to generate the raw data and the Data Analysis is used to elaborate data.

9.8 NET: quantification and visualization by confocal microscopy.

dHL-60 cells (or primary cells) were resuspended in HBSS (ThermoFisher) medium and seeded in a 96-well plate. Untreated and 10 µg/mL PMA-treated cells represented negative and positive controls for NET production, respectively. Subsequently, untreated cells were infected with *M. catarrhalis* BBH18 or NTHi 658 individually at MOI 50 or in their combination (MOI 25 each). Cells were treated with PMA and infected or not by *M. catarrhalis* (MOI50). The cells were incubated at 37 °C in an incubator for 4 h (in the case of PMNs, 2 h). To quantify NET-structures, the supernatant was carefully removed, and the cells were treated with micrococcal nuclease (500mU/ml, ThermoFisher) for 15 min in the presence of CaCl₂ (1.5mM, Sigma). EDTA (5mM, Sigma) was added to inhibit nuclease activity. The amount of extracellular DNA in the supernatant of cells was then quantified using PicoGreen (ThermoFisher) staining; the fluorescence was detected using a TECAN Infinite 200 plate reader. Each sample was analysed in triplicate to avoid any bias in the reading. To visualize NET-structures, samples were spotted onto a POLYSINE slide (Menzel-Glaser). After 4 hours, samples were fixed with 4% (v/v) formaldehyde (Sigma) for 1h then incubated for one hour with the mouse monoclonal anti-myeloperoxidase (MPO) antibody diluted 1:1000 in PBS + 5% BSA. Samples were washed with of PBS and incubated for 20-30 min at RT in the dark with 100 µL of PBS containing a secondary goat anti-mouse immunoglobulin G (whole molecule) Alexa fluor 488-conjugated (ThermoFisher) diluted 1:500. For the experiments performed with primary cells, adherent and not internalized *M. catarrhalis* and NTHi bacteria were detected by staining UspA2 or whole cell, respectively (rabbit polyclonal antibodies diluted 1:1000) with a secondary goat anti-rabbit immunoglobulin G (whole molecule) Alexa fluor 594-conjugated (ThermoFisher) diluted 1:500. After two washes with PBS, a droplet of a mounting solution containing DAPI was applied. The final step consisted in placing a cover glass on each spot and analysing the samples with a confocal ZEISS LSM700 microscope. 10 fields were observed, with at least 5 cells/field. Images of NET structures were analyzed using the ZEN software.

9.9 Autophagic response and intracellular survival assay

ROS-stimulated dHL-60 cells were non-infected or incubated with *M. catarrhalis* or NTHi individually at MOI 50 or in their combination (MOI 50 each) for 40 minutes after which 400 µg/ml gentamicin (Sigma) was added to inhibit growth of extracellular bacteria. After 20 minutes, medium was changed with new pre-warmed RPMI 1640 (no phenol red), supplemented with PMA. The reactions proceeded for 3 additional hours. Immediately after the removal of gentamicin (control groups) and after three hours, samples were processed for autophagic response and bacterial intracellular survival. For the former, samples were fixed with 4% (v/v) formaldehyde (Sigma) for 1

h . then incubated for one hour with the rabbit anti-LC3B antibody diluted 1:500 in permeabilization buffer. Samples were incubated for 20-30 min at RT in the dark with permeabilization buffer containing a secondary goat anti-rabbit immunoglobulin G (whole molecule) Alexa fluor 633-conjugated (Invitrogen) diluted 1:500. After two washes with PBS, LC3B expression levels were evaluated by flow cytometry. All data were collected using a BD FACS CANTO II (BD Bioscience) by acquiring 100,000 events, and the data analysed using the Flow-Jo software (v.8.6, TreeStar Inc). For bacterial intracellular survival, dHL-60 cells were permeabilized and colony formation unit (CFU)/ml was determined by dilution plating on BHI and HAE2 agar for *M. catarrhalis* and NTHi, respectively.

9.10 Electron microscopy (EM)

The cells were fixed in 4% paraformaldehyde solution in PBS pH 7.2 overnight at 4°C, washed in PBS, post-fixed in 1% OsO₄ in water for 1 hour at 4 °C, dehydrated in an ascending alcohol series. For scanning electron microscopy (SEM) observations, samples were processed by critical point drying in a Balzer's CPD030. Samples were gold-evaporated in a Balzer's MED 010 sputterer and observed in a SEM Quanta 400 scanning electron microscope operating at 20 kV. For transmission electron microscopy (TEM) observations, after the alcohol series, samples were infiltrated and embedded in epon resin that was polymerized at 60 °C for 48 hours. Ultrathin sections were cut from samples on a Reichert-Jung Ultracut E ultramicrotome. They were mounted on 200-mesh copper grids, routinely counterstained, and observed in a FEI Tecnai G2 SPIRIT transmission electron microscope at an electron accelerating voltage of 120 kV equipped with a Tvips TemCam F216.

9.11 Mcat and NTHi opsonization with human sera

5×10^7 of exponentially growing Mcat and NTHi bacteria were resuspended in DPBS +1%BSA +0.1% glucosio+0.5% Tween20 with or without 10% of human sera, hereafter called NHS. Tre sera (ID: 2543, 6002, 2151) from Phleb001_20180404-AXB-1805_Phleb001 generic were pooled and used as complement source at 10%. After an incubation of 30 min at 37 °C, bacteria were washed and then stained for 30 min using 1:200 of both Fluorescein isothiocyanate (FITC) conjugated polyclonal anti-human C3 antibody and AlexaFluor 594 conjugated anti-human IgG, then washed and fixed with 2% paraformaldehyde. Labeled bacteria were analyzed by flow cytometry for the binding to C3b and human IgG antibodies using a BD FACSCantoII and results reported as mean

fluorescence intensity (MFI). 2 h post-infection, opsonized and unopsonized bacteria were used to evaluate their uptake and intracellular ROS production in dHL-60 cells, in as described above.

9.12 Isolation of human neutrophils

Human neutrophils were isolated using a density gradient method. Blood was collected from healthy individuals, diluted 1:1 with Dulbecco's PBS (Sigma) and separated using a Ficoll gradient (Ficoll-plaque PLUS, 1.078 g/ml, GE Healthcare Life Science) and Histopaque 1,119 g/ml (Sigma). The layers containing plasma and peripheral blood mononuclear cells were aspirated carefully, preserving the erythrocyte/granulocyte layer. Hyperosmotic shock for erythrocytes lysis was performed with sterile cold water and PBS 10X. Finally, granulocytes were collected by centrifugation at 1,000 g for 5 min. The cell pellet was reconstituted in RPMI no phenol red (Gibco).

9.13 Statistical Analysis

All data are expressed as the mean and standard error of the mean. A one-way analysis of variance (ANOVA) was performed when multiple independent groups needed to be tested for their difference in the mean, student's t-tests were used for paired values (R version 3.6.0). $P < 0.05$ was considered to be significant.

9.14 Determination of the H₂O₂ and CuSO₄ MBC for *M. catarrhalis*.

For the Minimum bactericidal concentrations (MBC) determination, 2×10^6 of early exponential phase (c.a. 0.5 O.D.₆₀₀) bacteria were transferred to a 96-well plate, and H₂O₂ (9.8 M; Sigma) or CuSO₄ was added to each well to achieve a range of final concentrations. The suspension was incubated at 37°C for 30 min without shaking, and then the contents of the wells were serially diluted and plated onto BHI agar. The lowest concentration in which no viable bacteria are observed is called MBC.

9.15 RNA isolation for and real-time reverse transcription-PCR (RT-PCR) analyses.

Bacterial cells were grown in BHI at 37°C, 185 rpm with agitation to an OD₆₀₀ of 0.6/0.7 and then untreated or exposed for 15 min to H₂O₂ or CuSO₄ to a final concentration of 50 mM and 5 mM, respectively. From three independent experiments, total RNA was extracted with the Rneasy Mini Kit (Qiagen) according to the manufacturer's instructions. The RNA samples were treated with DNase (Qiagen) for 15 min at 25 °C and precipitated by sodium acetate and ethanol treatment. The integrity of the RNA samples was measured with the Agilent 2100 bioanalyzer (Agilent Technologies). Whole transcriptome RNA-seq library preparation was performed by using Universal RNA-Seq Library Preparation Kit with NuQuant (TECAN). Briefly, cDNA library preparation was performed using UMI technology. rRNA was removed by using an *ad hoc* designed probes after library construction and paired-end 101-bp sequencing was performed using Illumina MiSeq system. For validation of RNA-Seq data, three other independently isolated RNA samples were used for the relative real-time RT-PCR experiments. The endogenous control was *MCR_1683* or *polA* encoding a predicted DNA polymerase I. qPCR primers are listed in Table S1 in the supplementary materials. RT-qPCR was performed on cDNA was obtained from 1 ug of RNA using SuperScript IV Reverse Transcriptase (ThermoFisher) using Platinum SYBR Green qPCR SuperMix-UDG (Invitrogen) on a MX2000, Real-Time Detection system. Fold change values were calculated using the cycle threshold ($2^{-\Delta\Delta CT}$) method, and the values presented represent the geometric means of data from all biological replicate experiments.

9.16 RNA-Seq data analysis

Raw reads were first quality-checked using FastQC (version 0.11.3), and all samples showed a peak in the distribution of the mean sequence quality (Phred score) over all sequences around 38. Reads were mapped in paired-end mode to *Moraxella catarrhalis* BBH18 complete genome using Bowtie2 (version 2.2.6). Furthermore, reads were aligned to Bowtie2 indexes created using bacterial rRNA sequences in order to evaluate the extent of ribodepletion efficacy. Finally, mapped reads were also visualized with IGV (version 2.6.0). Next, gene counts were obtained using featureCounts function by Rsubread Bioconductor package (R version 3.4.4, Rsubread version 1.28.1) and the NCBI annotation, without considering multi-mapping reads. Differential expression analysis was performed with DESeq2 Bioconductor package (R version 3.6.0, DESeq2 version 1.24.0) (Love et al., 2014). Before to build the generalized linear model, the remaining counts associated to rRNA genes were removed from the count matrix, and both an examination of gene dispersion values in relation to the mean of normalized counts and a principal component analysis (PCA) on transformed and normalized

read counts were conducted. The transformation before PCA was applied to make counts data approximately homoskedastic. Differentially expressed genes were called upon building a generalized linear model comparing the data for the two treatments to the data for untreated controls with a design of the type \sim replicate + condition and considering the following threshold: Benjamini-Hochberg (BH)-adjusted P value \leq 0.01. Results were visualized in different ways. Heatmaps depicted mean-centered variance-stabilized read counts (normalized with respect to library size), with colours from yellow to red representing up-regulated genes and colours from light blue to blue representing down-regulated ones. Before any other visualization, like for the volcano plots, the log₂ fold changes were shrunken in order to correct for poorly reliable large estimates related to genes having low or highly variable read counts, using apegglm method (Zhu et al., 2018).

9.17 Mcat O35E and CCRI-195ME experiment data retrieval and mapping.

Whole genome alignment between *Moraxella catarrhalis* BBH18, O35E and CCRI-195ME strains was achieved and visualized through BLAST Ring Image Generator (BRIG) (v0.95), upon genome and annotation files download from NCBI and contigs concatenation for strain O35E. Unknown genes and 6S RNA sequence conservation in O35E and CCRI-195ME was analyzed via BLAST alignment. Raw reads for the experiment on O35E strain and for the experiment on CCRI-195ME strain were retrieved from NCBI Sequence Read Archive (SRA) depository and converted to compressed fastq files using the SRA toolkit (v2.10.8). Next, fastq files from the two experiments were aligned to the reference (and actually the most represented in our data) *Moraxella catarrhalis* BBH18 complete genome using Bowtie2 (version 2.2.6). Finally, count matrices were obtained via featureCounts function by Rsubread Bioconductor package (R version 3.4.4, Rsubread version 1.28.1), taking in consideration only uniquely mapping reads.

9.18 Co-expression network analysis

The co-expression network analysis was performed using WGCNA package (R version 3.6.0, WGCNA version 1.69) (Langfelder and Horvath, 2008). Before to build the network, the counts associated to rRNA genes were removed from the count matrix. Furthermore, genes whose counts were consistently low (less than 10 in 90% of the samples) were filtered out. This step naturally excluded from the analysis also those genes that were absent in at least one among O35E and CCRI-195ME strains. Next, read counts were normalized respect to library size and variance-stabilized.

From a principal component analysis (PCA) on transformed and normalized read counts a strong batch effect emerged, so ComBat method by Bioconductor sva package (R version 3.6.0, sva version 3.32.1) was applied to adjust for such effect. Finally, sample quantile scatterplots were inspected and quantile normalization was performed to remove systematic shifts between samples. Briefly, WGCNA pipeline started constructing a weighted gene co-expression network using pairwise similarity values based on Pearson correlation. Co-expression similarity to calculate adjacency was raised to the soft thresholding power $b = 9$, that demonstrated to be the lowest power for which the scale free topology fit index for the network reached 0.90. Next, based on the resulting network, topological overlap measures (TOM), that takes in consideration the context of a gene pair when calculating its similarity, were derived. To perform module detection, the algorithm run the agglomerative hierarchical clustering on TOM similarity matrix and average linkage together with a dynamic tree cutting procedure to make sure that obtained clusters satisfied criteria linked to cluster cohesion and separation. A minimum size of 30 genes in clusters was considered and a height cut of 0.20, corresponding to correlation of 0.80, was used to merge similar clusters. KEGG pathway enrichment analyses on genes falling in each module were performed through a hypergeometric test via `kegga` function by `limma` Bioconductor package (R version 3.6.0, `limma` version 3.40.6), considering as significant the pathways associated to a BH-adjusted P value ≤ 0.05 . Genes in modules were ranked using both module membership, defined by the correlation between a gene expression profile and the module eigengene (derived by the first principal component of the expression matrix), and intramodular connectivity. To define the strong neighborhood for genes of interest (particularly, unknown genes emerging from DE analyses) only connections with a weight higher or equal to the third quantile of the distribution of all the TOM values for the relative module were considered. Subnetworks showing the most strongly connected genes for modules of interest were visualized by Cytoscape (version 3.7.2).

9.19 Generation of directed mutants

Directed gene deletion mutants of *M. catarrhalis* BBH18 were obtained by allelic exchange of the target gene with a kanamycin resistance cassette. A kanamycin resistance cassette substituting the coding sequence of the gene is fused to its 5' and 3' ~500 bp flanking regions and transformed into naturally competent *M. catarrhalis* BBH18 bacteria. To this aim, ~ 1 μ g of the purified PCR product was mixed with 25 μ l of bacteria resuspended in PBS, incubated for 5-6 h at 37°C and transformants were selected twice on BHI + 30 μ g/ml kanamycin plates. Transformants were verified by PCR for recombination at the correct location on the genome, for the absence of the gene CDS

and confirmed by sequencing. The list of the oligonucleotides used in this study (obtained from Sigma) is shown in Table S1.

9.20 Genetic complementation of *badM* and *MCR_0349* directed mutants

For genetic complementation of the BBH18 *badM* and *MCR_0349* mutants, the CDS and upstream region was amplified from BBH18 and ligated into the BamHI and SacI sites of a modified pWW115, called pMA-WW115, containing an additional 2342 bp scaffold region that make this plasmid suitable for subcloning into *Escherichia coli*. Subsequently, XhoI restriction site was used to eliminate the *E. coli* scaffold, as it can be easily distinguishable from the pWW115 (4395 nt). To obtain the complemented mutants, 10 ul of plasmid ligation mixtures were transformed into $\Delta badM$ and ΔMCR_0349 of *M. catarrhalis* BBH18. For ΔMCR_0349 mutant, an additional construct includes also the CDS of *MCR_0348* joined with the CDS and upstream region of *MCR_0349*. As a control, empty pWW115 was transformed into the wt strain.

9.21 Use of growth curves to assess the response to exogenous H₂O₂

M. catarrhalis strains BBH18 wt, wt + empty pWW115, $\Delta badM$, $\Delta badM + badM$, $\Delta afeA$, $\Delta cysP$, $\Delta vapB$, $\Delta katA$, ΔMCR_0644 , ΔMCR_0349 , $\Delta MCR_0349 + MCR_0349$, $\Delta MCR_0349 + MCR_0349-MCR_0348$ were grown in BHI broth to mid-logarithmic phase (OD₆₀₀, 0.7). The culture is then splitted in two: untreated or 50 mM H₂O₂ was added; the flask was incubated at 37°C with agitation; Measurements of OD₆₀₀ were recorded over time.

9.22 Intracellular survival of deletion mutants and complementant strains in dHL-60 cells

ROS-stimulated dHL-60 cells (1×10^6) were incubated with the different *M. catarrhalis* strains at MOI 50 for 40 minutes after which 400 µg/ml gentamicin (Sigma) was added to inhibit growth of extracellular bacteria. After 20 minutes, medium was changed with new pre-warmed RPMI 1640 (no phenol red), supplemented with PMA. The reactions proceeded for 3 additional hours. For bacterial intracellular survival, Immediately after the removal of gentamicin (control groups) and after three hours, dHL-60 cells were permeabilized and colony formation unit (CFU)/ml was determined by dilution plating on BHI agar.

9.23 *In vivo* virulence assay of *Galleria mellonella* infected with Mcat

Larvae were purchased from a local vendor (Sagip, Italy) and stored at 15°C before use. Healthy larvae were selected of a body weight of approximately 250-380 mg and put into 25 cm Petri dishes containing a layer of filter paper. Once selected, no food was made available. Prior to each experiment, disinfection of larvae surface was done with ethanol 70% , and by using sterile Hamilton syringe, 10-20 larvae per group were infected with 10 μ l aliquots containing 2×10^7 bacteria into the *G. mellonella* hindmost left proleg. The control group was injected with 10 μ l 10 mM MgSO₄ in order to measure any potentially lethal effects of the physical injection process. Following the injections, larvae were incubated at 37°C, 5 % CO₂ for six days (24-, 48-, 72- and 144 h) to allow the progression of Mcat infection. According to the Health Index Score, larvae were monitored for their survival (dead or alive), activity (no movement, or inability to right themselves, movement that is minimal or upon stimulat shaking of the petri dish or touching with a pipette tip) and melanization (black, brown or creamy-colored larvae in the absence or presence of <3 or > 3 spots). For each strain, 5 independent repeats were carried out.

10. REFERENCES

- <ber e ner.pdf>.
- <Beyond oxidative stress an immunologists guide.pdf>.
- <G-Protein-Coupled Receptors in t.pdf>.
- <Garcia-Garcia and Rosales, 2002.pdf>.
- <high and low-affinity Fc receptors.pdf>.
- <Inhibitory and bactericidal effects of hydrogen peroxide production by Streptococcus.pdf>.
- <Kulkani,PI3K neutrophil.pdf>.
- <May JR. The bacteriology of chronic bronchitis. Lancet 1953.pdf>.
- <Metals, Toxicity and Oxidative Stress.pdf>.
- <MID and UspA1A2 of the human respiratory pathogen Moraxella.pdf>.
- <Moraxella catarrhalis from interactions with the host immune system to vaccine development.pdf>.
- <ompCD-mucin.pdf>.
- <OMPCD PROTEIN.pdf>.
- <P. aeruginosa has a type III secretion system (T3SS).pdf>.
- <Prall, F. et al. CD66a (BGP), an adhesion molecule of.pdf>.
- <A Study of the Reactivity of H0202- with Unsaturated Fatty Acids.pdf>.
- AKIMANA, C. & LAFONTAINE, E. R. 2007. The Moraxella catarrhalis outer membrane protein CD contains two distinct domains specifying adherence to human lung cells. *FEMS Microbiol Lett*, 271, 12-9.
- ALI, S. R., FONG, J. J., CARLIN, A. F., BUSCH, T. D., LINDEN, R., ANGATA, T., ARESCHOUG, T., PARAST, M., VARKI, N., MURRAY, J., NIZET, V. & VARKI, A. 2014. Siglec-5 and Siglec-14

are polymorphic paired receptors that modulate neutrophil and amnion signaling responses to group B Streptococcus. *J Exp Med*, 211, 1231-42.

- ANJEM, A., VARGHESE, S. & IMLAY, J. A. 2009. Manganese import is a key element of the OxyR response to hydrogen peroxide in Escherichia coli. *Mol Microbiol*, 72, 844-58.
- ASAD, L. M. B. O., MEDEIROS, D. C., FELZENSZWALB, I., LEITÃO, A. C. & ASAD, N. R. 2000. Participation of stress-inducible systems and enzymes involved in BER and NER in the protection of Escherichia coli against cumene hydroperoxide. *Mutation Research/DNA Repair*, 461, 31-40.
- AYDEMIR, Y., AYDEMIR, O., SENGUL, A., GUNGEN, A. C., COBAN, H., TASDEMIR, C., DUZENLI, H. & SEHITOGULLARI, A. 2019. Comparison of oxidant/antioxidant balance in COPD and non-COPD smokers. *Heart Lung*, 48, 566-569.
- BAGDONAS, E., RAUDONIUTE, J., BRUZAUSKAITE, I. & ALDONYTE, R. 2015. Novel aspects of pathogenesis and regeneration mechanisms in COPD. *Int J Chron Obstruct Pulmon Dis*, 10, 995-1013.
- BARKER, B. L., HALDAR, K., PATEL, H., PAVORD, I. D., BARER, M. R., BRIGHTLING, C. E. & BAFADHEL, M. 2015. Association between pathogens detected using quantitative polymerase chain reaction with airway inflammation in COPD at stable state and exacerbations. *Chest*, 147, 46-55.
- BEAVERS, W. N. & SKAAR, E. P. 2016. Neutrophil-generated oxidative stress and protein damage in Staphylococcus aureus. *Pathog Dis*, 74.
- BECKER, K. W. & SKAAR, E. P. 2014. Metal limitation and toxicity at the interface between host and pathogen. *FEMS Microbiol Rev*, 38, 1235-49.
- BECKER, P. D., BERTOT, G. M., SOUSS, D., EBENSEN, T., GUZMAN, C. A. & GRINSTEIN, S. 2007. Intranasal vaccination with recombinant outer membrane protein CD and adamantylamide dipeptide as the mucosal adjuvant enhances pulmonary clearance of Moraxella catarrhalis in an experimental murine model. *Infect Immun*, 75, 1778-84.
- BEGG, S. L. 2019. The role of metal ions in the virulence and viability of bacterial pathogens. *Biochemical Society Transactions*, 47, 77-87.
- BEHRENS, I. K., BUSCH, B., ISHIKAWA-ANKERHOLD, H., PALAMIDES, P., SHIVELY, J. E., STANNERS, C., CHAN, C., LEUNG, N., GRAY-OWEN, S. & HAAS, R. 2020. The HopQ-CEACAM Interaction Controls CagA Translocation, Phosphorylation, and Phagocytosis of Helicobacter pylori in Neutrophils. *mBio*, 11.
- BEITER, K., WARTHA, F., ALBIGER, B., NORMARK, S., ZYCHLINSKY, A. & HENRIQUES-NORMARK, B. 2006. An endonuclease allows Streptococcus pneumoniae to escape from neutrophil extracellular traps. *Curr Biol*, 16, 401-7.
- BERNSTEIN, J. M. & REDDY, M. 2000. Bacteria-mucin interaction in the upper aerodigestive tract shows striking heterogeneity: implications in otitis media, rhinosinusitis, and pneumonia. *Otolaryngol Head Neck Surg*, 122, 514-20.
- BESOLD, A. N., CULBERTSON, E. M. & CULOTTA, V. C. 2016. The Yin and Yang of copper during infection. *J Biol Inorg Chem*, 21, 137-44.
- BLAKEWAY, L. V., TAN, A., JURCISEK, J. A., BAKALETZ, L. O., ATTACK, J. M., PEAK, I. R. & SEIB, K. L. 2019. The Moraxella catarrhalis phase-variable DNA methyltransferase ModM3 is an epigenetic regulator that affects bacterial survival in an in vivo model of otitis media. *BMC Microbiol*, 19, 276.
- BLAKEWAY, L. V., TAN, A., PEAK, I. R. A. & SEIB, K. L. 2017. Virulence determinants of Moraxella catarrhalis: distribution and considerations for vaccine development. *Microbiology*, 163, 1371-1384.
- BONSIGNORE, P., KUIPER, J. W. P., ADRIAN, J., GOOB, G. & HAUCK, C. R. 2019. CEACAM3-A Prim(at)e Invention for Opsonin-Independent Phagocytosis of Bacteria. *Front Immunol*, 10, 3160.
- BOTOS, I., SEGAL, D. M. & DAVIES, D. R. 2011. The structural biology of Toll-like receptors. *Structure*, 19, 447-59.
- BOUCHON, A., DIETRICH, J. & COLONNA, M. 2000. Cutting edge: inflammatory responses can be triggered by TREM-1, a novel receptor expressed on neutrophils and monocytes. *J Immunol*, 164, 4991-5.
- BOULTON, I. C. & GRAY-OWEN, S. D. 2002. Neisserial binding to CEACAM1 arrests the activation and proliferation of CD4+ T lymphocytes. *Nat Immunol*, 3, 229-36.
- BOYLAN, J. A., LAWRENCE, K. A., DOWNEY, J. S. & GHERARDINI, F. C. 2008. Borrelia burgdorferi membranes are the primary targets of reactive oxygen species. *Mol Microbiol*, 68, 786-99.

- BROCKSON, M. E., NOVOTNY, L. A., JURCISEK, J. A., MCGILLIVARY, G., BOWERS, M. R. & BAKALETZ, L. O. 2012. Respiratory syncytial virus promotes *Moraxella catarrhalis*-induced ascending experimental otitis media. *PLoS One*, 7, e40088.
- BROOKS, M. J., SEDILLO, J. L., WAGNER, N., WANG, W., ATTIA, A. S., WONG, H., LAURENCE, C. A., HANSEN, E. J. & GRAY-OWEN, S. D. 2008. *Moraxella catarrhalis* binding to host cellular receptors is mediated by sequence-specific determinants not conserved among all UspA1 protein variants. *Infect Immun*, 76, 5322-9.
- BROWNE, N., HEELAN, M. & KAVANAGH, K. 2013. An analysis of the structural and functional similarities of insect hemocytes and mammalian phagocytes. *Virulence*, 4, 597-603.
- BRUHNS, P. 2012. Properties of mouse and human IgG receptors and their contribution to disease models. *Blood*, 119, 5640-9.
- BUNTRU, A., KOPP, K., VOGES, M., FRANK, R., BACHMANN, V. & HAUCK, C. R. 2011. Phosphatidylinositol 3'-kinase activity is critical for initiating the oxidative burst and bacterial destruction during CEACAM3-mediated phagocytosis. *J Biol Chem*, 286, 9555-66.
- BUNTRU, A., ROTH, A., NYFFENEGGER-JANN, N. J. & HAUCK, C. R. 2012. HemITAM signaling by CEACAM3, a human granulocyte receptor recognizing bacterial pathogens. *Arch Biochem Biophys*, 524, 77-83.
- CARLIN, A. F., CHANG, Y. C., ARESCHOUG, T., LINDAHL, G., HURTADO-ZIOLA, N., KING, C. C., VARKI, A. & NIZET, V. 2009. Group B *Streptococcus* suppression of phagocyte functions by protein-mediated engagement of human Siglec-5. *J Exp Med*, 206, 1691-9.
- CHAKRABORTY, S. & KENNEY, L. J. 2018. A New Role of OmpR in Acid and Osmotic Stress in *Salmonella* and *E. coli*. *Front Microbiol*, 9, 2656.
- CHANG, Y. C. & NIZET, V. 2014. The interplay between Siglecs and sialylated pathogens. *Glycobiology*, 24, 818-25.
- CHANG, Y. C. & NIZET, V. 2020. Siglecs at the Host-Pathogen Interface. *Adv Exp Med Biol*, 1204, 197-214.
- CHERESH, P., KIM, S. J., TULASIRAM, S. & KAMP, D. W. 2013. Oxidative stress and pulmonary fibrosis. *Biochim Biophys Acta*, 1832, 1028-40.
- CHIANG, S. M. & SCHELLHORN, H. E. 2012. Regulators of oxidative stress response genes in *Escherichia coli* and their functional conservation in bacteria. *Arch Biochem Biophys*, 525, 161-9.
- CHITKARA, R. & HURST, J. R. 2012. Chronic obstructive pulmonary disease: aetiology, pathology, physiology and outcome. *Medicine*, 40, 257-261.
- CHOI, A. M. K., RYTER, S. W. & LEVINE, B. 2013. Autophagy in Human Health and Disease. *New England Journal of Medicine*, 368, 651-662.
- CHOUDHURY, G. & MACNEE, W. 2017. Role of Inflammation and Oxidative Stress in the Pathology of Ageing in COPD: Potential Therapeutic Interventions. *COPD*, 14, 122-135.
- COOK, S. M. & MCARTHUR, J. D. 2013. Developing *Galleria mellonella* as a model host for human pathogens. *Virulence*, 4, 350-3.
- COOLS, F., TORFS, E., VANHOUTTE, B., DE MACEDO, M. B., BONOFIOLIO, L., MOLLERACH, M., MAES, L., CALJON, G., DELPUTTE, P., CAPPOEN, D. & COS, P. 2018. *Streptococcus pneumoniae* galU gene mutation has a direct effect on biofilm growth, adherence and phagocytosis in vitro and pathogenicity in vivo. *Pathog Dis*, 76.
- CUTULI, M. A., PETRONIO PETRONIO, G., VERGALITO, F., MAGNIFICO, I., PIETRANGELO, L., VENDITTI, N. & DI MARCO, R. 2019. *Galleria mellonella* as a consolidated in vivo model hosts: New developments in antibacterial strategies and novel drug testing. *Virulence*, 10, 527-541.
- D'ANNA, S. E., MANISCALCO, M., CAPPELLO, F., CARONE, M., MOTTA, A., BALBI, B., RICCIARDOLO, F. L. M., CARAMORI, G. & STEFANO, A. D. 2020. Bacterial and viral infections and related inflammatory responses in chronic obstructive pulmonary disease. *Annals of Medicine*, 53, 135-150.
- DAN DUNN, J., ALVAREZ, L. A., ZHANG, X. & SOLDATI, T. 2015. Reactive oxygen species and mitochondria: A nexus of cellular homeostasis. *Redox Biol*, 6, 472-485.
- DAVIE, J. J., EARL, J., DE VRIES, S. P., AHMED, A., HU, F. Z., BOOTSMA, H. J., STOL, K., HERMANS, P. W., WADOWSKY, R. M., EHRlich, G. D., HAYS, J. P. & CAMPAGNARI, A. A. 2011. Comparative analysis and supragenome modeling of twelve *Moraxella catarrhalis* clinical isolates. *BMC Genomics*, 12, 70.

- DE VRIES, S. P., ELEVELD, M. J., HERMANS, P. W. & BOOTSMA, H. J. 2013. Characterization of the molecular interplay between *Moraxella catarrhalis* and human respiratory tract epithelial cells. *PLoS One*, 8, e72193.
- DE VRIES, S. P., VAN HIJUM, S. A., SCHUELER, W., RIESBECK, K., HAYS, J. P., HERMANS, P. W. & BOOTSMA, H. J. 2010. Genome analysis of *Moraxella catarrhalis* strain BBH18, [corrected] a human respiratory tract pathogen. *J Bacteriol*, 192, 3574-83.
- DECRAMER, M., JANSSENS, W. & MIRAVITLLES, M. 2012. Chronic obstructive pulmonary disease. *The Lancet*, 379, 1341-1351.
- DELGADO-RIZO, V., MARTINEZ-GUZMAN, M. A., INIGUEZ-GUTIERREZ, L., GARCIA-OROZCO, A., ALVARADO-NAVARRO, A. & FAFUTIS-MORRIS, M. 2017. Neutrophil Extracellular Traps and Its Implications in Inflammation: An Overview. *Front Immunol*, 8, 81.
- DEMIDENOK, O. I., KAPRELYANTS, A. S. & GONCHARENKO, A. V. 2014. Toxin-antitoxin vapBC locus participates in formation of the dormant state in *Mycobacterium smegmatis*. *FEMS Microbiol Lett*, 352, 69-77.
- DERETIC, V., SAITOH, T. & AKIRA, S. 2013. Autophagy in infection, inflammation and immunity. *Nat Rev Immunol*, 13, 722-37.
- DI STEFANO, A., CARAMORI, G., RICCIARDOLO, F. L., CAPELLI, A., ADCOCK, I. M. & DONNER, C. F. 2004. Cellular and molecular mechanisms in chronic obstructive pulmonary disease: an overview. *Clin Exp Allergy*, 34, 1156-67.
- DIAZ-OCHOA, V. E., JELLBAUER, S., KLAUS, S. & RAFFATELLU, M. 2014. Transition metal ions at the crossroads of mucosal immunity and microbial pathogenesis. *Front Cell Infect Microbiol*, 4, 2.
- DUPRE-CROCHET, S., ERARD, M. & NUBETA, O. 2013. ROS production in phagocytes: why, when, and where? *J Leukoc Biol*, 94, 657-70.
- EARL, J. P., DE VRIES, S. P., AHMED, A., POWELL, E., SCHULTZ, M. P., HERMANS, P. W., HILL, D. J., ZHOU, Z., CONSTANTINIDOU, C. I., HU, F. Z., BOOTSMA, H. J. & EHRlich, G. D. 2016. Comparative Genomic Analyses of the *Moraxella catarrhalis* Serosensitive and Seroresistant Lineages Demonstrate Their Independent Evolution. *Genome Biol Evol*, 8, 955-74.
- EL-BENNA, J., DANG, P. M., GOUGEROT-POCIDALO, M. A., MARIE, J. C. & BRAUT-BOUCHER, F. 2009. p47phox, the phagocyte NADPH oxidase/NOX2 organizer: structure, phosphorylation and implication in diseases. *Exp Mol Med*, 41, 217-25.
- ESCOLL, P., ROLANDO, M. & BUCHRIESER, C. 2016. Modulation of Host Autophagy during Bacterial Infection: Sabotaging Host Munitions for Pathogen Nutrition. *Front Immunol*, 7, 81.
- ESCOLL, P., ROLANDO, M. & BUCHRIESER, C. 2017. MAMs are attractive targets for bacterial repurposing of the host cell: MAM-functions might be key for undermining an infected cell. *Bioessays*, 39.
- ESSILFIE, A. T., SIMPSON, J. L., HORVAT, J. C., PRESTON, J. A., DUNKLEY, M. L., FOSTER, P. S., GIBSON, P. G. & HANSBRO, P. M. 2011. Haemophilus influenzae infection drives IL-17-mediated neutrophilic allergic airways disease. *PLoS Pathog*, 7, e1002244.
- EZRATY, B., GENNARIS, A., BARRAS, F. & COLLET, J.-F. 2017. Oxidative stress, protein damage and repair in bacteria. *Nature Reviews Microbiology*, 15, 385-396.
- FAUCHER, S. P., FRIEDLANDER, G., LIVNY, J., MARGALIT, H. & SHUMAN, H. A. 2010. *Legionella pneumophila* 6S RNA optimizes intracellular multiplication. *Proc Natl Acad Sci U S A*, 107, 7533-8.
- FIRACATIVE, C., KHAN, A., DUAN, S., FERREIRA-PAIM, K., LEEMON, D. & MEYER, W. 2020. Rearing and Maintenance of *Galleria mellonella* and Its Application to Study Fungal Virulence. *J Fungi (Basel)*, 6.
- FU, Y., CHANG, F. M. & GIEDROC, D. P. 2014. Copper transport and trafficking at the host-bacterial pathogen interface. *Acc Chem Res*, 47, 3605-13.
- FUCHS, T. A., ABED, U., GOOSMANN, C., HURWITZ, R., SCHULZE, I., WAHN, V., WEINRAUCH, Y., BRINKMANN, V. & ZYCHLINSKY, A. 2007. Novel cell death program leads to neutrophil extracellular traps. *J Cell Biol*, 176, 231-41.
- GARCHA, D. S., THURSTON, S. J., PATEL, A. R., MACKAY, A. J., GOLDRING, J. J., DONALDSON, G. C., MCHUGH, T. D. & WEDZICHA, J. A. 2012. Changes in prevalence and load of airway bacteria using quantitative PCR in stable and exacerbated COPD. *Thorax*, 67, 1075-80.
- GARCÍA-GARCÍA, E. & ROSALES, C. 2002. Signal transduction during Fc receptor-mediated phagocytosis. *J Leukoc Biol*, 72, 1092-108.

- GEORGE, S. N., GARCHA, D. S., MACKAY, A. J., PATEL, A. R., SINGH, R., SAPSFORD, R. J., DONALDSON, G. C. & WEDZICHA, J. A. 2014. Human rhinovirus infection during naturally occurring COPD exacerbations. *Eur Respir J*, 44, 87-96.
- GERMAN, N., LUTHJE, F., HAO, X., RONN, R. & RENSING, C. 2016. Microbial Virulence and Interactions With Metals. *Prog Mol Biol Transl Sci*, 142, 27-49.
- GLASAUER, A. & CHANDEL, N. S. 2013. Ros. *Curr Biol*, 23, R100-2.
- GOMES, L. C., DI BENEDETTO, G. & SCORRANO, L. 2011. During autophagy mitochondria elongate, are spared from degradation and sustain cell viability. *Nat Cell Biol*, 13, 589-98.
- GOULART, C. L., BARBOSA, L. C., BISCH, P. M. & VON KRÜGER, W. M. A. 2016. Catalases and PhoB/PhoR system independently contribute to oxidative stress resistance in *Vibrio cholerae* O1. *Microbiology (Reading)*, 162, 1955-1962.
- GRABCANOVIC-MUSIJA, F., OBERMAYER, A., STOIBER, W., KRAUTGARTNER, W. D., STEINBACHER, P., WINTERBERG, N., BATHKE, A. C., KLAPPACHER, M. & STUDNICKA, M. 2015. Neutrophil extracellular trap (NET) formation characterises stable and exacerbated COPD and correlates with airflow limitation. *Respir Res*, 16, 59.
- GREENE, C. M., MARCINIAK, S. J., TECKMAN, J., FERRAROTTI, I., BRANTLY, M. L., LOMAS, D. A., STOLLER, J. K. & MCELVANEY, N. G. 2016. alpha1-Antitrypsin deficiency. *Nat Rev Dis Primers*, 2, 16051.
- GUTIERREZ, M. G., MASTER, S. S., SINGH, S. B., TAYLOR, G. A., COLOMBO, M. I. & DERETIC, V. 2004. Autophagy is a defense mechanism inhibiting BCG and *Mycobacterium tuberculosis* survival in infected macrophages. *Cell*, 119, 753-66.
- HAINES-MENGES, B. L., WHITAKER, W. B., LUBIN, J. B. & BOYD, E. F. 2015. Host Sialic Acids: A Delicacy for the Pathogen with Discerning Taste. *Microbiol Spectr*, 3.
- HAINES, S., ARNAUD-BARBE, N., PONCET, D., REVERCHON, S., WAWRZYNIAK, J., NASSER, W. & RENAULD-MONGENIE, G. 2015. IscR Regulates Synthesis of Colonization Factor Antigen I Fimbriae in Response to Iron Starvation in Enterotoxigenic *Escherichia coli*. *J Bacteriol*, 197, 2896-907.
- HAKKIM, A., FUCHS, T. A., MARTINEZ, N. E., HESS, S., PRINZ, H., ZYCHLINSKY, A. & WALDMANN, H. 2011. Activation of the Raf-MEK-ERK pathway is required for neutrophil extracellular trap formation. *Nat Chem Biol*, 7, 75-7.
- HALDAR, K., GEORGE, L., WANG, Z., MISTRY, V., RAMSHEH, M. Y., FREE, R. C., JOHN, C., REEVE, N. F., MILLER, B. E., TAL-SINGER, R., WEBB, A. J., BROOKES, A. J., TOBIN, M. D., SINGH, D., DONALDSON, G. C., WEDZICHA, J. A., BROWN, J. R., BARER, M. R. & BRIGHTLING, C. E. 2020. The sputum microbiome is distinct between COPD and health, independent of smoking history. *Respir Res*, 21, 183.
- HARMS, A., BRODERSEN, D. E., MITARAI, N. & GERDES, K. 2018. Toxins, Targets, and Triggers: An Overview of Toxin-Antitoxin Biology. *Mol Cell*, 70, 768-784.
- HEINRICH, A., HAARMANN, H., ZAHRADNIK, S., FRENZEL, K., SCHREIBER, F., KLASSERT, T. E., HEYL, K. A., ENDRES, A. S., SCHMIDTKE, M., HOFMANN, J. & SLEVOGT, H. 2016a. *Moraxella catarrhalis* decreases antiviral innate immune responses by down-regulation of TLR3 via inhibition of p53 in human bronchial epithelial cells. *FASEB J*, 30, 2426-34.
- HEINRICH, A., HEYL, K. A., KLAILE, E., MULLER, M. M., KLASSERT, T. E., WIESSNER, A., FISCHER, K., SCHUMANN, R. R., SEIFERT, U., RIESBECK, K., MOTER, A., SINGER, B. B., BACHMANN, S. & SLEVOGT, H. 2016b. *Moraxella catarrhalis* induces CEACAM3-Syk-CARD9-dependent activation of human granulocytes. *Cell Microbiol*, 18, 1570-1582.
- HOGG, M., WALLACE, S. S. & DOUBLIE, S. 2005. Bumps in the road: how replicative DNA polymerases see DNA damage. *Curr Opin Struct Biol*, 15, 86-93.
- HOOPMAN, T. C., LIU, W., JOSLIN, S. N., PYBUS, C., BRAUTIGAM, C. A. & HANSEN, E. J. 2011. Identification of gene products involved in the oxidative stress response of *Moraxella catarrhalis*. *Infect Immun*, 79, 745-55.
- HOUGHTON, A. M. 2013. Mechanistic links between COPD and lung cancer. *Nat Rev Cancer*, 13, 233-45.
- IMLAY, J. A. 2008. Cellular defenses against superoxide and hydrogen peroxide. *Annu Rev Biochem*, 77, 755-76.
- IMLAY, J. A. 2013. The molecular mechanisms and physiological consequences of oxidative stress: lessons from a model bacterium. *Nat Rev Microbiol*, 11, 443-54.

- IMLAY, J. A. 2015. Transcription Factors That Defend Bacteria Against Reactive Oxygen Species. *Annu Rev Microbiol*, 69, 93-108.
- IWADATE, Y. & KATO, J. I. 2017. Involvement of the ytfK gene from the PhoB regulon in stationary-phase H₂O₂ stress tolerance in Escherichia coli. *Microbiology (Reading)*, 163, 1912-1923.
- JAFARINEJAD, H., MOGHOOFEI, M., MOSTAFAEI, S., SALIMIAN, J., AZIMZADEH JAMALKANDI, S. & AHMADI, A. 2017. Worldwide prevalence of viral infection in AECOPD patients: A meta-analysis. *Microb Pathog*, 113, 190-196.
- JAROENPOOL, J., PATTANAPANYASAT, K., NOONIN, N. & PRACHONGSAI, I. 2016. Aberrant neutrophil function among heavy smokers and chronic obstructive pulmonary disease patients. *Asian Pac J Allergy Immunol*, 34, 278-283.
- JAYAPRAKASH, K., DEMIREL, I., KHALAF, H. & BENGTSSON, T. 2015. The role of phagocytosis, oxidative burst and neutrophil extracellular traps in the interaction between neutrophils and the periodontal pathogen Porphyromonas gingivalis. *Mol Oral Microbiol*, 30, 361-75.
- JEON, J. & YONG, D. 2019. Two Novel Bacteriophages Improve Survival in Galleria mellonella Infection and Mouse Acute Pneumonia Models Infected with Extensively Drug-Resistant Pseudomonas aeruginosa. *Appl Environ Microbiol*, 85.
- JO, E. K., YUK, J. M., SHIN, D. M. & SASAKAWA, C. 2013. Roles of autophagy in elimination of intracellular bacterial pathogens. *Front Immunol*, 4, 97.
- JO, I., CHUNG, I. Y., BAE, H. W., KIM, J. S., SONG, S., CHO, Y. H. & HA, N. C. 2015. Structural details of the OxyR peroxide-sensing mechanism. *Proc Natl Acad Sci U S A*, 112, 6443-8.
- JOHNSON, M. B. & CRISS, A. K. 2013. Neisseria gonorrhoeae phagosomes delay fusion with primary granules to enhance bacterial survival inside human neutrophils. *Cell Microbiol*, 15, 1323-40.
- JOHNSON, M. D., KEHL-FIE, T. E., KLEIN, R., KELLY, J., BURNHAM, C., MANN, B. & ROSCH, J. W. 2015a. Role of copper efflux in pneumococcal pathogenesis and resistance to macrophage-mediated immune clearance. *Infect Immun*, 83, 1684-94.
- JOHNSON, M. D., KEHL-FIE, T. E. & ROSCH, J. W. 2015b. Copper intoxication inhibits aerobic nucleotide synthesis in Streptococcus pneumoniae. *Metallomics*, 7, 786-94.
- JOMOVA, K. & VALKO, M. 2011. Advances in metal-induced oxidative stress and human disease. *Toxicology*, 283, 65-87.
- JUNEAU, R. A., PANG, B., WEIMER, K. E., ARMBRUSTER, C. E. & SWORDS, W. E. 2011. Nontypeable Haemophilus influenzae initiates formation of neutrophil extracellular traps. *Infect Immun*, 79, 431-8.
- JUNEAU, R. A., STEVENS, J. S., APICELLA, M. A. & CRISS, A. K. 2015. A thermonuclease of Neisseria gonorrhoeae enhances bacterial escape from killing by neutrophil extracellular traps. *J Infect Dis*, 212, 316-24.
- KALOGRAIAKI, I., EUBA, B., PROVERBIO, D., CAMPANERO-RHODES, M. A., AASTRUP, T., GARMENDIA, J. & SOLIS, D. 2016. Combined Bacteria Microarray and Quartz Crystal Microbalance Approach for Exploring Glycosignatures of Nontypeable Haemophilus influenzae and Recognition by Host Lectins. *Anal Chem*, 88, 5950-7.
- KHATUA, B., BHATTACHARYA, K. & MANDAL, C. 2012. Sialoglycoproteins adsorbed by Pseudomonas aeruginosa facilitate their survival by impeding neutrophil extracellular trap through siglec-9. *J Leukoc Biol*, 91, 641-55.
- KILLINY, N. 2018. Generous hosts: Why the larvae of greater wax moth, Galleria mellonella is a perfect infectious host model? *Virulence*, 9, 860-865.
- KIM, S. Y., PARK, C., JANG, H. J., KIM, B. O., BAE, H. W., CHUNG, I. Y., KIM, E. S. & CHO, Y. H. 2019. Antibacterial strategies inspired by the oxidative stress and response networks. *J Microbiol*, 57, 203-212.
- KING, P. T., SHARMA, R., O'SULLIVAN, K., SELEMIDIS, S., LIM, S., RADHAKRISHNA, N., LO, C., PRASAD, J., CALLAGHAN, J., MCLAUGHLIN, P., FARMER, M., STEINFORT, D., JENNINGS, B., NGUI, J., BROUGHTON, B. R., THOMAS, B., ESSILFIE, A. T., HICKEY, M., HOLMES, P. W., HANSBRO, P., BARDIN, P. G. & HOLDSWORTH, S. R. 2015. Nontypeable Haemophilus influenzae induces sustained lung oxidative stress and protease expression. *PLoS One*, 10, e0120371.
- KLOCK, H. E., KOESEMA, E. J., KNUTH, M. W. & LESLEY, S. A. 2008. Combining the polymerase incomplete primer extension method for cloning and mutagenesis with microscreening to accelerate structural genomics efforts. *Proteins*, 71, 982-94.

- KULKARNI, S., SITARU, C., JAKUS, Z., ANDERSON, K. E., DAMOULAKIS, G., DAVIDSON, K., HIROSE, M., JUSS, J., OXLEY, D., CHESSA, T. A., RAMADANI, F., GUILLOU, H., SEGONDS-PICHON, A., FRITSCH, A., JARVIS, G. E., OKKENHAUG, K., LUDWIG, R., ZILLIKENS, D., MOCSAI, A., VANHAESEBROECK, B., STEPHENS, L. R. & HAWKINS, P. T. 2011. PI3K β plays a critical role in neutrophil activation by immune complexes. *Sci Signal*, 4, ra23.
- KUPIAINEN, H., KUOKKANEN, M., KONTTO, J., VIRTAMO, J., SALOMAA, V., LINDQVIST, A., KILPELAINEN, M. & LAITINEN, T. 2016. CHRNA5/CHRNA3 Locus Associates with Increased Mortality among Smokers. *COPD*, 13, 464-70.
- LADOMERSKY, E. & PETRIS, M. J. 2015. Copper tolerance and virulence in bacteria. *Metallomics*, 7, 957-64.
- LAMARK, T., KIRKIN, V., DIKIC, I. & JOHANSEN, T. 2009. NBR1 and p62 as cargo receptors for selective autophagy of ubiquitinated targets. *Cell Cycle*, 8, 1986-90.
- LEE, J., KIM, K. H., JO, D. S., MA, S. H., KIM, J. H., KIM, C. S., KIM, H. M. & KANG, J. H. 2020. A longitudinal hospital-based epidemiology study to assess acute otitis media incidence and nasopharyngeal carriage in Korean children up to 24 months. *Hum Vaccin Immunother*, 16, 3090-3097.
- LESHNER, M., WANG, S., LEWIS, C., ZHENG, H., CHEN, X. A., SANTY, L. & WANG, Y. 2012. PAD4 mediated histone hypercitrullination induces heterochromatin decondensation and chromatin unfolding to form neutrophil extracellular trap-like structures. *Front Immunol*, 3, 307.
- LETELIER, M. E., SANCHEZ-JOFRE, S., PEREDO-SILVA, L., CORTES-TRONCOSO, J. & ARACENA-PARKS, P. 2010. Mechanisms underlying iron and copper ions toxicity in biological systems: Pro-oxidant activity and protein-binding effects. *Chem Biol Interact*, 188, 220-7.
- LEVINE, B. & DERETIC, V. 2007. Unveiling the roles of autophagy in innate and adaptive immunity. *Nat Rev Immunol*, 7, 767-77.
- LEVINE, B. & KROEMER, G. 2008. Autophagy in the pathogenesis of disease. *Cell*, 132, 27-42.
- LEY, K., LAUDANNA, C., CYBULSKY, M. I. & NOURSHARGH, S. 2007. Getting to the site of inflammation: the leukocyte adhesion cascade updated. *Nat Rev Immunol*, 7, 678-89.
- LI, L., CHEN, H., LIU, Y., XU, S., WU, M., LIU, Z., QI, C., ZHANG, G., LI, J. & HUANG, X. 2020. Synergistic effect of linezolid with fosfomycin against *Staphylococcus aureus* in vitro and in an experimental *Galleria mellonella* model. *J Microbiol Immunol Infect*, 53, 731-738.
- LI, Y., SPIROPOULOS, J., COOLEY, W., KHARA, J. S., GLADSTONE, C. A., ASAI, M., BOSSE, J. T., ROBERTSON, B. D., NEWTON, S. M. & LANGFORD, P. R. 2018. *Galleria mellonella* - a novel infection model for the *Mycobacterium tuberculosis* complex. *Virulence*, 9, 1126-1137.
- LIU, D. F., MCMICHAEL, J. C. & BAKER, S. M. 2007. *Moraxella catarrhalis* outer membrane protein CD elicits antibodies that inhibit CD binding to human mucin and enhance pulmonary clearance of *M. catarrhalis* in a mouse model. *Infect Immun*, 75, 2818-25.
- LJUBIN-STERNAK, S. & MESTROVIC, T. 2014. Chlamydia trachomatis and Genital Mycoplasmas: Pathogens with an Impact on Human Reproductive Health. *J Pathog*, 2014, 183167.
- LUBBERS, R., VAN ESSEN, M. F., VAN KOOTEN, C. & TROUW, L. A. 2017. Production of complement components by cells of the immune system. *Clin Exp Immunol*, 188, 183-194.
- MACAULEY, M. S., CROCKER, P. R. & PAULSON, J. C. 2014. Siglec-mediated regulation of immune cell function in disease. *Nat Rev Immunol*, 14, 653-66.
- MAISONNEUVE, E. & GERDES, K. 2014. Molecular mechanisms underlying bacterial persisters. *Cell*, 157, 539-48.
- MALACHOWA, N., KOBAYASHI, S. D., FREEDMAN, B., DORWARD, D. W. & DELEO, F. R. 2013. *Staphylococcus aureus* leukotoxin GH promotes formation of neutrophil extracellular traps. *J Immunol*, 191, 6022-9.
- MALDONADO, R. F., SA-CORREIA, I. & VALVANO, M. A. 2016. Lipopolysaccharide modification in Gram-negative bacteria during chronic infection. *FEMS Microbiol Rev*, 40, 480-93.
- MARINO, E., CARUSO, M., CAMPAGNA, D. & POLOSA, R. 2015. Impact of air quality on lung health: myth or reality? *Ther Adv Chronic Dis*, 6, 286-98.
- MATHER, M. W., DRINNAN, M., PERRY, J. D., POWELL, S., WILSON, J. A. & POWELL, J. 2019. A systematic review and meta-analysis of antimicrobial resistance in paediatric acute otitis media. *International Journal of Pediatric Otorhinolaryngology*, 123, 102-109.
- MAY, J. R. 1953. The bacteriology of chronic bronchitis. *Lancet*, 265, 534-7.

- MAYADAS, T. N., CULLERE, X. & LOWELL, C. A. 2014. The multifaceted functions of neutrophils. *Annu Rev Pathol*, 9, 181-218.
- MAYHEW, D., DEVOS, N., LAMBERT, C., BROWN, J. R., CLARKE, S. C., KIM, V. L., MAGID-SLAV, M., MILLER, B. E., OSTRIDGE, K. K., PATEL, R., SATHE, G., SIMOLA, D. F., STAPLES, K. J., SUNG, R., TAL-SINGER, R., TUCK, A. C., VAN HORN, S., WEYNANTS, V., WILLIAMS, N. P., DEVASTER, J. M. & WILKINSON, T. M. A. 2018. Longitudinal profiling of the lung microbiome in the AERIS study demonstrates repeatability of bacterial and eosinophilic COPD exacerbations. *Thorax*, 73, 422-430.
- MCCAFFREY, R. L., SCHWARTZ, J. T., LINDEMANN, S. R., MORELAND, J. G., BUCHAN, B. W., JONES, B. D. & ALLEN, L. A. 2010. Multiple mechanisms of NADPH oxidase inhibition by type A and type B *Francisella tularensis*. *J Leukoc Biol*, 88, 791-805.
- MERLE, N. S., CHURCH, S. E., FREMEAUX-BACCHI, V. & ROUMENINA, L. T. 2015. Complement System Part I - Molecular Mechanisms of Activation and Regulation. *Front Immunol*, 6, 262.
- METZLER, K. D., GOOSMANN, C., LUBOJEMSKA, A., ZYCHLINSKY, A. & PAPAYANNOPOULOS, V. 2014. A myeloperoxidase-containing complex regulates neutrophil elastase release and actin dynamics during NETosis. *Cell Rep*, 8, 883-96.
- MOGHOOFEI, M., AZIMZADEH JAMALKANDI, S., MOEIN, M., SALIMIAN, J. & AHMADI, A. 2020. Bacterial infections in acute exacerbation of chronic obstructive pulmonary disease: a systematic review and meta-analysis. *Infection*, 48, 19-35.
- MONTEITH, A. J., MILLER, J. M., MAXWELL, C. N., CHAZIN, W. J. & SKAAR, E. P. 2021. Neutrophil extracellular traps enhance macrophage killing of bacterial pathogens. 7, eabj2101.
- MULLINS, E. A., RODRIGUEZ, A. A., BRADLEY, N. P. & EICHMAN, B. F. 2019. Emerging Roles of DNA Glycosylases and the Base Excision Repair Pathway. *Trends Biochem Sci*, 44, 765-781.
- MURPHY, M. P. 2009. How mitochondria produce reactive oxygen species. *Biochem J*, 417, 1-13.
- MURPHY, T. F., BRAUER, A. L., JOHNSON, A., WILDING, G. E., KOSZELAK-ROSENBLUM, M. & MALKOWSKI, M. G. 2017. A Cation-Binding Surface Protein as a Vaccine Antigen To Prevent *Moraxella catarrhalis* Otitis Media and Infections in Chronic Obstructive Pulmonary Disease. *Clin Vaccine Immunol*, 24.
- MURPHY, T. F., KIRKHAM, C., JOHNSON, A., BRAUER, A. L., KOSZELAK-ROSENBLUM, M. & MALKOWSKI, M. G. 2016. Sulfate-binding protein, CysP, is a candidate vaccine antigen of *Moraxella catarrhalis*. *Vaccine*, 34, 3855-61.
- MURPHY, T. F. & PARAMESWARAN, G. I. 2009. *Moraxella catarrhalis*, a human respiratory tract pathogen. *Clin Infect Dis*, 49, 124-31.
- NATHAN, C. & CUNNINGHAM-BUSSEL, A. 2013. Beyond oxidative stress: an immunologist's guide to reactive oxygen species. *Nature Reviews Immunology*, 13, 349-361.
- NGUYEN, G. T., GREEN, E. R. & MECSAS, J. 2017. Neutrophils to the ROScUE: Mechanisms of NADPH Oxidase Activation and Bacterial Resistance. *Front Cell Infect Microbiol*, 7, 373.
- NORIS, M. & REMUZZI, G. 2013. Overview of complement activation and regulation. *Semin Nephrol*, 33, 479-92.
- NYSTROM, T. 2005. Role of oxidative carbonylation in protein quality control and senescence. *EMBO J*, 24, 1311-7.
- PADHI, A., PATTNAIK, K., BISWAS, M., JAGADEB, M., BEHERA, A. & SONAWANE, A. 2019. *Mycobacterium tuberculosis* LprE Suppresses TLR2-Dependent Cathelicidin and Autophagy Expression to Enhance Bacterial Survival in Macrophages. *J Immunol*, 203, 2665-2678.
- PAPAYANNOPOULOS, V. 2018. Neutrophil extracellular traps in immunity and disease. *Nat Rev Immunol*, 18, 134-147.
- PAPAYANNOPOULOS, V., METZLER, K. D., HAKKIM, A. & ZYCHLINSKY, A. 2010. Neutrophil elastase and myeloperoxidase regulate the formation of neutrophil extracellular traps. *J Cell Biol*, 191, 677-91.
- PAVORD, I. D., JONES, P. W., BURGEL, P. R. & RABE, K. F. 2016. Exacerbations of COPD. *Int J Chron Obstruct Pulmon Dis*, 11 Spec Iss, 21-30.
- PELLEGRINI, M., FINETTI, F., PETRONILLI, V., ULIVIERI, C., GIUSTI, F., LUPETTI, P., GIORGIO, M., PELICCI, P. G., BERNARDI, P. & BALDARI, C. T. 2007. p66SHC promotes T cell apoptosis by inducing mitochondrial dysfunction and impaired Ca²⁺ homeostasis. *Cell Death Differ*, 14, 338-47.

- PEREIRA, M. F., ROSSI, C. C., DA SILVA, G. C., ROSA, J. N. & BAZZOLLI, D. M. S. 2020. *Galleria mellonella* as an infection model: an in-depth look at why it works and practical considerations for successful application. *Pathog Dis*, 78.
- PEREZ, A. C. & MURPHY, T. F. 2017. A *Moraxella catarrhalis* vaccine to protect against otitis media and exacerbations of COPD: An update on current progress and challenges. *Hum Vaccin Immunother*, 13, 2322-2331.
- PEREZ, A. C. & MURPHY, T. F. 2019. Potential impact of a *Moraxella catarrhalis* vaccine in COPD. *Vaccine*, 37, 5551-5558.
- PERICONE, C. D., OVERWEG, K., HERMANS, P. W. & WEISER, J. N. 2000. Inhibitory and bactericidal effects of hydrogen peroxide production by *Streptococcus pneumoniae* on other inhabitants of the upper respiratory tract. *Infection and immunity*, 68, 3990-3997.
- PINGAULT, N. M., LEHMANN, D., BOWMAN, J. & RILEY, T. V. 2007. A comparison of molecular typing methods for *Moraxella catarrhalis*. *J Appl Microbiol*, 103, 2489-95.
- PIRES, R. H., FELIX, S. B. & DELCEA, M. 2016. The architecture of neutrophil extracellular traps investigated by atomic force microscopy. *Nanoscale*, 8, 14193-202.
- PRADO ACOSTA, M. & LEPENIES, B. 2019. Bacterial glycans and their interactions with lectins in the innate immune system. *Biochem Soc Trans*, 47, 1569-1579.
- PRALL, F., NOLLAU, P., NEUMAIER, M., HAUBECK, H. D., DRZENIEK, Z., HELMCHEN, U., LÖNING, T. & WAGENER, C. 1996. CD66a (BGP), an adhesion molecule of the carcinoembryonic antigen family, is expressed in epithelium, endothelium, and myeloid cells in a wide range of normal human tissues. *J Histochem Cytochem*, 44, 35-41.
- PYZ, E., MARSHALL, A. S., GORDON, S. & BROWN, G. D. 2006. C-type lectin-like receptors on myeloid cells. *Ann Med*, 38, 242-51.
- QUILLIN, S. J. & SEIFERT, H. S. 2018. *Neisseria gonorrhoeae* host adaptation and pathogenesis. *Nat Rev Microbiol*, 16, 226-240.
- QUINTANA, J., NOVOA-APONTE, L. & ARGUELLO, J. M. 2017. Copper homeostasis networks in the bacterium *Pseudomonas aeruginosa*. *J Biol Chem*, 292, 15691-15704.
- RAJEEVE, K., DAS, S., PRUSTY, B. K. & RUDEL, T. 2018. *Chlamydia trachomatis* paralyses neutrophils to evade the host innate immune response. *Nat Microbiol*, 3, 824-835.
- REDDY, M. S., MURPHY, T. F., FADEN, H. S. & BERNSTEIN, J. M. 1997. Middle ear mucin glycoprotein: purification and interaction with nontypable *Haemophilus influenzae* and *Moraxella catarrhalis*. *Otolaryngol Head Neck Surg*, 116, 175-80.
- REN, D. & PICHICHERO, M. E. 2016. Vaccine targets against *Moraxella catarrhalis*. *Expert Opin Ther Targets*, 20, 19-33.
- REN, J., SANG, Y., QIN, R., CUI, Z. & YAO, Y. F. 2017. 6S RNA is involved in acid resistance and invasion of epithelial cells in *Salmonella enterica* serovar Typhimurium. *Future Microbiol*, 12, 1045-1057.
- RIEBISCH, A. K., MUHLEN, S., BEER, Y. Y. & SCHMITZ, I. 2021. Autophagy-A Story of Bacteria Interfering with the Host Cell Degradation Machinery. *Pathogens*, 10.
- RIESBECK, K., TAN, T. T. & FORSGREN, A. 2006. MID and UspA1/A2 of the human respiratory pathogen *Moraxella catarrhalis*, and interactions with the human host as basis for vaccine development. *Acta Biochim Pol*, 53, 445-56.
- RIQUELME, S. A., AHN, D. & PRINCE, A. 2018. *Pseudomonas aeruginosa* and *Klebsiella pneumoniae* Adaptation to Innate Immune Clearance Mechanisms in the Lung. *J Innate Immun*, 10, 442-454.
- RIQUELME, S. A. & PRINCE, A. 2020. Airway immunometabolites fuel *Pseudomonas aeruginosa* infection. *Respir Res*, 21, 326.
- ROBLEDO-AVILA, F. H., RUIZ-ROSADO, J. D., PARTIDA-SANCHEZ, S. & BROCKMAN, K. L. 2020. A Bacterial Epigenetic Switch in Non-typeable *Haemophilus influenzae* Modifies Host Immune Response During Otitis Media. *Front Cell Infect Microbiol*, 10, 512743.
- ROHRBACH, A. S., SLADE, D. J., THOMPSON, P. R. & MOWEN, K. A. 2012. Activation of PAD4 in NET formation. *Front Immunol*, 3, 360.
- ROLANDO, M., ESCOLL, P., NORA, T., BOTTI, J., BOITEZ, V., BEDIA, C., DANIELS, C., ABRAHAM, G., STOGIOS, P. J., SKARINA, T., CHRISTOPHE, C., DERVINS-RAVAULT, D., CAZALET, C., HILBI, H., RUPASINGHE, T. W., TULL, D., MCCONVILLE, M. J., ONG, S. Y., HARTLAND, E. L., CODOGNO, P., LEVADE, T., NADERER, T., SAVCHENKO, A. &

- BUCHRIESER, C. 2016. Legionella pneumophila S1P-lyase targets host sphingolipid metabolism and restrains autophagy. *Proc Natl Acad Sci U S A*, 113, 1901-6.
- ROMSANG, A., DUANG-NKERN, J., LEESUKON, P., SANINJUK, K., VATTANAVIBOON, P. & MONGKOLSUK, S. 2014. The iron-sulphur cluster biosynthesis regulator IscR contributes to iron homeostasis and resistance to oxidants in *Pseudomonas aeruginosa*. *PLoS One*, 9, e86763.
- ROWE, H. A., GRIFFITHS, N. J., HILL, D. J. & VIRJI, M. 2007. Co-ordinate action of bacterial adhesins and human carcinoembryonic antigen receptors in enhanced cellular invasion by capsule serum resistant *Neisseria meningitidis*. *Cell Microbiol*, 9, 154-68.
- SAMANOVIC, M. I., DING, C., THIELE, D. J. & DARWIN, K. H. 2012. Copper in microbial pathogenesis: meddling with the metal. *Cell Host Microbe*, 11, 106-15.
- SANTOS, J. A., PEREIRA, P. J. & MACEDO-RIBEIRO, S. 2015. What a difference a cluster makes: The multifaceted roles of IscR in gene regulation and DNA recognition. *Biochim Biophys Acta*, 1854, 1101-12.
- SARANTIS, H. & GRAY-OWEN, S. D. 2007. The specific innate immune receptor CEACAM3 triggers neutrophil bactericidal activities via a Syk kinase-dependent pathway. *Cell Microbiol*, 9, 2167-80.
- SARANTIS, H. & GRAY-OWEN, S. D. 2012. Defining the roles of human carcinoembryonic antigen-related cellular adhesion molecules during neutrophil responses to *Neisseria gonorrhoeae*. *Infect Immun*, 80, 345-58.
- SCHAAR, V., NORDSTROM, T., MORGELIN, M. & RIESBECK, K. 2011. *Moraxella catarrhalis* outer membrane vesicles carry beta-lactamase and promote survival of *Streptococcus pneumoniae* and *Haemophilus influenzae* by inactivating amoxicillin. *Antimicrob Agents Chemother*, 55, 3845-53.
- SCHMITTER, T., AGERER, F., PETERSON, L., MUNZNER, P. & HAUCK, C. R. 2004. Granulocyte CEACAM3 is a phagocytic receptor of the innate immune system that mediates recognition and elimination of human-specific pathogens. *J Exp Med*, 199, 35-46.
- SCHWAN, W. R., WARRENER, P., KEUNZ, E., STOVER, C. K. & FOLGER, K. R. 2005. Mutations in the *cueA* gene encoding a copper homeostasis P-type ATPase reduce the pathogenicity of *Pseudomonas aeruginosa* in mice. *Int J Med Microbiol*, 295, 237-42.
- SCHWARZ, F., PEARCE, O. M., WANG, X., SAMRAJ, A. N., LAUBLI, H., GARCIA, J. O., LIN, H., FU, X., GARCIA-BINGMAN, A., SECREST, P., ROMANOSKI, C. E., HEYSER, C., GLASS, C. K., HAZEN, S. L., VARKI, N., VARKI, A. & GAGNEUX, P. 2015. Siglec receptors impact mammalian lifespan by modulating oxidative stress. *Elife*, 4.
- SHAFFER, T. L., BALDER, R., BUSKIRK, S. W., HOGAN, R. J. & LAFONTAINE, E. R. 2013. Use of the Chinchilla model to evaluate the vaccinogenic potential of the *Moraxella catarrhalis* filamentous hemagglutinin-like proteins MhaB1 and MhaB2. *PLoS One*, 8, e67881.
- SHELDON, J. R. & SKAAR, E. P. 2019. Metals as phagocyte antimicrobial effectors. *Curr Opin Immunol*, 60, 1-9.
- SHI, X., FESTA, R. A., IOERGER, T. R., BUTLER-WU, S., SACCHETTINI, J. C., DARWIN, K. H. & SAMANOVIC, M. I. 2014. The copper-responsive RicR regulon contributes to *Mycobacterium tuberculosis* virulence. *mBio*, 5.
- SHUTO, T., KAMEI, S., NOHARA, H., FUJIKAWA, H., TASAKI, Y., SUGAHARA, T., ONO, T., MATSUMOTO, C., SAKAGUCHI, Y., MARUTA, K., NAKASHIMA, R., KAWAKAMI, T., SUICO, M. A., KONDO, Y., ISHIGAMI, A., TAKEO, T., TANAKA, K. I., WATANABE, H., NAKAGATA, N., UCHIMURA, K., KITAMURA, K., LI, J. D. & KAI, H. 2016. Pharmacological and genetic reappraisals of protease and oxidative stress pathways in a mouse model of obstructive lung diseases. *Sci Rep*, 6, 39305.
- SIES, H. 2015. Oxidative stress: a concept in redox biology and medicine. *Redox Biol*, 4, 180-3.
- SIES, H. 2018. On the history of oxidative stress: Concept and some aspects of current development. *Current Opinion in Toxicology*, 7, 122-126.
- SIES, H., BERNDT, C. & JONES, D. P. 2017. Oxidative Stress. *Annu Rev Biochem*, 86, 715-748.
- SINGER, B. B., KLAILE, E., SCHEFFRAHN, I., MULLER, M. M., KAMMERER, R., REUTTER, W., OBRINK, B. & LUCKA, L. 2005. CEACAM1 (CD66a) mediates delay of spontaneous and Fas ligand-induced apoptosis in granulocytes. *Eur J Immunol*, 35, 1949-59.
- SISINNI, L., CENDRON, L., FAVARO, G. & ZANOTTI, G. 2010. *Helicobacter pylori* acidic stress response factor HP1286 is a YceI homolog with new binding specificity. *FEBS J*, 277, 1896-905.
- SMIDT, M., BATTIG, P., VERHAEGH, S. J., NIEBISCH, A., HANNER, M., SELAK, S., SCHULER, W., MORFELDT, E., HELLBERG, C., NAGY, E., LUNDBERG, U., HAYS, J. P., MEINKE, A. &

- HENRIQUES-NORMARK, B. 2013. Comprehensive antigen screening identifies *Moraxella catarrhalis* proteins that induce protection in a mouse pulmonary clearance model. *PLoS One*, 8, e64422.
- SMIRNOV, A., DAILY, K. P. & CRISS, A. K. 2014. Assembly of NADPH oxidase in human neutrophils is modulated by the opacity-associated protein expression State of *Neisseria gonorrhoeae*. *Infect Immun*, 82, 1036-44.
- SPANIOL, V., WYDER, S. & AEBI, C. 2013. RNA-Seq-based analysis of the physiologic cold shock-induced changes in *Moraxella catarrhalis* gene expression. *PLoS One*, 8, e68298.
- STOCKLEY, J. A., WALTON, G. M., LORD, J. M. & SAPEY, E. 2013. Aberrant neutrophil functions in stable chronic obstructive pulmonary disease: the neutrophil as an immunotherapeutic target. *Int Immunopharmacol*, 17, 1211-7.
- SU, Y. C., SINGH, B. & RIESBECK, K. 2012. *Moraxella catarrhalis*: from interactions with the host immune system to vaccine development. *Future Microbiol*, 7, 1073-100.
- SUAREZ-ARRABAL, M. C., MELLA, C., LOPEZ, S. M., BROWN, N. V., HALL, M. W., HAMMOND, S., SHIELS, W., GRONER, J., MARCON, M., RAMILO, O. & MEJIAS, A. 2015. Nasopharyngeal bacterial burden and antibiotics: Influence on inflammatory markers and disease severity in infants with respiratory syncytial virus bronchiolitis. *J Infect*, 71, 458-69.
- SUN, J., MARESSO, A. W., KIM, J.-J. P. & BARBIERI, J. T. 2004. How bacterial ADP-ribosylating toxins recognize substrates. *Nature Structural & Molecular Biology*, 11, 868-876.
- SUN, Y., MCCORVIE, T. J., YATES, L. A. & ZHANG, X. 2020. Structural basis of homologous recombination. *Cell Mol Life Sci*, 77, 3-18.
- TAN, T. T., MORGELIN, M., FORSGREN, A. & RIESBECK, K. 2007. *Haemophilus influenzae* survival during complement-mediated attacks is promoted by *Moraxella catarrhalis* outer membrane vesicles. *J Infect Dis*, 195, 1661-70.
- THAMMAVONGSA, V., MISSIAKAS, D. M. & SCHNEEWIND, O. 2013. *Staphylococcus aureus* degrades neutrophil extracellular traps to promote immune cell death. *Science*, 342, 863-6.
- THEPRUNGSIRIKUL, J., SKOPELJA-GARDNER, S., WIERZBICKI, R. M., SESSIONS, K. J. & RIGBY, W. F. C. 2021. Differential Enhancement of Neutrophil Phagocytosis by Anti-Bactericidal/Permeability-Increasing Protein Antibodies. *J Immunol*, 207, 777-783.
- TOOZE, S. A. & DIKIC, I. 2016. Autophagy Captures the Nobel Prize. *Cell*, 167, 1433-1435.
- TRAORE, D. A., EL GHAZOUANI, A., JACQUAMET, L., BOREL, F., FERRER, J. L., LASCoux, D., RAVANAT, J. L., JAQUINOD, M., BLONDIN, G., CAUX-THANG, C., DUARTE, V. & LATOUR, J. M. 2009. Structural and functional characterization of 2-oxo-histidine in oxidized PerR protein. *Nat Chem Biol*, 5, 53-9.
- TSAI, C. J., LOH, J. M. & PROFT, T. 2016. *Galleria mellonella* infection models for the study of bacterial diseases and for antimicrobial drug testing. *Virulence*, 7, 214-29.
- TUMER, Z. & MOLLER, L. B. 2010. Menkes disease. *Eur J Hum Genet*, 18, 511-8.
- TWADDELL, S. H., BAINES, K. J., GRAINGE, C. & GIBSON, P. G. 2019. The Emerging Role of Neutrophil Extracellular Traps in Respiratory Disease. *Chest*, 156, 774-782.
- UCHIYAMA, S., DOHRMANN, S., TIMMER, A. M., DIXIT, N., GHOSHANI, M., BHANDARI, T., TIMMER, J. C., SPRAGUE, K., BUBECK-WARDENBURG, J., SIMON, S. I. & NIZET, V. 2015. Streptolysin O Rapidly Impairs Neutrophil Oxidative Burst and Antibacterial Responses to Group A *Streptococcus*. *Front Immunol*, 6, 581.
- VAN ACKER, H. & COENYE, T. 2017. The Role of Reactive Oxygen Species in Antibiotic-Mediated Killing of Bacteria. *Trends Microbiol*, 25, 456-466.
- VAN ACKER, H., SASS, A., BAZZINI, S., DE ROY, K., UDINE, C., MESSIAEN, T., RICCARDI, G., BOON, N., NELIS, H. J., MAHENTHIRALINGAM, E. & COENYE, T. 2013. Biofilm-grown *Burkholderia cepacia* complex cells survive antibiotic treatment by avoiding production of reactive oxygen species. *PLoS One*, 8, e58943.
- VANHOVE, A. S., RUBIO, T. P., NGUYEN, A. N., LEMIRE, A., ROCHE, D., NICOD, J., VERGNES, A., POIRIER, A. C., DISCONZI, E., BACHERE, E., LE ROUX, F., JACQ, A., CHARRIERE, G. M. & DESTOUMIEUX-GARZON, D. 2016. Copper homeostasis at the host vibrio interface: lessons from intracellular vibrio transcriptomics. *Environ Microbiol*, 18, 875-88.
- VAREECHON, C., ZMINA, S. E., KARMAKAR, M., PEARLMAN, E. & RIETSCH, A. 2017. *Pseudomonas aeruginosa* Effector ExoS Inhibits ROS Production in Human Neutrophils. *Cell Host Microbe*, 21, 611-618 e5.

- VARGHESE, S., WU, A., PARK, S., IMLAY, K. R. & IMLAY, J. A. 2007. Submicromolar hydrogen peroxide disrupts the ability of Fur protein to control free-iron levels in *Escherichia coli*. *Mol Microbiol*, 64, 822-30.
- VERDUIN, C. M., HOL, C., FLEER, A., VAN DIJK, H. & VAN BELKUM, A. 2002. *Moraxella catarrhalis*: from emerging to established pathogen. *Clin Microbiol Rev*, 15, 125-44.
- VERHAEGH, S. J. C., SCHAAR, V., SU, Y. C., RIESBECK, K. & HAYS, J. P. 2015. *Moraxella catarrhalis*. *Molecular Medical Microbiology*.
- WANG, X. & QUINN, P. J. 2010. Lipopolysaccharide: Biosynthetic pathway and structure modification. *Prog Lipid Res*, 49, 97-107.
- WARTHA, F., BEITER, K., ALBINGER, B., FERNEBRO, J., ZYCHLINSKY, A., NORMARK, S. & HENRIQUES-NORMARK, B. 2007. Capsule and D-alanylated lipoteichoic acids protect *Streptococcus pneumoniae* against neutrophil extracellular traps. *Cell Microbiol*, 9, 1162-71.
- WHITE, C., LEE, J., KAMBE, T., FRITSCH, K. & PETRIS, M. J. 2009. A role for the ATP7A copper-transporting ATPase in macrophage bactericidal activity. *J Biol Chem*, 284, 33949-56.
- WILD, P., FARHAN, H., MCEWAN, D. G., WAGNER, S., ROGOV, V. V., BRADY, N. R., RICHTER, B., KORAC, J., WAIDMANN, O., CHOUDHARY, C., DOTSCHE, V., BUMANN, D. & DIKIC, I. 2011. Phosphorylation of the autophagy receptor optineurin restricts *Salmonella* growth. *Science*, 333, 228-33.
- WILLIAMS MCMACKIN, E. A., DJAPGNE, L., CORLEY, J. M. & YAHR, T. L. 2019. Fitting Pieces into the Puzzle of *Pseudomonas aeruginosa* Type III Secretion System Gene Expression. *J Bacteriol*, 201.
- WINTERBOURN, C. C., KETTLE, A. J. & HAMPTON, M. B. 2016. Reactive Oxygen Species and Neutrophil Function. *Annu Rev Biochem*, 85, 765-92.
- WRIGHT, T. K., GIBSON, P. G., SIMPSON, J. L., MCDONALD, V. M., WOOD, L. G. & BAINES, K. J. 2016. Neutrophil extracellular traps are associated with inflammation in chronic airway disease. *Respirology*, 21, 467-75.
- WU, C. C., WANG, C. K., CHEN, Y. C., LIN, T. H., JINN, T. R. & LIN, C. T. 2014. IscR regulation of capsular polysaccharide biosynthesis and iron-acquisition systems in *Klebsiella pneumoniae* CG43. *PLoS One*, 9, e107812.
- WYPYCH, T. P., WICKRAMASINGHE, L. C. & MARSLAND, B. J. 2019. The influence of the microbiome on respiratory health. *Nat Immunol*, 20, 1279-1290.
- XIA, Y., WENG, Y., XU, C., WANG, D., PAN, X., TIAN, Z., XIA, B., LI, H., CHEN, R., LIU, C., JIN, Y., BAI, F., CHENG, Z., KUIPERS, O. P. & WU, W. 2020. Endoribonuclease YbeY Is Essential for RNA Processing and Virulence in *Pseudomonas aeruginosa*. *mBio*, 11.
- YAGI, K., HUFFNAGLE, G. B., LUKACS, N. W. & ASAI, N. 2021. The Lung Microbiome during Health and Disease. *Int J Mol Sci*, 22.
- YAMANAKA, N., HOTOMI, M. & BILLAL, D. S. 2008. Clinical bacteriology and immunology in acute otitis media in children. *J Infect Chemother*, 14, 180-7.
- YOSHIMORI, T. 2004. Autophagy: a regulated bulk degradation process inside cells. *Biochem Biophys Res Commun*, 313, 453-8.
- ZHAO, Z., PENG, T., OH, J. I., GLAESER, J., WEBER, L., LI, Q. & KLUG, G. 2019. A response regulator of the OmpR family is part of the regulatory network controlling the oxidative stress response of *Rhodobacter sphaeroides*. *Environ Microbiol Rep*, 11, 118-128.

11. SUPPLEMENTARY MATERIALS

Table S1. List of cell lines, bacterial strains and oligonucleotides used in this study.

REAGENT or RESOURCE	SOURCE	IDENTIFIER
Cell lines		

HL-60	ATCC	CCL-240
Bacterial strains		
Stellar Competent cells	Takara Bio	Cat# 636763
T7 Express Iq Competent <i>E. coli</i>	NEB	Cat# C3013I
<i>Moraxella catarrhalis</i> BBH18, wt strain		GCA_000092265.1
<i>M. catarrhalis</i> BBH18, $\Delta badM$ mutant	This paper	N/A
<i>M. catarrhalis</i> BBH18, $\Delta cysP$ mutant	This paper	N/A
<i>M. catarrhalis</i> BBH18, $\Delta afeA$ mutant	This paper	N/A
<i>M. catarrhalis</i> BBH18, $\Delta katA$ mutant	This paper	N/A
<i>M. catarrhalis</i> BBH18, ΔMCR_{1638} mutant	This paper	N/A
<i>M. catarrhalis</i> BBH18, ΔMCR_{0644} mutant	This paper	N/A
<i>M. catarrhalis</i> BBH18, ΔMCR_{0349} mutant	This paper	N/A
<i>M. catarrhalis</i> BBH18, wt + empty pWW115	This paper	N/A
<i>M. catarrhalis</i> BBH18, $\Delta badM$ + pWW115_ <i>badM</i>	This paper	N/A
<i>M. catarrhalis</i> BBH18, ΔMCR_{0349} + pWW115_ <i>MCR_{0349}</i>	This paper	N/A
<i>M. catarrhalis</i> BBH18, ΔMCR_{0349} + pWW115_ <i>MCR_{0349-MCR_{0348}}</i>	This paper	N/A
Oligonucleotides		
pET15bF: CTAGCATAACCCCTTGGGGCCTCTAAACGG	Sigma-Aldrich	<i>E. coli</i> subcloning
pET15bR: GCTGCCGCGCGCACACCAGGCCGCTGCTGTG	Sigma-Aldrich	<i>E. coli</i> subcloning
OmpCDHisF: CTGTACTTCCAGGGCGGTGTGACAGTCAGCCCACTACTAC		
OmpCDHisR: AATTAAGTCGCGTTATTGAACAATCATATCTTTGGTTTGATC		
Kan_KOFor: TGACTAACTAGGAGGAATAAATGGC	Sigma-Aldrich	KanR amplification
Kan_KORev: TCATTATTCCTTCCAGGTACTAAAAC	Sigma-Aldrich	KanR amplification
Kan_CDSRev: CAATCAGGCTTGATCCCCAGTAAGTC		To check the quality of mutants
katA_UP: AGGAGATATACCATGCACACCGATGATGAGTTATTTTGGGA	Sigma-Aldrich	To generate $\Delta katA$
katA_DW: CAAGGGGTTATGCTAGGTCTTTATCGGCGGTGGTGCTGGT	Sigma-Aldrich	To generate $\Delta katA$
katA_KANFor: CTGGAAGGAATAATGATTCAGTGATAATCATAAAAGCTG	Sigma-Aldrich	To generate $\Delta katA$
katA_KANRev: CCTCCTAGTTAGTCATCCTTCCTATTTCGGTGGGTTAATG	Sigma-Aldrich	To generate $\Delta katA$
katA_extFor: GCATTGGCGACAGTACAACCAATATC	Sigma-Aldrich	To check the quality of $\Delta katA$
katA_CDSRev: GCAAAAGCGGATTGTTCAACGTC	Sigma-Aldrich	To check the quality of $\Delta katA$
lpxC_UP: AGGAGATATACCATGGTGATGCTGCACAGTGGCTAAAAG	Sigma-Aldrich	To generate $\Delta lpxC$
lpxC_DW: AAGGGGTTATGCTAGCAAAGACAACCTTCGCCAAAATTGGTGTC	Sigma-Aldrich	To generate $\Delta lpxC$
lpxC_KANFor: GTACCTGGAAGGAATAATGACTAAAGTGTCATTGAGTAAGCAAA GG	Sigma-Aldrich	To generate $\Delta lpxC$

lpxC_KANRev: TTATTCCTCCTAGTTAGTCACTCGTTATAATTCTCA GTCAAAACCG	Sigma-Aldrich	To generate $\Delta lpxC$
lpxC_extFor: CCTGAGACTTTTGAGCAATTGCAAGC	Sigma-Aldrich	To check the quality of $\Delta lpxC$
lpxC_CDSRev: CTATGTCTTTTAGAAAGCCAAAAGTACG	Sigma-Aldrich	To check the quality of $\Delta lpxC$
cysP_UP: AGGAGATATACCATGGGTATGCCAAACACATGGTCAAAATAG	Sigma-Aldrich	To generate $\Delta cysP$
cysP_DW: CAAGGGGTTATGCTAGTGGCAGTTTGGGCAGGCTAGCAATG	Sigma-Aldrich	To generate $\Delta cysP$
cysP_KANFOR: CTGGAAGGAATAATGACATTTTTGCTCAAACAGTTGTCAAAC	Sigma-Aldrich	To generate $\Delta cysP$
cysP_KANREV: CCTCCTAGTTAGTCATCCAAACCAAATAAACAAGATAG	Sigma-Aldrich	To generate $\Delta cysP$
cysP_extFor: CTTAGCACAAAGCAAATGATCGCCTGC	Sigma-Aldrich	To check the quality of $\Delta cysP$
cysP_CDSRev: CATTGAACAAAATCTTGGCAGCAGC	Sigma-Aldrich	To check the quality of $\Delta cysP$
afeA_UP: AGGAGATATACCATGGACCTAGTGCCAACACAGGTGCGATG	Sigma-Aldrich	To generate $\Delta afeA$
afeA_DW: AAGGGGTTATGCTAGCATAATGGCTTTTTTCGGTTTTTACATC	Sigma-Aldrich	To generate $\Delta afeA$
afeA_KANFOR: CTGGAAGGAATAATGATGGATAAAAATCACCATCAGCCTTG	Sigma-Aldrich	To generate $\Delta afeA$
afeA_KANREV: CCTCCTAGTTAGTCAATTAACCTAATTGCTTGACTGGC	Sigma-Aldrich	To generate $\Delta afeA$
afeA_extFor: AGGTGCGATGATTTTTAGTGCTTTC	Sigma-Aldrich	To check the quality of $\Delta afeA$
afeA_CDSRev: CTAAAAGATTCATAATGGCTTTTTTCGG	Sigma-Aldrich	To check the quality of $\Delta afeA$
vapB_UP: AGGAGATATACCATGCGAGCTTGGCTATTCTAGTGATGCC	Sigma-Aldrich	To generate $\Delta vapB$
vapB_DW: AAGGGGTTATGCTAGGGTGTGTAATGAACGCCATTTAGATAG	Sigma-Aldrich	To generate $\Delta vapB$
vapB_KANFOR: GTACCTGGAAGGAATAATGACTGCTTGATACCAATATTTGTATTT ATC	Sigma-Aldrich	To generate $\Delta vapB$
vapB_KANREV: TTATTCCTCCTAGTTAGTCAGATGATCCCCTAAGTAATGATTATTT G	Sigma-Aldrich	To generate $\Delta vapB$
vapB_extFor: GGTTTAGGCACATTGGTAGTACCG	Sigma-Aldrich	To check the quality of $\Delta vapB$
vapB_CDSRev: CACCAGTCACGCTCCACATCATC	Sigma-Aldrich	To check the quality of $\Delta vapB$
badM_UP: AGGAGATATACCATGGCTGATTAATACCCTAATCAATCATAAC	Sigma-Aldrich	To generate $\Delta badM$
badM_DW: AAGGGGTTATGCTAGGCCAACTGCTTGGGCAGCATCCACATG	Sigma-Aldrich	To generate $\Delta badM$

badM_KANFor:GTACCTGGAAGGAATAATGAGCCAGACTTCACTC ATCTATTTAGAC	Sigma-Aldrich	To generate $\Delta badM$
badM_KANRev:TTATTCCTCCTAGTTAGTCAGAAATACTTCCATAA TTGCCTAATTTTG	Sigma-Aldrich	To generate $\Delta badM$
badM_extFor: GACATCACCATCAATGGTTATAGCTTC	Sigma-Aldrich	To check the quality of $\Delta badM$
badM_CDSRev: CATGCTGGATTCCCAATTAAAGTGATG	Sigma-Aldrich	To check the quality of $\Delta badM$
MCR_0644_UP: AGGAGATATACCATGGGCATAACCTGCAATCAGACTGTGCG	Sigma-Aldrich	To generate ΔMCR_0644
MCR_0644_DW: AAGGGTTATGCTAGCCATTAATAACGGCTATGTCATGCCTG	Sigma-Aldrich	To generate ΔMCR_0644
MCR_0644_KANFor: GTACCTGGAAGGAATAATGACCATTCACTTAAAATCACCCATAG C	Sigma-Aldrich	To generate ΔMCR_0644
MCR_0644_KANRev:TTATTCCTCCTAGTTAGTCACACTACTCATAG ATAACTGTTTATCTAC	Sigma-Aldrich	To generate ΔMCR_0644
MCR_0644_extFor: TACACCCAAAGATAGACTTTGG	Sigma-Aldrich	To check the quality of ΔMCR_0644
MCR_0644_CDSRev: GTATTTTTTGGGTGTACGATACTC	Sigma-Aldrich	To check the quality of ΔMCR_0644
MCR_0349_UP: AGGAGATATACCATGGCTCTAAACATCTGCTGGCAGGCATC	Sigma-Aldrich	To generate ΔMCR_0349
MCR_0349_DW: AAGGGTTATGCTAGGTA AAAATTTGGTGCTTATTTTCAGATGGG	Sigma-Aldrich	To generate ΔMCR_0349
MCR_0349_KANFor:GTACCTGGAAGGAATAATGACATGAGCAAAC AAATCATTACATACAG	Sigma-Aldrich	To generate ΔMCR_0349
MCR_0349_KANRev:TTATTCCTCCTAGTTAGTCAGACATCCTTATT TTGACTGAAGTGAC	Sigma-Aldrich	To generate ΔMCR_0349
MCR_0349_extFor: GGCTGATGACCATGAAATTACTC	Sigma-Aldrich	To check the quality of ΔMCR_0349
MCR_0349_CDSRev: GATGTGCTTGGTGCGAAAATAGGC	Sigma-Aldrich	To check the quality of ΔMCR_0349
badM_complFor: GTGTCAGGATCCCAAATTAATAAAAATCAATCCATTAG	Sigma-Aldrich	To obtain complemented $\Delta badM$
badM_complRev: GAAACAGAGCTCTCATGCTGGATTCCCAATTAAAGTG	Sigma-Aldrich	To obtain complemented $\Delta badM$
MCR_0349_complFor: GTGTCAGGATCCCGCACATTGCTTGGCTATCCAAACATC	Sigma-Aldrich	To obtain single and double complemented ΔMCR_0349
MCR_0349_singlecomplRev: GAAACAGAGCTCGATGCATTAGATGTGCTTGGTGCG	Sigma-Aldrich	To obtain single complemented ΔMCR_0349
MCR_0349_doublecomplRev: GAAACAGAGCTCCTTGTTGACCAAAGACTAACATACCGC	Sigma-Aldrich	To obtain double complemented ΔMCR_0349

rpoD_RTFor: GAGCTGGATCTTGGATCACC	Sigma-Aldrich	qPCR_ housekeeping gene
rpoD_RTRev: GGCTTCTTGGGCTACATCAT	Sigma-Aldrich	qPCR_ housekeeping gene
MCR_1477_RTFor: CGATGTCTATACAGGTTTGGATGC	Sigma-Aldrich	qPCR_MCR_1477
MCR_1477_RTRev: GTCTGAAATTTAGTACCCATTCC	Sigma-Aldrich	qPCR_MCR_1477
MCR_0644_RTFor: CTTGCCAAATTGAGCGTATCATTC	Sigma-Aldrich	qPCR_MCR_0644
MCR_0644_RTRev: GTATTTTTGGGTGTACGATACTC	Sigma-Aldrich	qPCR_MCR_0644
iscS_RTFor: GTGGCACATTTTTATGAAGGTCGTG	Sigma-Aldrich	qPCR_iscS
iscS_RTRev: GTGTCATCACGCAATGCGTTTTCAAC	Sigma-Aldrich	qPCR_iscS
lpxC_RTFor: GAACGCACCGATATTGGTGCAACAGTTC	Sigma-Aldrich	qPCR_lpxC
lpxC_RTRev: GATACCTGCTTGATCAATCAGATAC	Sigma-Aldrich	qPCR_lpxC
badM_RTFor: GCGTTTAACTCGTGGACGGTATG	Sigma-Aldrich	qPCR_badM
badM_RTRev: CATGCTGGATTCCCAATTAAGTGATG	Sigma-Aldrich	qPCR_badM
katA_RTFor: CAAACGAGACCCACGCACCAACATG	Sigma-Aldrich	qPCR_katA
katA_RTRev: GCAAAAGCGGATTGTTCAACGTC	Sigma-Aldrich	qPCR_katA
MCR_1049_RTFor: GAGCAGTACGCCAGCCACCCTTTGG	Sigma-Aldrich	qPCR_MCR_1049
MCR_1049_RTRev: CCATGTCTCTAGACCAATAAATTTGG	Sigma-Aldrich	qPCR_MCR_1049
Fur_RTFor: GATTGAAGAAGGGTTGATTCACCAG	Sigma-Aldrich	qPCR_fur
Fur_RTRev: GTGCTACGCTCAACCAAAAAGTTTGC	Sigma-Aldrich	qPCR_fur
Recombinant DNA		
pET15b	Novagen	
Genomic DNA (gDNA) from <i>M. catarrhalis</i> BBH18	This paper	N/A
gDNA <i>M. catarrhalis</i> BBH18, Δ <i>badM</i> mutant	This paper	N/A
gDNA <i>M. catarrhalis</i> BBH18, Δ <i>cysP</i> mutant	This paper	N/A
gDNA <i>M. catarrhalis</i> BBH18, Δ <i>afeA</i> mutant	This paper	N/A
gDNA <i>M. catarrhalis</i> BBH18, Δ <i>katA</i> mutant	This paper	N/A
gDNA <i>M. catarrhalis</i> BBH18, Δ <i>MCR_1638</i> mutant	This paper	N/A
gDNA <i>M. catarrhalis</i> BBH18, Δ <i>MCR_0644</i> mutant	This paper	N/A
gDNA <i>M. catarrhalis</i> BBH18, Δ <i>MCR_0349</i> mutant	This paper	N/A
PCR product to obtain Δ <i>badM</i> mutant	This paper	N/A
PCR product to obtain Δ <i>cysP</i> mutant	This paper	N/A
PCR product to obtain Δ <i>afeA</i> mutant	This paper	N/A
PCR product to obtain Δ <i>katA</i> mutant	This paper	N/A
PCR product to obtain Δ <i>MCR_1638</i> mutant	This paper	N/A
PCR product to obtain Δ <i>MCR_0644</i> mutant	This paper	N/A
PCR product to obtain Δ <i>MCR_0349</i> mutant	This paper	N/A
pMA_WW115	GenArt	An <i>E.coli</i> scaffold joined with pWW115 for subcloning steps
pWW115		GenBank: DQ311662.1
pMA_WW115_ <i>badM</i>	This paper	Subcloning steps
pWW115_ <i>badM</i>	This paper	To obtain complemented Δ <i>badM</i>
pMA_WW115_ <i>MCR_0349</i>	This paper	Subcloning steps
pWW115_ <i>MCR_0349</i>	This paper	To obtain single complemented Δ <i>MCR_0349</i>

pMA_WW115__MCR_0349-MCR_0348	This paper	Subcloning steps
pWW115__MCR_0349-MCR_0348	This paper	To obtain double complemented Δ MCR_0349

Table S2. Health Index Score system in *Galleria mellonella*

Health Index Scoring System	
Activity	
no movement	0,0
<i>minimal movement on stimulation</i>	1,0
<i>move when stimulated</i>	2,0
move without stimulation	3
Melanization	
black larvae	0,0
<i>Brown larvae</i>	1,0
<i>3 spots on beige larvae and or tail/line</i>	2,0
<3 spots on beige larvae or tail/line	3
no melanization	4
Survival	
<i>dead</i>	0,0
<i>alive</i>	2,0